Towards a damage model for articular cartilage

Citation for published version (APA):
Hosseini, S. M. (2014). *Towards a damage model for articular cartilage*. [Phd Thesis 1 (Research TU/e / Graduation TU/e), Biomedical Engineering]. Technische Universiteit Eindhoven.
https://doi.org/10.6100/IR762410

DOI:
10.6100/IR762410

Document status and date:
Published: 01/01/2014

Document Version:
Publisher’s PDF, also known as Version of Record (includes final page, issue and volume numbers)

Please check the document version of this publication:

• A submitted manuscript is the version of the article upon submission and before peer-review. There can be important differences between the submitted version and the official published version of record. People interested in the research are advised to contact the author for the final version of the publication, or visit the DOI to the publisher's website.
• The final author version and the galley proof are versions of the publication after peer review.
• The final published version features the final layout of the paper including the volume, issue and page numbers.

Link to publication

General rights
Copyright and moral rights for the publications made accessible in the public portal are retained by the authors and/or other copyright owners and it is a condition of accessing publications that users recognise and abide by the legal requirements associated with these rights.

- Users may download and print one copy of any publication from the public portal for the purpose of private study or research.
- You may not further distribute the material or use it for any profit-making activity or commercial gain
- You may freely distribute the URL identifying the publication in the public portal.

If the publication is distributed under the terms of Article 25fa of the Dutch Copyright Act, indicated by the “Taverne” license above, please follow below link for the End User Agreement:

www.tue.nl/taverne

Take down policy
If you believe that this document breaches copyright please contact us at:

openaccess@tue.nl

providing details and we will investigate your claim.

Download date: 04. Oct. 2023

Briefly, several issues can be addressed for the computational importance and contribution of this thesis. The important role of the superficial tangential zone of the cartilage which used to be a kind of general accepted idea with less supportive documents has been computationally demonstrated in this thesis. This has been done by taking into account the role of horizontal collagen fibers in STZ as well as considering the depth dependent composition and structure of the main components of articular cartilage (proteoglycans, collagen network, water content). Moreover, in this thesis it has been demonstrated that even in computational modeling of biological tissues, the effect of preconditioning has to be considered. Investigating the equilibrium condition of viscoelasticity of collagen fibers and that of the poroelasticity of the whole matrix individually as well as simultaneously showed that essentially, if one of them is not in equilibrium, then by definition the other one is not in equilibrium as well. The equilibrium condition of the whole tissue only would be achieved when both effects reach equilibrium. In addition, in this thesis, our cartilage computational code has been developed by the linear softening damage mechanics model which could implement a softening behavior to both the ground substance and collagen network of the cartilage individually as well as both together. By this development, we were able to understand how damage initiates and progresses in each cartilage component as well as how the damage in one component affects the damage in the other component.

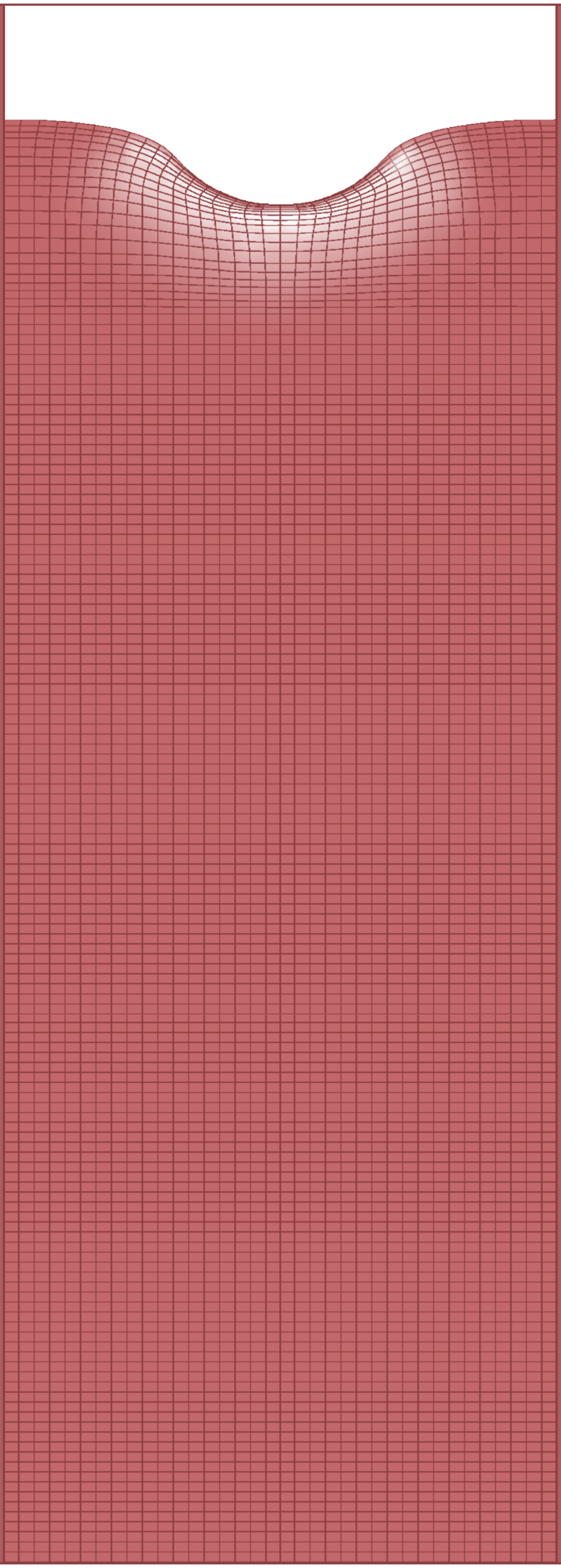

Towards a Damage Model for Articular Cartilage

Sayyed Mohsen Hosseini

Towards a Damage Model for Articular Cartilage

Sayyed Mohsen Hosseini

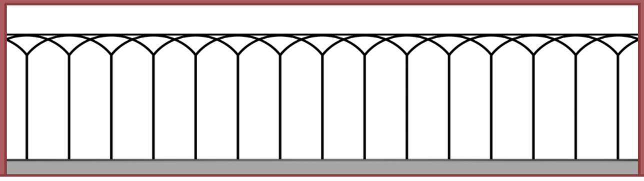

Towards a Damage Model for Articular Cartilage

Sayyed Mohsen Hosseini

The financial support for doing this research as well as for publishing this thesis by the Dutch Arthritis Foundation (Reumafonds) is gratefully acknowledged.

- Dutch Arthritis Foundation (Reumafonds)
  Dr. Jan van Breemenstraat 4
  1056 AB Amsterdam
  Postbus 59091
  1040 KB Amsterdam

Reumafonds
Dutch Arthritis Foundation

Also, financial support for the publication of this thesis by the following institutes / companies is gratefully acknowledged.

- Stichting Anna Fonds | NOREF
  Postbus 1021
  2340 BA Oegstgeest
  The Netherlands

Anna Fonds
Nederlands
Orthopedisch
Research en
Educatie
Fonds

- Biomet Nederland B.V.
  Toermalijnring 600
  3316 LC Dordrecht
  Postbus 3060
  3301 DB Dordrecht
  The Netherlands

BIOMET® One Surgeon. One Patient:

A catalogue record is available from the Eindhoven University of Technology Library
ISBN: 978-90-386-3526-2
Copyright © 2013 by Sayyed Mohsen Hosseini

The knee photo on the cover has been bought by the author from www.fotolia.com. The copyright information is: © Artem Furman - Fotolia.com
Cover design: Sayyed Saeed Hosseini (ssdhosseini@gmail.com)
Print: Wöhrmann Print Service B.V., Zutphen, The Netherlands

All rights reserved. No part of this book may be reproduced, stored in a database or retrieval system, or published, in any form or in any way, electronically, mechanically, by print, photoprint, microfilm or any other means without prior written permission of the author.

Towards a Damage Model for Articular Cartilage

PROEFSCHRIFT

ter verkrijging van de graad van doctor aan de
Technische Universiteit Eindhoven, op gezag van de
rector magnificus prof.dr.ir. C.J. van Duijn, voor een
commissie aangewezen door het College voor
Promoties, in het openbaar te verdedigen
op dinsdag 14 januari 2014 om 16:00 uur

door

Sayyed Mohsen Hosseini

geboren te Gonbadekavoos, Iran

Dit proefschrift is goedgekeurd door de promotoren en de samenstelling van de promotiecommissie is als volgt:

voorzitter:	prof.dr. K. Nicolay
1e promotor:	prof.dr. K. Ito
copromotor:	dr. C.C. van Donkelaar
leden:	prof.dr.ir. N. Verdonschot (Radboud UMC and University of Twente)
	prof.dr. D.L. Bader (University of Southampton)
	prof.dr.ir. M.G.D. Geers
adviseur:	dr.ir. W. Wilson

To my parents and my brothers

for their

unconditional love, endless kindness and never ending encouragement

Contents

Summary III

Chapter 1 1

General Introduction 1

1.1 Articular cartilage (AC) 2

1.2 Articular cartilage mechanics 3

1.3 Articular cartilage damage and osteoarthritis (OA) 4

1.4 A brief background of articular cartilage computational models 6

1.5 Rational and outline of the thesis 8

Chapter 2 11

The Importance of Superficial Collagen Fibrils for the Function of Articular Cartilage 11

2.1 Introduction 12

2.2 Materials and methods 14

2.2.1 Model theory 14

2.2.2 Depth-dependent composition and structure 17

2.2.3 Simulations 18

2.3 Results 19

2.4 Discussion 25

2.5 Appendix 28

Chapter 3 31

Is Collagen Fiber Damage the Cause of Early Softening in Articular Cartilage? .. 31

3.1 Introduction 32

3.2 Materials and methods 34

3.2.1 Sample preparation and setup description 34

3.2.2 Loading protocols and force relaxation parameters (FRPs) 34

3.2.3 Histology and biochemical analyses 36

3.2.4 Statistical analyses 37

3.3 Results 37

3.3.1 FRP variations 37

3.3.2 Biochemical analyses 40

3.3.3 Histology 40

3.4 Discussion 42

Chapter 4 47

How Preconditioning Affects the Measurement of Poro-viscoelastic Mechanical Properties in Biological Tissues 47

4.1 Introduction 48

4.2 Materials and methods 50
4.2.1 Finite element model 50
4.2.2 Loading protocol 54
4.2.3 Simulations 54
4.2.4 Data analysis 55
4.3 Results 55
4.4 Discussion 61
4.5 Conclusion 65
Chapter 5 67
A Numerical Model to Study Mechanically Induced Initiation and Progression of Damage in Articular Cartilage 67
5.1 Introduction 68
5.2 Materials and methods 69
5.2.1 Cartilage mechanics model 69
5.2.2 Damage model 71
5.2.3 Simulations 73
5.3 Results 75
5.4 Discussion 81
5.5 Conclusion 86
Chapter 6 87
General Discussion 87
6.1 Discussion 88
6.2 Recommendations for future studies in the field cartilage damage 93
6.2.1 Follow up of the present work 93
6.2.2 Towards a clinically viable tool 94
6.3 General conclusion 96
References 97
Acknowledgements 111
Curriculum Vitae 113

Summary

Towards a Damage Model for Articular Cartilage

Articular cartilage (AC) in diarthrodial joints functions as a mechanical load bearing surface. It is generally accepted that excessive mechanical loading may initiate cartilage damage and stimulate damage progression. Ultimately, this may result in osteoarthritis (OA), which is a painful and disabling disease. By the age of 55–65, up to 85% of all people will have some degree of OA in one or more joints. Unfortunately, it is still difficult to treat OA, and treatment mostly addresses late stages of the disease. Better therapeutic outcome for aggressive cases of OA could probably be obtained if earlier treatment was possible. To predict disease progression for a particular patient requires more insight in the development of OA over time.

One of the earliest signs of OA clinically seen is roughening of the articular surface, meaning that the superficial tangential zone (STZ) of cartilage has been compromised. It has been proposed that the STZ is essential to the tissue's load-distributing function, and therefore, any kind of structural disintegration to this layer may lead to OA initiation. However, the exact mechanism by which the STZ fulfills this function has not yet been revealed. Using a channel-indentation experiment, it was recently shown that compared to intact tissue, cartilage without STZ behaves slightly stiffer, and deforms significantly different in regions adjacent to mechanically compressed areas. In Chapter 2, this channel indentation experiment was extensively evaluated computationally, showing that the horizontally oriented collagen fibers in an intact STZ result in superior load-bearing properties, because they distribute the applied load over a larger deep zone area compared to cartilage in which the STZ is compromised.

We subsequently aimed to explore even earlier aspects of cartilage damage. Experimental data are sparsely available. Therefore, we performed an experimental study in which we aimed to monitor cartilage softening in response to mechanical overloading (Chapter 3). We hypothesized that excessive mechanical loading would initiate collagen damage, which would result in tissue softening. However, in contrast with our hypothesis, in samples that did show softening, we were unable to detect collagen damage. Thus, our results demonstrate that cartilage softening may be caused by another mechanism that most likely precedes collagen damage.

Although we hypothesized that the long-term changes in mechanical properties of cartilage do result from damage, we could not exclude the effect of time dependent behavior of AC on the results of Chapter 3. As the tissue contains abundant water, surrounded by a matrix containing viscoelastic components, in Chapter 4, we questioned whether part of the observed tissue response in the experiments may be the result of a physiological time dependent complex responses of cartilage. This is also important because it has long been observed that initial loading curves generated by experimental loading of soft biological tissues are substantially different from subsequent loadings. Slow viscoelastic phenomena related to fluid flow or collagen viscoelasticity are initiated during the first loading cycles (preconditioning) and may persist during the actual collection of the data. The results of this investigation showed that not having satisfied the required time for recovery of the tissue in each loading cycle will lead to an inconsistent response from the tissue.

Having understood the effect of time dependent behavior of the AC, in Chapter 5 we developed a damage model which simulates the AC softening behavior. Because in our experiments we observed softening without detecting collagen damage, while collagen damage is known to occur even at relatively early phases during OA, in the model we included damage in both the fibrillar network and the ground substance. This model assumes that when the tensile strain in the fibrillar network or the deviatoric strain in the ground substance exceed certain thresholds, the damage initiates in that particular constituent of the tissue and subsequently the material reduces its stiffness.

Using this model, PG damage was predicted to localize near the surface of cartilage, while collagen damage penetrated deeper into the tissue. These distinct patterns resemble damage locations reported in the literature. Strain patterns in the tissue significantly differed, depending on the nature of damage to the ground substance or the collagen fibers. Finally it was predicted that ground substance softening developed relatively independent of collagen fiber damage, while collagen fiber damage increased with damage to the ground substance.

Briefly, the first steps towards the development of a cartilage damage model have been made in this thesis. Starting from a fibril reinforced poroviscoelastic swelling model, damage was introduced such that it could be attributed to particular aspects of the tissue, i.e. to collagen and ground substance. The potential benefits of this model include possibilities for understanding fundamental aspects of OA initiation and progression. For instance, it allows unraveling the specific effects of collagen damage or ground substance weakening. Such questions are extremely challenging to study experimentally. Future developments could then focus towards more clinical issues, for instance to develop and validate a computational tool that can be used to objectively predict the time course of OA progression in a patient-specific manner.

Chapter 1

General Introduction

1.1 Articular cartilage (AC)

Articular cartilage is a very thin layer of soft tissue which covers the end of bones in the joints in which the two bones meet each other and there is a relative motion between them, such as in the hip, knee, shoulders, fingers and etc. Articular cartilage is a wear resistant and fluid saturated tissue providing smooth sliding at the joints. Moreover, articular cartilage performs as a load distributer and absorber. This functionality is important in the hip and knee joint where many times the body weight is being carried. This important mechanical function makes biomechanical analysis of this tissue an interesting research field.

Mechanical performance of articular cartilage is directly related to its composition and structure (Kempson et al. 1973; Schinagl et al. 1997; Charlebois et al. 2004). From a biomechanical point of view, articular cartilage is a biphasic material consisting of a fluid phase and a solid phase. Water, which consists between 65% to 80% of the tissue volume fraction has a very important role in absorbing the load applied to the cartilage as well as it is partly responsible for the time dependent biomechanical behavior of the tissue. The content of the water in the tissue varies through the depth of the tissue. Higher volume fraction of the water can be seen in the top layer of the tissue and the water content decreases with increasing in the depth of the tissue (Lipshitz et al. 1975; Shapiro et al. 2001; Rieppo et al. 2004, Wilson et al. 2007).

The major biomechanically important solid constituents of the extracellular matrix (ECM) of the articular cartilage are collagen fibers and proteoglycans (PGs). Collagen fibers (mainly collagen type II) constitute 70% of the tissue dry weight, and its concentration is highest in the superficial and deep zones (Buckwalter et al. 1991; Mow and Guo 2002; Rieppo et al. 2004; Rieppo et al. 2005). PGs constitute 20–30% of the dry weight; their concentration is lowest near the surface and highest in the middle zone. The large negatively charged molecules of proteoglycans are actually entrapped in a network of collagen fibers. The interaction between the proteoglycans and collagen fibers produces a fiber-reinforced composite solid matrix (Buckwalter et al. 1991; Hunziker 1992; Wong et al. 1996).

Beside the variation of the collagen content through the depth of the tissue, the orientation of the collagen fibers changes through the depth as well (Benninghoff 1925). This characteristic of the collagen network has a major contribution in the mechanical role of the tissue. The collagen fibers are vertical in the deep zone of the tissue and they bend over in the middle zone to become parallel to the surface in the superficial zone (Benninghoff 1925). The horizontally parallel collagen fibers at the surface try to distribute the applied load over a larger part of the cartilage surface (Glaser and Putz 2002; Thambyah and Broom 2006; Thambyah et al. 2009, Bevill et al. 2010).

Another characteristic of articular cartilage which is important for its mechanical functionality is a phenomenon called Donnan osmotic swelling. In swelling, due to the fixed charge density (FCD) of the negatively charged PGs, the cation concentration inside the tissue is higher than in the surrounding synovial fluid. This creates an osmotic pressure difference that results in absorbing water into the tissue (Maroudas 1968; Maroudas and Bannon 1981; Chen et al. 2001). Fluid flow into the tissue due to Donnan osmotic swelling will expand the tissue. However, collagen fibers in the ECM stabilize the matrix by resisting against swelling pressure. By this mechanism the combination of collagen fibrils and swelling pressure determines the compressive stiffness of AC.

Chondrocytes are the cells in articular cartilage tissue. They are responsible for biosynthesis of collagen fibers and proteoglycans but they are not important for the mechanical function of the tissue. They make up 2% to 5% of the total volume fraction of cartilage tissue (Urban 1994; Wong et al. 1997; Wang et al. 2002).

1.2 Articular cartilage mechanics

The structure and composition of articular cartilage as well as the interaction between the solid and fluid phases define the tissue mechanical behavior (Donzelli et al. 1999; Huang et al. 2001; Huang et al. 2003; Park et al. 2004; Boschetti and Peretti 2008). Because of the fluid flow through a porous media as well as the intrinsic viscoelasticity of the solid phase, articular cartilage behaves as a time dependent material. This means that the response of the tissue to mechanical loads depends on loading rate (Langelier and Buschmann 2003). Like other viscoelastic materials, articular cartilage shows higher stiffness if the load is applied faster. During deformation, the external load is first supported by the (incompressible) fluid fraction, and next gradually transmitted to the solid matrix as the fluid is expelled. Given enough time, the force will equilibrate over time from a peak and sharp response to a plateau (Boschetti and Peretti 2008). The fluid phase does not support external loads at equilibrium so at the time that fluid transport has stopped then all loads are transmitted to the solid part. However, since the time dependency of the material comes from both the solid and the fluid phase, the ultimate internal equilibrium of the tissue depends on the component which takes most time to reach equilibrium (June et al. 2009; Cheng et al. 2009).

In addition to the time dependent mechanical characteristic of articular cartilage, nonlinear tension-compression behavior is another articular cartilage characteristic (Huang et al. 2001; Huang et al. 2003). The solid phase, specifically the interaction between the collagen fiber network and the swelling behavior of the tissue, is responsible for the nonlinear tension-compression behavior. Collagen fibers can only withstand the tensile forces. When swelling occurs, due to the increase in size, the fibers will be placed under tension as they resist the swelling pressure. When subsequently compressive loads are applied, first this residual tension in the collagen fibers decreases. Increasing compressive load will be counterbalanced by the swelling pressure, which means that the fibers will no longer be in tension. By increasing the compressive load from this level, the fibers will buckle and will not withstand loading (Wilson et al. 2004). Only proteoglycans and fluid pressurization will balance the compressive load thereafter (Bank et al. 2000; Kurz et al. 2001; Huang et al. 2005; Rolauffs et al. 2010; Nishimuta and Levenston 2012; Julkunen et al. 2013).

The above mechanisms make it difficult to analyze the response of cartilage to external loads that are different from standard unconfined or confined compression loading. In the regions which are under tension, the fibers are active and reinforce the tissue. In the regions under compression, the fibers will not participate in bearing the load. The tissue response depends on the kind of deformation the tissue receives, and may differ for various locations within the cartilage. The more deformation, the more displacement of water, which means more time needed for equilibrium. In addition, the collagen fibers themselves behave viscoelasticly, adding another time-dependency to the tissue response.

1.3 Articular cartilage damage and osteoarthritis (OA)

The mechanical functionality of articular cartilage in the hip and knee joint is more important than that of the other joints because many times the weight of the whole body is carried by these joints. Different kinds of mechanical loads are being applied to these joints in a normal life style such as static loads (body weight), dynamic loads (walking and running) and impact loads (jumping). As a consequence of overloading and overuse, articular cartilage is known to undergo substantial wear and degeneration potentially leading to mechanical damage and eventually osteoarthritis (OA) (Natoli and Athanasiou 2009).

Osteoarthritis (OA), also known as degenerative arthritis or degenerative joint disease, may be caused by acute or sustained mechanical abnormalities. OA involves degradation of articular cartilage and changes in the synovium and in the subchondral bone (Lorenz and Richter 2006). An increase in thickness, decrease in stiffness (softening), increase in permeability and an increase in water content are the typical characteristics of early degenerated articular cartilage (Lorenz and Richter 2006; Temple et al. 2007; Temple-Wong et al. 2009). These tissue level characteristics of degenerated articular cartilage originate from the changes that happen in molecular structure and content of the tissue. For example, damage to collagen fibers has clear influence on the swelling properties of the tissue. When fibrillation and disintegration occur in the collagen network, the fibers cannot withstand the swelling pressure as stiffly as before. Therefore the tissue will increase in thickness by absorbing more water into the tissue (Bank et al. 2000). Fibrillation and disintegration of the collagen network, which includes torn fibers as well as fibers which are peeled apart from each other, are among the reasons for the weakening of the degenerated articular cartilage. This weakening originates from the fact that the interfibrillar bonding in the collagen network has been partly or completely lost due to mechanical overloading. The loss of interfibrillar bonding due to mechanical overloading may happen inside the cartilage network even while the surface of the tissue is still intact. When this occurs, the collagen network is thought to become softer and less effective in resisting tensile loading (Temple et al. 2007; Shirazi et al. 2008; Siegmund et al. 2008; Temple-Wong et al. 2009). Changes in proteoglycan molecules both in content and structure also characterize the tissue level characteristics of degenerated articular cartilage. Mechanical overloading and/or repetitive loading break the large PG molecules into smaller molecules (Pearle et al 2005; Mankin et al. 2000). In case this is accompanied by fibrillation and disintegration of the superficial collagen network, the small PG molecules will escape the tissue from the gaps opened on the surface of the tissue. This will lead to a decrease in PG content and consequently a decrease in compressive properties of the tissue. It has been shown that the compressive stiffness of articular cartilage decreases by 20% in early stages of tissue degeneration (Temple et al. 2007; Temple-Wong et al. 2009).

Although there is much data on the differences between normal and degenerated cartilage, the importance of softening in the ground substance, damage to the collagen network, and the possible interaction between them for the progression of cartilage damage remains speculative. Yet, such insight may be useful for future development of therapies to treat early OA. Computational models have matured where it has become possible to predict mechanical behavior of articular cartilage, time courses of tissue differentiation and bone adaptation under (patho)physiological conditions (Wilson et al. 2005c; Halloran et al. 2012). Together they capture the essential aspects of progressive OA. However, a model that captures damage development in articular cartilage does not yet exist (Wilson et al. 2005c; Halloran et al. 2012). Such a model is necessary for simulating the (early) development of OA. Thus, the general aim of this thesis is to develop a damage model for articular cartilage, which is able to predict the earlier stages of disease progression, when collagen damage and ground substance softening are observed. We base our cartilage damage progression model on an existing, validated model on cartilage mechanics that incorporates a physiological collagen network and a swelling, non-fibrillar proteoglycan-rich matrix, and we extend this model with descriptions of damage in both the fibrillar and the non-fibrillar matrix.

1.4 A brief background of articular cartilage computational models

Articular cartilage is a biphasic material which means it contains both a solid and a fluid phase. The fluid phase includes water and the solid phase consists of a collagen network and a ground substance, mainly consisting of proteoglycans. Mow et al. (1980) first introduced a biphasic mixture theory in order to study mechanical behavior of cartilage. In a biphasic model the total stress of the tissue will be the sum of the fluid and solid stresses. In most biphasic models the solid matrix has been assumed linear elastic and isotropic. A biphasic model can also take into account the flow dependent viscoelasticity which comes from the flow of water through small pores of the tissue (Torzilli and Mow 1976a; Torzilli and Mow 1976b; Mansour and Mow 1976; McCutchen 1982; Li and Herzog 2004; Macirowski et al. 1994; Soltz and Ateshian 1998; Setton et al. 1993). Though an isotropic biphasic model could explain the mechanical behavior of cartilage in some standard tests, such model is unable to capture experimental results under many other conditions because important features of cartilage are neglected. These include anisotropy caused by the collagen network, strain-dependent permeability, flow-independent viscoelasticity and the swelling behavior of cartilage (Brown and Singerman 1986; Armstrong et al. 1984).

Biphasic models were improved by transversely isotropic models in which part of the compression-tension nonlinearity originating from having different mechanical properties in the direction of compression and perpendicular to that direction was compensated (Garcia et al. 1998; Bursac et al. 1999; Donzelli et al. 1999). However, the transversely isotropic models could not capture the nonlinear behavior of articular cartilage in compression-tension tests that was originating from collagen fibers (Laasanen et al. 2003; Mow et al. 1989; Boschetti and Peretti 2008). The conewise linear elastic model could capture this effect in confined and unconfined compression tests, tensile and torsional tests (Huang et al. 2001; Soltz and Ateshian 2000; Huang et al. 2003).

Fibril reinforced models which have been developed in late nineties (Soulhat et al. 1999) are models that can simulate the role of collagen fibers more effectively. In these models, the solid phase consists of two different components, the collagen fiber network and proteoglycans, respectively referred to as fibrillar and nonfibrillar parts of the ECM. In these models, collagen fibers reinforce the nonfibrillar part by having higher tensile stiffness along their directions. The solid stress is then the sum of the fibrillar and nonfibrillar stresses.

Another improvement of cartilage mechanics models was the inclusion of Donnan osmotic swelling. Effects of electrical charges were included by adding a third and even a fourth phase to the biphasic models (Lai et al. 1991; Lai et al. 2000; Huyghe and Janssen 1997; Huyghe et al. 2009). This allowed to not only simulate the effects of confined and unconfined compression experiments, but also free swelling experiments in baths with various saline concentrations.

Advanced models take both fiber reinforcement and osmotic swelling into account (Wilson et al. 2005b; Wilson et al. 2006a). This combination of is important for the mechanical behavior of cartilage, because the swelling caused by the proteoglycans in the nonfibrillar part tends to expand the tissue, while the collagen fibers resist this expansion and stabilize the shape and volume of the tissue at equilibrium.

Finally, in these fibril reinforced swelling models, the depth dependent composition and structure of the cartilage tissue such as arcade-like orientation of collagen fibers and changing water content and proteoglycan density through the depth of the tissue have also been considered in recent advanced fibril reinforced models (Wilson et al. 2005b; Wilson et al. 2006a). This allows to fully base the mechanical properties of cartilage on the biochemical composition of the tissue, which is a major advantage when a translation from experimental to numerical studies and vice versa are aimed for.

Computational models of cartilage not only have been used to simulate and investigate the mechanical behavior of cartilage, but also they have been employed to predict the damage in cartilage. Since it is believed that mechanical overloading is one of the important causes of damage initiation and progression, the cartilage models have been used to calculate the high stresses and strains occurring in the tissue due to mechanical overloading. Then the regions with these high stresses and strains have been reported as the most potential regions for damage initiation. Wilson et al. (2006b) reported that the location of the maximum shear strain along the collagen fibrils corresponded well with location of collagen damage in relatively thin samples. However, to the best of our knowledge, a computational model which really includes a description of damage development in order to explore damage initiation and progression in cartilage has not yet been developed. Such model would allow for instance to study the interaction between different components of cartilage in damage development.

1.5 Rational and outline of the thesis

The general aim of this thesis is to develop a damage model for articular cartilage, which is able to predict the earlier stages of tissue degeneration. During these earlier stages, collagen damage and ground substance softening have been observed. Therefore, we base our degenerated tissue model on an existing, validated model on cartilage mechanics that incorporates a physiological collagen network and a swelling, non-fibrillar proteoglycan-rich matrix.

One of the earliest signs of clinically observed OA is roughening of the articular surface, meaning that the superficial tangential zone (STZ) of cartilage has been compromised. It has been proposed that the superficial tangential zone (STZ) of articular cartilage is essential to the tissue’s load-distributing function, and therefore, any kind of structural disintegration to this layer may lead to OA initiation. However, the exact mechanism by which the STZ fulfills this function has not yet been revealed. Using a channel-indentation experiment, it was recently shown that compared to intact tissue, cartilage without STZ behaves slightly stiffer, and deforms significantly different in regions adjacent to mechanically compressed areas. In Chapter 2, this channel indentation experiment was extensively evaluated computationally, showing that the horizontally oriented collagen fibers in an intact STZ result in superior load-bearing properties, because they distribute the applied load over a larger deep zone area compared to cartilage in which the STZ is compromised.

After showing that the model is able to capture STZ damage effects, we aimed to investigate even earlier aspects of cartilage damage. Since experimental data are sparsely available, in Chapter 3, we performed an experimental study in which we aimed to monitor cartilage mechanical softening in response to mechanical overloading. Based on earlier work, we hypothesized that excessive mechanical loading would initiate collagen damage, which would result in tissue softening due to early collagen damage. We questioned if a loading magnitude threshold exists above which softening occurs in cartilage. We approached this question by first identify a threshold load above which significant softening would be induced in articular cartilage. The premise was that when we identified initial tissue softening, collagen damage should have reached detectable levels. Therefore, we subsequently evaluated whether collagen damage could be detected by using immunohistochemical probe for denatured collagen.

Although we hypothesized that the long-term changes do result from damage, attributing the results of Chapter 3 directly to damage was dangerous. As the tissue contains abundant water, surrounded by a matrix that contains viscoelastic components, part of the observed tissue response in the experiments may have been the result of a physiological time dependent complex response of cartilage. Therefore, in Chapter 4, we thoroughly explored the time-dependent behavior of cartilage in response to mechanical loading (indentation). This was also important because it has long been observed that initial loading curves generated by experimental loading of soft biological tissues are substantially different from subsequent loadings. Slow viscoelastic phenomena related to fluid flow or collagen viscoelasticity are initiated during the first loading cycles (preconditioning) and may persist during the actual collection of the data.

With insights in the effect of time dependent behavior of the tissue, in Chapter 5, we aimed to capture the very early effects of loading on damage development with a damage model. This model is the beginning of a model that should be able to simulate the development of tissue softening as a consequence of damage to cartilage tissue.

This model works in such a way that as soon as strain levels in either the non-fibrillar or the fibrillar matrix exceed a certain threshold, damage accumulates and subsequently the material stiffness is reduced. Simulations showing how this model predicts damage progression over time are provided in this chapter.

Finally, in Chapter 6, the insights achieved in the present thesis are generally discussed and summarized.

Chapter 2

The Importance of Superficial Collagen Fibrils for the Function of Articular Cartilage

Abstract

It has been proposed that the superficial tangential zone (STZ) of articular cartilage is essential to the tissue's load-distributing function. However, the exact mechanism by which the STZ fulfills this function has not yet been revealed. Using a channel-indentation experiment, it was recently shown that compared to intact tissue, cartilage without STZ behaves slightly stiffer and deforms significantly different in regions adjacent to mechanically compressed areas (Bevill et al. 2010). We aim to further explore the role of STZ in the load-transfer mechanism of AC by thorough biomechanical analysis of these experiments. Using our previously validated fibril-reinforced swelling model of articular cartilage, which accounts for the depth-dependent collagen structure and biochemical composition of articular cartilage, we simulated the above-mentioned channel-indenter compression experiments for both intact and STZ-removed cartilage. First, we show that the composition of the deep zone in cartilage is most effective in carrying cartilage compression, which explains the apparent tissue stiffening after STZ removal. Second, we show that tangential fibrils in the STZ are responsible for transferring compressive loads from directly loaded regions to adjacent tissue. Cartilage with an intact STZ has superior load-bearing properties compared to cartilage in which the STZ is compromised, because the STZ is able to recruit a larger area of deep zone cartilage to carry compressive loads.

This chapter is based on the following publication:

Hosseini SM, Wu Y, Ito K, van Donkelaar CC (2013) The importance of superficial collagen fibrils for the function of articular cartilage. Biomechanics and Modeling in Mechanobiology DOI: 10.1007/s10237-013-0485-0

2.1 Introduction

Articular cartilage covers the ends of bones in diarthrodial joints. It distributes loads in the joint and reduces contact stresses. For cartilage to perform this function, the interplay between its contents of water, proteoglycans (PGs) and collagen is essential. The fluid fraction in cartilage is approximately 80% and decreases from the surface to the deep zone (Shapiro et al. 2001; Rieppo et al. 2004). PGs constitute 20–30% of the dry weight; their concentration is lowest near the surface and highest in the middle zone (Hunziker 1992; Wong et al. 1996). The fixed charge density (FCD), defined as the number of fixed negative charges in the PG network divided by the free water content, is highest in the deep zone (Maroudas and Bannon 1981; Maroudas et al. 1991). Collagen constitutes 70% of the tissue dry weight, and its concentration is highest in the superficial and deep zones (Mow and Guo 2002; Rieppo et al. 2005). Collagen is organized such that it contains densely packed fibrils tangential to the surface in the superficial tangential zone (STZ), and perpendicular fibrils in the deep zone, extending to the subchondral bone (Benninghoff 1925; Wilson et al. 2004). The transitional zone occupies several times the volume of the superficial zone. In this zone, the collagen fibrils have a larger diameter and are more randomly arranged. The chondrocytes appear rounded and are larger and more active than in the superficial zone. PG content is high in this zone, and aggrecan aggregates are larger than in the superficial zone.

This structural organization is thought to be essential for the load-bearing capacity of cartilage. Indeed, the earliest visible changes in arthritic articular cartilage involve roughening and fibrillation of the superficial zone (Buckwalter and Lane 1997; Buckwalter and Mankin 1998), which is accompanied by cartilage softening (Thibault et al. 2002; McCormack and Mansour 1998; Kleemann et al. 2005). These processes are thought to represent the onset of further structural and mechanical deterioration, ultimately leading to full cartilage degeneration and severe osteoarthritis (Boschetti and Peretti 2008). Therefore, the existence of an intact STZ appears to be essential to the functioning and maintenance of cartilage.

Although cartilage softening is observed clinically when the STZ is compromised, the literature shows that the Young's modulus and the compressive modulus increase with distance from the articular surface in intact cartilage (Schinagl et al. 1996; Schinagl et al. 1997; Shirazi and Shirazi-Adl 2008; Wang et al. 2003; Chahine et al. 2004). The experiments by Shinagl et al. (1997) were further evaluated computationally, showing that this depth-dependency originates from pre-stress in the radial collagen fibrils (Wilson et al. 2007), as earlier suggested by Chahine et al. (2004) and in agreement with Kempson et al. (1973) who showed that tensile properties correlate with collagen content in the STZ, but not with proteoglycan content. In agreement with these data, Bevill et al. (2010) showed that cartilage appeared stiffer after removal of the STZ. However, the question remains how this relates to the contrasting clinical findings that cartilage behaves softer when the STZ is compromised (Buckwalter and Lane 1997; Buckwalter and Mankin 1998; Thibault et al. 2002; McCormack and Mansour 1998; Kleemann et al. 2005).

To explore the mechanical effect of the STZ in more detail, Bevill et al. (2010) and Thambyah et al. (2009) loaded intact cartilage and cartilage from which the STZ was removed, with a channel indenter. With this setup, they showed that the collagen network deforms significantly different, depending on the integrity of the STZ. This confirms previous data by Glaser and Putz (2002), who analyzed the influence of removal of the STZ during compressive loading with another indentation setup. They concluded that removal of the STZ would impair distribution of a locally applied compressive load sideways. The biomechanical mechanism behind this load transfer is, however, not completely understood. This study aims to further explore the mechanism of load transfer by the STZ in articular cartilage, by biomechanical evaluation of the experimental work of Bevill et al. (2010). For that, a previously validated fibril-reinforced poroviscoelastic swelling model of articular cartilage is employed which accounts for the depth-dependent collagen structure and biochemical composition of articular cartilage (Wilson et al. 2006a; Wilson et al. 2007). Specifically, compression tests in healthy and STZ-removed cartilage are simulated, and results are compared with experimental observations of deformation and collagen structural responses. The stresses and strains in the STZ and inside the directly compressed and adjacent cartilage provide insight into the biomechanical of load transfer in articular cartilage. The results explain why removal of the STZ results in stiffening of the cartilage tissue, yet leads to apparent softening of the cartilage under physiological loading conditions, with clinical implications.

2.2 Materials and methods

2.2.1 Model theory

In the fibril-reinforced poroviscoelastic swelling theory articular cartilage is assumed as biphasic, consisting of a solid and a fluid phase. In the standard biphasic theory the total stress is given by (Wilson et al. 2007; Mow et al. 1980):

$$\boldsymbol{\sigma}_{tot} = -p\mathbf{I} + \boldsymbol{\sigma}_s \tag{1}$$

where p is the hydrostatic pressure, $\boldsymbol{\sigma}_s$ the effective solid stress and $\mathbf{I}$ the unit tensor. Typically, the effective stress depends on strain only. Hence, the relative fluid and solid volume fractions do not influence the total stress in the tissue. However, in the biphasic model not only the amount of deformation but also the amount of solid has an influence on the stress contribution of the solid matrix. Therefore, if the dependency of the solid fraction on the effective stress is included then the total stress can be written as:

$$\boldsymbol{\sigma}_{tot} = -p\mathbf{I} + n_s\boldsymbol{\sigma}_{rs} = -p\mathbf{I} + \frac{n_{s,0}}{J}\boldsymbol{\sigma}_{rs} = -p\mathbf{I} + n_{s,0}\boldsymbol{\sigma}_{rs,J}(J) \tag{2}$$

where $n_{s,0}$ and n_s are the initial and current solid volume fraction, and J the volumetric deformation. Note that the dependency of the solid fraction on the volumetric deformation is included in the function for the real solid stress ($\boldsymbol{\sigma}_{rs,J}$).

In this computational model, the effective solid stress in articular cartilage consists of three terms: the stress in the non-fibrillar part of the extracellular matrix (ECM) representing proteoglycan molecules (PG), the tensile stress in the fibrillar part of the ECM representing the collagen network and the swelling pressure due to negatively charged PGs.

$$\boldsymbol{\sigma}_{tot} = -p\mathbf{I} + n_{s,0}\left(\left(1 - \sum_{i=1}^{totf}\rho_c^i\right)\boldsymbol{\sigma}_{nf} + \sum_{i=1}^{totf}\rho_c^i\boldsymbol{\sigma}_f^i\right) - \Delta\pi\mathbf{I} \tag{3}$$

where $\boldsymbol{\sigma}_{nf}$ is the Cauchy stress in the non-fibrillar matrix, $\boldsymbol{\sigma}^i_f$ is the fibril Cauchy stress in the i^{th} fibril with respect to the global coordinate system, ρ^i_c is the volume fraction of the collagen fibrils in the i^{th} direction with respect to the total volume of the solid matrix and $\Delta\pi$ is the osmotic pressure gradient. The non-fibrillar and fibrillar stress terms are defined per unit area of the non-fibrillar and fibrillar areas respectively.

2.2.1.1 Non-fibrillar part

Although the solid itself is incompressible, because of its porous structure the entire solid matrix is compressible. The amount of compressibility depends on the water fraction, i.e. with a water fraction of zero or one, the matrix is fully incompressible or fully compressible, respectively. To include this in the model, the following expression for the Poisson's ratio is proposed.

$$\nu_m = 0.5 n_s = 0.5 \frac{n_{s,0}}{J} \tag{4}$$

Note that as the total solid is assumed to be incompressible, the relative fractions of the fibrillar and non-fibrillar matrix remain constant. By substituting this formula into the equations of bulk and shear moduli and implementing them into the energy function of the compressible neo-Hookean model (Wilson et al. 2007), the total stress of the non-fibrillar matrix can be calculated by the following formula, which depends on the amount of deformation, the amount of solid and shear modulus G_m (Wilson et al. 2006a; Wilson et al. 2007):

$$\boldsymbol{\sigma}_{nf} = -\frac{1}{6}\frac{\ln(J)}{J} G_m \mathbf{I}\left[-1 + \frac{3(J+n_{s,0})}{(-J+n_{s,0})} + \frac{3\ln(J)Jn_{s,0}}{(-J+n_{s,0})^2}\right] + \frac{G_m}{J}(\mathbf{F}\cdot\mathbf{F}^T - J^{2/3}\mathbf{I}) \tag{5}$$

where $\boldsymbol{\sigma}_{nf}$ is the Cauchy stress of the non-fibrillar matrix and $\mathbf{F}$ is the deformation gradient tensor.

2.2.1.2 Fibrillar part

The fibril Cauchy stress tensor is as follows:

$$\boldsymbol{\sigma}_f = \frac{\lambda}{J} P_f \vec{e}_f \vec{e}_f \tag{6}$$

where λ is the elongation of the fibril, P_f is the first Piola-Kirchhoff stress, and e_f is the current fibril direction. Note that this total Cauchy stress of the fibrils is expressed as a function of the deformed surface that a fibril works on (Wilson et al. 2006a).

Because the loading procedure of the reference experiments (Bevill et al. 2010) occurred over a very long duration (3 hours), the transient behavior of the tissue (viscoelasticity) for both fibrillar and non-fibrillar part were neglected and only the equilibrium state of the tissue was of interest. However, the equilibrium stiffness of the collagen fibrils was considered strain-dependent (Charlebois et al. 2004). Therefore, the collagen fibrils were represented by:

$$\begin{aligned} P_f &= E(e^{k\varepsilon_f} - 1) && \text{for} \quad \varepsilon_f > 0 \\ P_f &= 0 && \text{for} \quad \varepsilon_f \leq 0 \end{aligned} \qquad (7)$$

where $\mathcal{E}_f$ is the logarithmic fibril strain ($\mathcal{E}_f = \log(\lambda)$), and E (MPa) and k (dimensionless) are positive material constants. It was also assumed that fibrils do not withstand load when they receive compressive strain ($\mathcal{E}_f \leq 0$).

2.2.1.3 Osmotic swelling

Owing to the fixed charges of the PGs, the cation concentration inside the tissue is higher than in the surrounding synovial fluid. This excess of ion particles within the matrix creates a pressure gradient referred to as "Donnan osmotic pressure gradient", which is a driving force for fluid flow. However, part of the water inside cartilagenous tissues is absorbed by the collagen network, and PGs are excluded from this intra-fibrillar space because of their large size. This means that their effective concentrations are much higher in the extra-fibrillar space than if they were distributed uniformly throughout the entire matrix. When the distinction between intra- and extra-fibrillar water is made the osmotic pressure gradient is given as follows (Wilson et al. 2005b; Wilson et al. 2006a; Wilson et al. 2007):

$$\Delta\pi = \phi_{int} RT \sqrt{c_{F,exf}^2 + 4\frac{\gamma_{ext}^{\pm\,2}}{\gamma_{int}^{\pm\,2}} c_{ext}^2} - 2\phi_{ext} RTc_{ext} \qquad (8)$$

where $\phi\alpha$ (α = internal, external) is the osmotic coefficient, $c_{F,exf}$ is the effective fixed charge density (FCD), $\gamma^{\pm}_{\alpha}$ is the activity coefficients, and c_{ext} is the external salt concentration (Huyghe et al. 2003). R and T represent the gas constant (8.3145 J/molK) and absolute temperature (293 K) respectively. The approach to use this equation in a biphasic swelling formulation was extensively evaluated for applicability in cartilage (Wilson et al. 2005a).

2.2.1.4 Permeability

The present study only addressed the deformation of the tissue at equilibrium. At equilibrium, fluid flow does not occur and therefore the value for permeability was not important. It was set to a constant value of 1×10^{-12} m^4/Ns for the whole tissue (Wilson et al. 2007).

2.2.2 Depth-dependent composition and structure

The fluid fraction, collagen fraction and fixed charge density distributions as a function of the normalized depth *z** (0 at the articular surface and 1 at the cartilage bone interface) were taken the same as in Wilson et al. (2006a) which is below (Figure 1).

$$n_f = -0.2z^* + 0.9 \tag{9}$$

$$\rho_{c,tot} = 1.4{z^*}^2 - 1.1z^* + 0.59 \tag{10}$$

$$c_F = -0.1{z^*}^2 + 0.24z^* + 0.035 \tag{11}$$

where n_f is the total fluid volume fraction, $\rho_{c,tot}$ is the total collagen volume fraction per total solid volume, and c_F the fixed charge density in mEq/ml water.

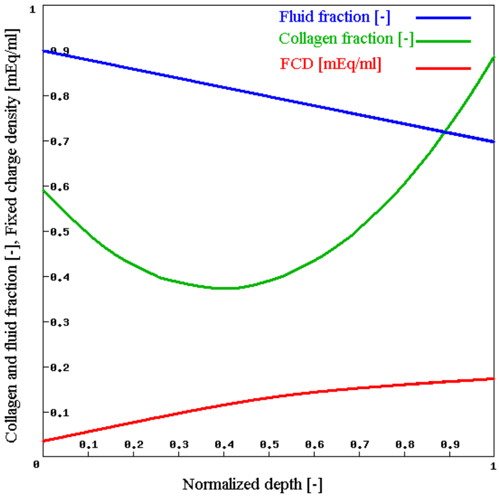

***Figure 1** Depth-dependent contents of articular cartilage.*

The 3D-collagen network was captured as a combination of two fibril components (Wilson et al. 2006a; Wilson et al. 2007): one representing the dominant primary fibril orientation in cartilage (Benninghoff 1925), and a secondary less dense component, representing a quasi-isotropic fibril network as observed by scanning electron microscopy (Clark 1985; Clark 1991). Primary fibril directions extended perpendicular from the subchondral bone and then bended to align with the articular surface (Figure 2). To enable bending into medial, lateral, posterior and anterior directions, 4 primary fibril directions were accounted for. To include fibrils under 45 degree angles in 3D, in total 13 secondary fibril are included (Wilson et al. 2004). The density of collagen fibrils in primary and secondary directions are defined as follows:

$$\begin{aligned} \rho_c &= \rho_{c,tot} \frac{C}{4C+13} \quad \text{primary directions} \\ \rho_c &= \rho_{c,tot} \frac{1}{4C+13} \quad \text{secondary directions} \end{aligned} \tag{12}$$

where *C* is a positive constant equal to 3.009 (Wilson et al. 2005a; Wilson et al. 2007).

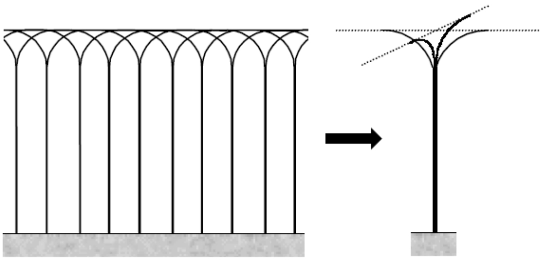

***Figure 2** Orientation of the primary fibril direction as a function of depth. **Left** Cartoon of the arcade model of the fibrillar network. **Right** Orientation of four primary collagen fibril directions as implemented in the FEA model.*

2.2.3 Simulations

In the experiments of Bevill et al. (2010), osteochondral blocks (14×14 mm) were equilibrated in 0.15 M saline, before a nominal compressive stress of 4.5 MPa was applied with a channel indenter consisting of two rectangular platens (8×3 mm) separated by a 1 mm channel relief zone (Figure 3a) for three hours. While compressed, the tissue was formalin-fixed and processed for histology. Tissue shape and structure was examined by DIC microscopy to enhance the contrast in unstained samples. This was done for intact cartilage (average height 1.74 mm) as well as for samples from which the STZ had been removed (average height 1.07 mm) (Figure 3b). From the DIC images, strains in the tissue were computed for both the directly compressed region (*dc*) and the channel relief zone (*cr*) as:

$$\varepsilon_\alpha = \frac{h_\alpha - h_0}{h_0} \quad with\ \alpha\ \in \{dc, cr\} \tag{13}$$

where h_0 is the height before compression, determined from the periphery of the sample, and h_{dc} and h_{cr} the height of the respective zones during loading (Figure 3a).

This experiment was simulated using the above model in ABAQUS 6.9 (Abaqus Inc., Providence, RI). Cartilage height was 1.74 mm, and sample size was reduced from 14 to 0.5 mm in the *x*-direction, and plane strain conditions were prescribed at the cut surfaces. The mesh contained 2464 eight-node brick elements, refined near the corners of the indenter. The STZ-removed samples were modeled by simply using the lower 1.07 mm of the entire model (Figure 3b). Consequently, the main differences between intact and STZ-removed samples were sample height, the absence of tangential collagen fibrils, and a difference in tissue composition where the STZ-removed samples contain the contents as visualized in Figure 1 between $z^* = 0.4$ and 1.0.

As a starting point, the model parameters that were previously determined for simulating healthy cartilage with this model were used (Wilson et al. 2006a). However, these parameters were determined from deformation experiments up to 20% strain, while in the present experiments strains reached over 50% strain. At these high compressive strains, collagen contributes to the compressive stiffness, making the tissues behave significantly stiffer (Römgens et al. 2013). This effect was compensated for by increasing the stiffness of the non-fibrillar matrix (G_m), using the strain under the indenters and the bulge height in the channel as reference. The final set of material parameters was $G_m = 12.18$ MPa, $E = 45$ MPa and $k = 56$.

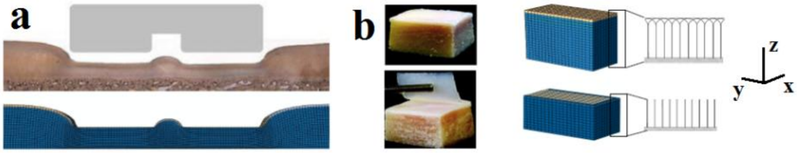

Figure 3 a *Channel indenter: cartilage-on-bone* ***(top)*** *(Bevill et al. 2010), model simulation* ***(bottom) b*** *Intact-1.74 mm thick* ***(top)****, STZ-removed-1.07 mm thick* ***(bottom)*** *adapted from Bevill et al. (2010).*

2.3 Results

The tissue is severely compressed under the indenter, while the height of the cartilage in the channel region is less reduced and therefore appears as a bulge. This general appearance of the deformation was similar for the simulations (Figure 3a). After removing the STZ, the tissue was found to be 1.06-fold stiffer in the directly compressed region. This effect was also matched in the simulation (1.09-fold increase) (Table 1). Furthermore, it was experimentally shown that the strain in the bulge was decreased after removal of the STZ from 0.71 to 0.23. This effect was also apparent from the simulations, although quantitatively the effect of removing the STZ is more prominent in the experiment than in the simulation (0.68 to 0.39) (Table 1).

Table 1 *Comparison between observed (Bevill et al. 2010) and computed strains in the bulged and directly compressed regions. All strains are calculated relative to the original undeformed height (Eq. 13).*

	Experimental Strain (%)		Simulation Strain (%)		Bulge/indenter	
	Indenter	Bulge	Indenter	Bulge	Experiment	Simulation
Intact	56	40	50	34	0.71	0.68
STZ-removed	53	12	46	18	0.23	0.39
Intact/STZ-removed	1.06	3.33	1.09	1.89	3.09	1.74

To evaluate tissue stiffening after STZ removal, additional simulations were performed. First, structure and composition of the STZ-removed sample were used, while sample height was kept identical to the intact sample. Second, the height of the intact sample was changed to that of the STZ-removed sample, while the composition was taken identical to the intact sample. In addition, the effect of tissue composition was explored by applying homogeneous fixed charge density and/or non-fibrillar matrix stiffness over the construct height in simulations with samples of the different heights. With similar heights and different compositions, the ratio of stiffness between intact and STZ-removed samples increased from 1.09 to 1.13. With homogeneous FCD and homogeneous non-fibrillar stiffness, STZ-removal did not result in stiffening of the tissue (stiffness ratio reversed from 1.09 to 0.96), independent of sample height.

For evaluating the biomechanics involved in the compression of the tissue in the channel region such that a bulge develops, first the stress distribution in the intact sample is considered. Compressive stress in the non-fibrillar matrix was localized in the superficial zone of the directly loaded region, but stress was lower and rather homogeneous in the bulge area (Figure 4a). Shear stress was localized superficially near the corners of the indenter (Figure 4b). High tensile stresses developed in the superficial tangential collagen fibrils, with highest values located in the channel region (Figure 4c). Maximum principal stresses were highest in the superficial zone, gradually declining in the transitional area (Figure 4d).

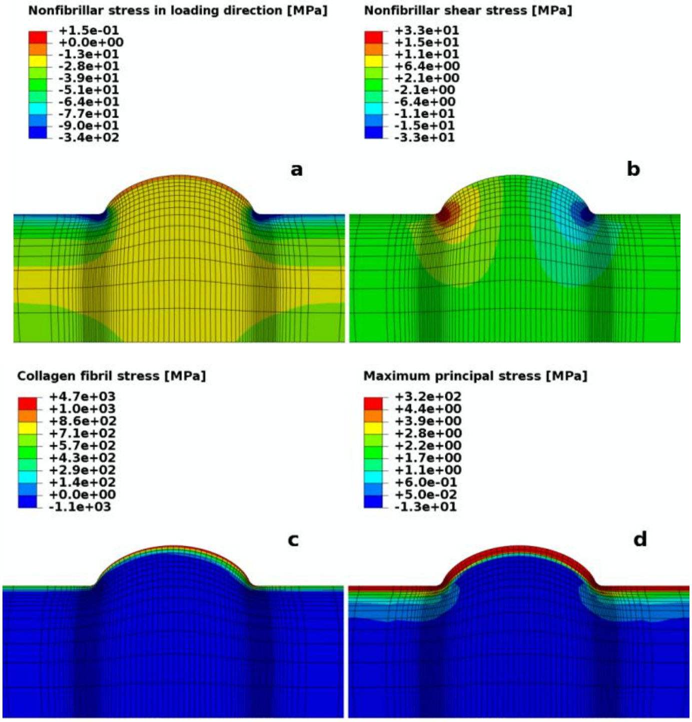

Figure 4 ***a*** *Stress in the direction of loading (vertical in the image).* ***b*** *Shear stress.* ***c*** *Stress in the collagen fibrils that bend from the deep zone toward the left when they approach the surface. Fibrils that bend the other direction show mirrored stress distribution.* ***d*** *Maximal principal stress in the cartilage.*

After removing the STZ, the tissue bulge in the channel region is higher than the tissue bulge in intact samples. (Table 1), and the total stress in the fibrils and the non-fibrillar matrix remains low (Figure 5).

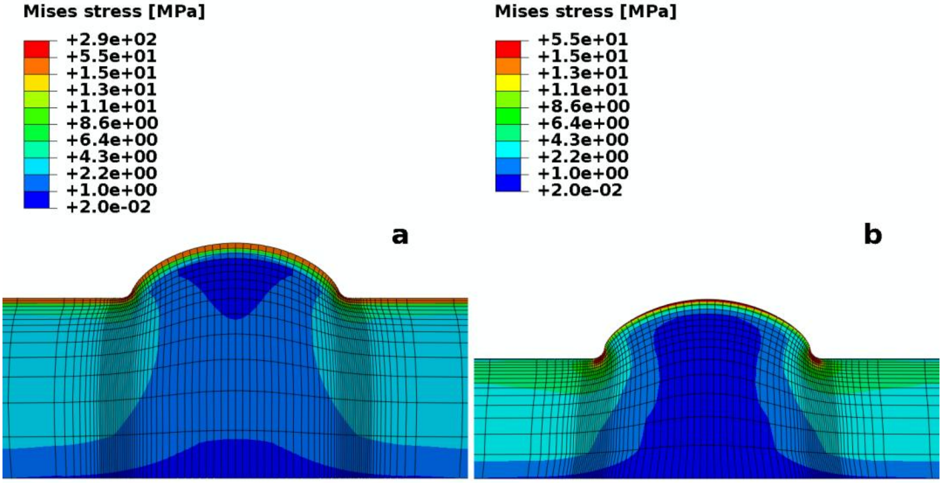
Mises stress [MPa]
+2.9e+02
+5.5e+01
+1.5e+01
+1.3e+01
+1.1e+01
+8.6e+00
+6.4e+00
+4.3e+00
+2.2e+00
+1.0e+00
+2.0e-02
a
Mises stress [MPa]
+5.5e+01
+1.5e+01
+1.3e+01
+1.1e+01
+8.6e+00
+6.4e+00
+4.3e+00
+2.2e+00
+1.0e+00
+2.0e-02
b

Figure 5** von Mises stress in intact cartilage **(a)** in STZ-removed cartilage **(b).

In the directly indented regions, both with and without superficial zone, fluid loss reaches almost 18-20%. The bulging part of the intact cartilage lost approximately 10% of its water content, while the bulge in the STZ-removed tissue remained well hydrated with fluid loss below 5% (Figure 6a,b). Consequently, the swelling pressure, which is a function of the free water in the tissue, increased more in the channel region of the intact than the STZ-removed tissue cartilage (Figure 6c,d).

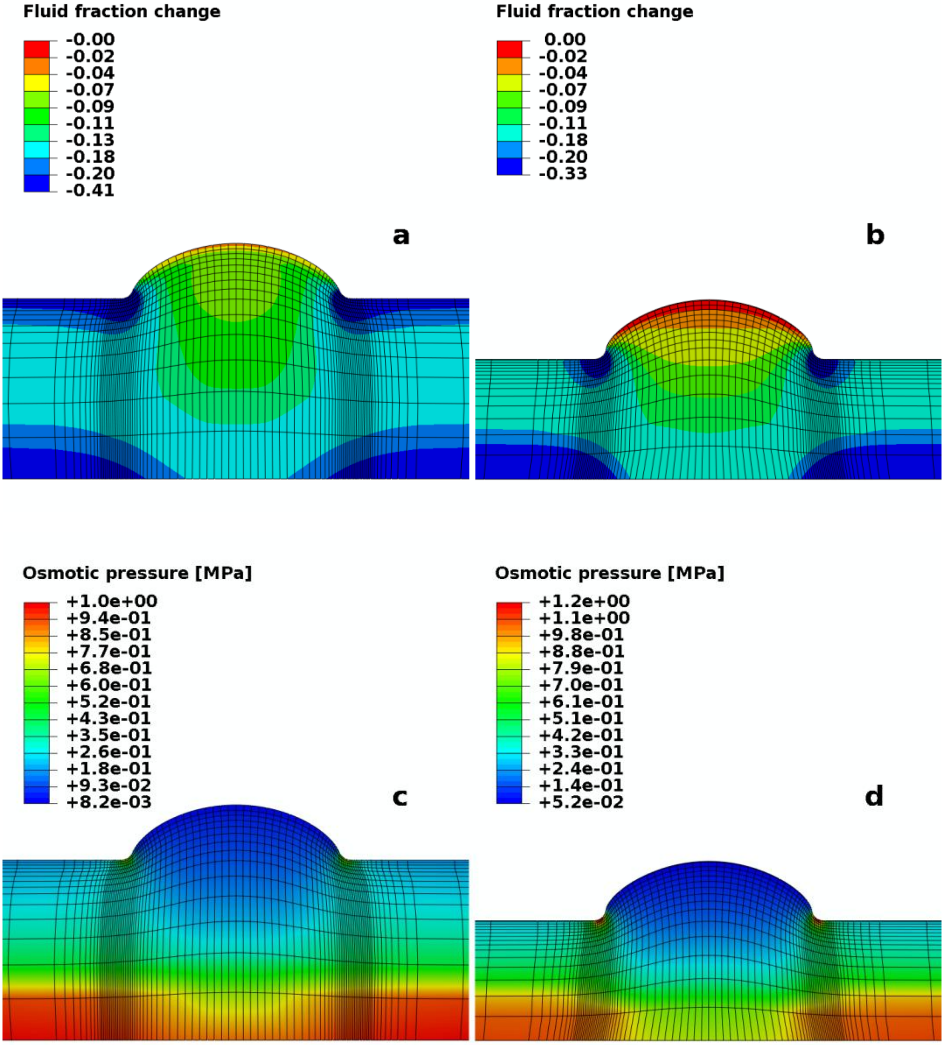

Figure 6 *Fluid fraction change is negative under all conditions, showing significant compression in the indented as well as in the channel region. Fluid expression in the bulge area as a consequence of the loading is more excessive in intact cartilage* ***(a)*** *than in STZ-removed cartilage* ***(b)****. Swelling pressure for intact* ***(c)*** *and the STZ-removed samples* ***(d)*** *follow the fluid fraction decrease.*

The final evaluations involved a comparison between simulation parameters and structural phenomena that were observed experimentally (Bevill et al. 2010). First, intact and STZ-removed cartilage differed in appearance of bright and dark areas using DIC microscopy. The intact cartilage showed a small dark area covering the surface of the bulge and a larger triangular region in the deeper areas, while in the STZ-removed cartilage the dark color extended throughout the bulge (arrows in Figure 7c,d). The peculiar shapes of these dark areas in both samples coincided with the distribution of minimal principal strains in the simulations (Figure 7a,b).

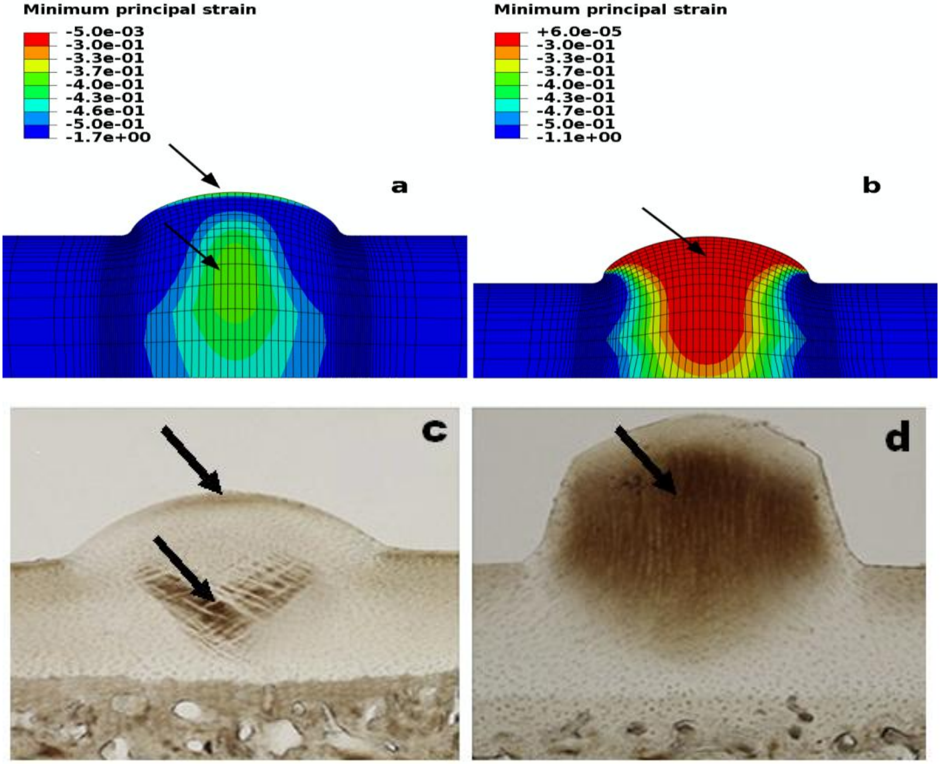
Minimum principal strain
-5.0e-03
-3.0e-01
-3.3e-01
-3.7e-01
-4.0e-01
-4.3e-01
-4.6e-01
-5.0e-01
-1.7e+00
a
Minimum principal strain
+6.0e-05
-3.0e-01
-3.3e-01
-3.7e-01
-4.0e-01
-4.3e-01
-4.7e-01
-5.0e-01
-1.1e+00
b
c
d

Figure 7 *Minimum principal strain for intact cartilage* ***(a)*** *and STZ-removed cartilage* ***(b)*** *compared with DIC microscopy images of intact cartilage* ***(c)*** *and STZ-removed cartilage* ***(d)****. Arrows indicate areas with comparable characteristics, i.e. darker areas in DIC microscopy and least minimal principal strains (Bottom images are adapted from Bevill et al. (2010)).*

The second observation involved a sharp transition in color of the DIC images in the lateral areas of the bulge, well below the surface of the tissue (Figure 8b). This sharp band co-localized with the maximal principal strain (Figure 8a), where the sharp transition was in the zone where fibrils were bent over and continue approximately tangential to the surface.

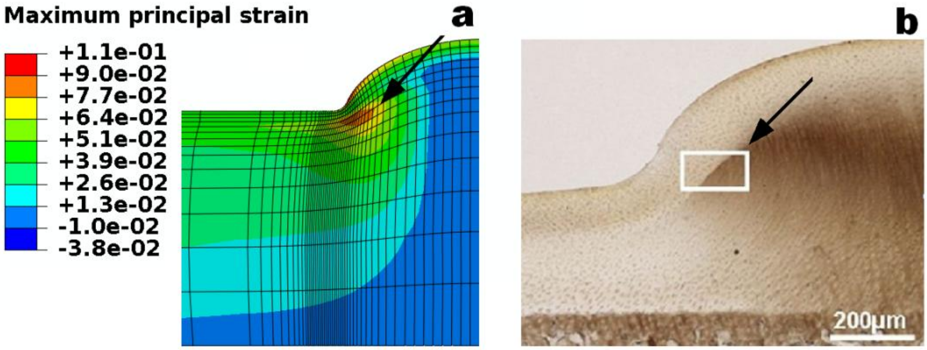

***Figure 8** Maximum principal strain **(a)** compared with DIC microscopy in intact cartilage **(b)**.*

2.4 Discussion

A thorough comparison between experiments of Bevill et al. (2010) and simulations using our composition-based FE model of articular cartilage, explains two phenomena related to cartilage mechanics and function. First, the tangential collagen fibrils in the STZ of cartilage are fundamental to the transfer of stresses between directly loaded regions and adjacent regions that are not directly loaded (Figure 4, Figure 5). Hence, the STZ recruits a larger cartilage surface for loadbearing. Second, as a consequence of its depth-dependent composition, and because the superficial zone is the weakest zone under compression, the cartilage average tissue stiffness increases after removal of the STZ (Table 1). Together, this means that the deep zone of cartilage is the most effective zone to resist compression, while the STZ ensures that externally applied load is carried not only by the deep zone tissue that is directly under the loaded surface, but also by adjacent deep zone tissue. Removal of the STZ abolishes this surface-area recruiting function. Consequently, after removal of the STZ, the tissue may behave stiffer in directly compressed regions, but load applied to the cartilage is carried by a smaller area than in intact tissue.

Our analyses also allows for a more detailed interpretation of the original data of Bevill et al. (2010). Based on appearance of the tissue, they identified so-called shear-bands in the channeled area, underneath the tissue surface. Our analyses however show that the largest shear strains occur at a distinct location, at the surface of the tissue close to the corners of the channel indenter (Figure 4b). The location of ‘shear bands’ is best represented by the triangular area where neither compressive nor tensile stresses are excessive (Figure 7). How these mechanical variables would translate into the structural observation of ‘shear bands’ under DIC remains unexplained. Similarly, the peculiar, sharp transition between dark and bright colors that was observed in the tissue under the edge of the indenter (Figure 8) correlates nicely with high principal strains. Apparently, both low and high principal strains affect the appearance of DIC images, but a direct interpretation of the structural phenomena is difficult.

Simulations provide additional insight in the importance of hydrostatic and osmotic pressures and fluid flows for the bulge to develop, as proposed by Bevill et al. (2010). In agreement with their speculations, fluid flows from the compressed region into the bulge from where it leaves the tissue. This causes temporal effects on bulge shape. The experimental data, however, involve equilibrium conditions during which fluid flow is absent by definition. Under these prevailing equilibrium conditions, hydrostatic pressure is zero. Thus, the remaining factor pressurizing the fluid is the internal osmotic pressure. Indeed, the bulge shape is larger when total swelling pressure is increased, as nicely shown experimentally in a follow-up study in which the tissue is osmotically challenged (Bevill et al. 2010). Under given external osmotic conditions, however, our analyses show that the osmotic pressure is lower in the bulge than in the directly compressed region (Figure 6c,d). The rationale is that the number of fixed charges per fluid volume increases when water is expelled from the tissue. Consequently, we postulate that the tissue bulge does not appear because of excessive osmotic pressure in the channel. Rather than being pushed upward, the bulge in the channel region is less compressed than the directly loaded region. The channeled region is subsequently compressed by the effective stress in the tangential collagen fibrils and the magnitude of this effective stress depends on the integrity of the superficial collagen (Figure 6). In the absence of an intact superficial layer, the compressive load is not transferred to the channeled area. Therefore, the tissue is less deformed and the bulge remains more pronounced.

To obtain deformations that are consistent with those measured in the experiments by Bevill et al. (2010), the compressive stiffness of the matrix is increased to 12 MPa. This high compressive stiffness cannot be explained by variability in composition or structure between sample-origin or species. We postulate that the reason for the excessive deformation is that the generally used values for cartilage stiffness underestimate the tissue stiffness at high strains. Previously, physiological properties for the poroviscoelastic fiber-reinforced swelling model were obtained from simultaneous fits to distinct sets of experimental data (Wilson et al. 2006a). The cartilage sample used in these fits has the same representative composition (Shapiro et al. 2001; Rieppo et al. 2004; Maroudas and Bannon 1981; Lipshitz et al. 1975; Chen et al. 2001) and collagen structure (Benninghoff 1925; Clark 1985; Clark 1991) as the one used in the present study. The experimental data used in the fitting procedure include osmotic swelling, and up to 20% confined and unconfined compression and indentation. Variations in this constitution and fibril structure between joints or species affects the macroscopic mechanical behavior of the tissue, and may be adjusted for specimen-specific modeling, while using the original material parameters for these constituents. However, these are valid up to the 20% strain range for which they are originally fitted. In the present study, the strains exceed 50% (Table 1). It has recently been shown that in cartilaginous tissues, at strain levels above 35% the collagen contributes significantly and strongly non-linear to the compressive stiffness of the tissue (Römgens et al. 2013). To accommodate for this effect, the bulk modulus has been increased in the present study to a value that is excessive for physiological loading conditions, but is appropriate for the high compressions used in the experiments by Bevill et al. (2010). Also, to evaluate the applicability of the model to study these high strains, a tensile test has been performed in which the strain behavior was evaluated (Appendix A).

Both the magnitude of compression and the channel indentation are not physiological loading conditions, but were deliberately chosen by Bevill et al. (2010) to study the importance of the superficial zone without adverse boundary effects due to sample preparation and aiming to exaggerate findings by Glazer and Putz (2002). Indeed, the channel indenter experiment reveals new aspects of tissue deformation before and after removal of the STZ. However, due to the complexity of the experimental conditions it is difficult to interpret these findings. The present study provides more insights in these aspects by simulating the experiment using a numerical model.

In addition to providing more insight in the experimental data by Bevill et al. (2010), two general conclusions are derived from the present numerical evaluation. First, we explain that cartilage without STZ appears stiffer than intact cartilage, because of the depth-dependent composition of cartilage. This confirms literature showing that the compressive modulus of the STZ is lower than that of the middle and deep zones (Schinagl et al. 1997; Shirazi and Shirazi-Adl 2008; Schinagl et al. 1996; Wang et al. 2003; Chahine et al. 2004; Wilson et al. 2007; Kempson et al. 1973). The present study shows that this effect prevails even though the integrity of the collagen network is lost. Second, we reveal the mechanism by which superficial fibrils transfer load from loaded to non-loaded regions, thus recruiting a larger cartilage surface for carrying mechanical loads. In the absence of these fibrils, this load-sharing effect is significantly impaired.

The latter insight has clinical implications. First, it explains why mild fibrillation is a strong indicator for progressive cartilage damage in osteoarthritis. Stress transfer within the STZ is essential for load distribution over a larger cartilage surface, and therefore also for reducing peak stresses that may be transferred between bones. This load transfer is prohibited when the STZ is removed, and also when the tangential fibrils become discontinuous, i.e. when the tissue is fibrillated. Second, as a consequence of the mechanical importance of an intact STZ, we propose that surgical debridement of the cartilage surface during arthroscopy, even when the surface is mildly fibrillated, should be done with care. Removal of any intact STZ is detrimental to load-sharing between directly loaded and adjacent cartilage, and therefore increases peak stresses in cartilage, putting it at risk for further damage. Third, these findings suggest that an implant to replace diseased cartilage should preferably include an STZ-like zone. This agrees with studies showing that the reproduction of an appropriate STZ would likely stimulate the integration of tissue engineered implants with the surrounding host cartilage (Khoshgoftar et al. 2013).

2.5 Appendix

In order to verify model behavior under the large range conditions used in the present study, a large deformation tension and compression test has been simulated for a 3D cylinder with 2 mm diameter and 1 mm height. The material is identical to the material used in the present study. Top and bottom of the cylinder were fixed in the plane perpendicular to the loading direction, and nodes were allowed to move freely within that plane.

After an initial swelling phase, the axial and radial strains in tension (140% strain) and compression (50% strain) have been plotted against each other (Figure 9). The result of deformation shows that the model does not collapse, with realistic strain behavior in both tension and compression, with more loss of volume (fluid) in compression than in tension (Figure 9). This verifies that the cartilage model used in the present work can be applied to the large strain range in the present study.

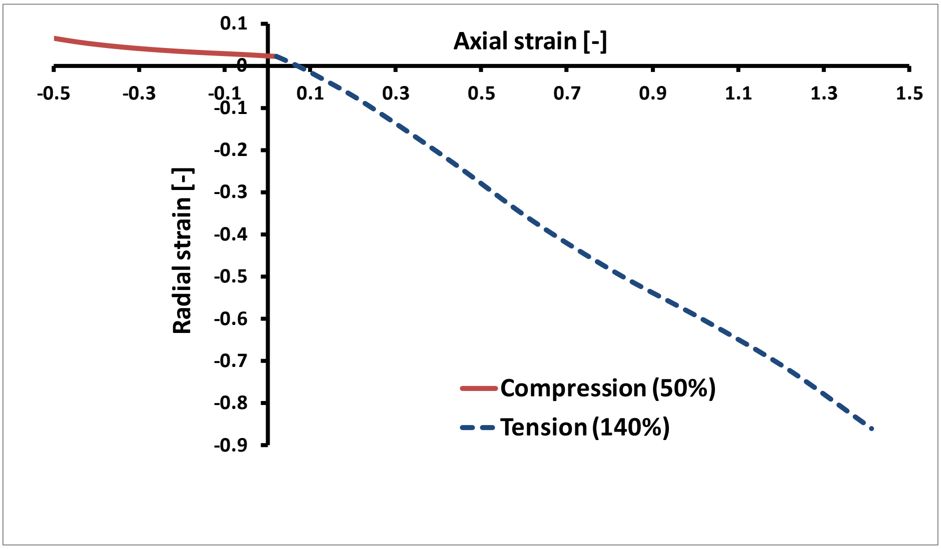

Figure 9 *Axial strain against radial strain in the whole range of deformation for a swollen disk of diameter 2 mm and height 1 mm. The axial and radial strains start at positive values, because prior to the compression and tension testing, the tissue is allowed to swell to equilibrium.*

CHAPTER 2

Chapter 3

Is Collagen Fiber Damage the Cause of Early Softening in Articular Cartilage?

Abstract

Because collagen damage and cartilage softening have not yet been determined simultaneously in one study for the very early onset of osteoarthritis (OA), it remains questionable whether they are associated. The aim of the present chapter is therefore to evaluate whether indeed, initial collagen damage can be found when tissue softening occurs as a result of excessive mechanical loading. To investigate this aim, a series of specific indentation loading protocols were designed to induce and monitor cartilage softening in osteochondral explants of bovine carpometacarpal joints. The experiment contained one control group (*n* = 6) in which no damage was induced and four experimental groups in which samples received either a constant load of 3 (*n* = 5), 6 (*n* = 5) or 15 N (*n* = 6), or an increasing load (*n* = 7) from 2 to 13 N in 11 steps. Moreover, to determine mechanically induced collagen damage, Col2-3/4M (cumulative collagen damage) and Col2-3/4C_{short} (only enzymatic damage) staining were compared. The normalized peak and equilibrium reaction forces decreased in the groups that received increasing and 15 N peak loading. However, Col2-3/4M staining was negative in all samples, while enzymatic damage (Col2-3/4C_{short}) appeared similar in experiments and in unloaded control groups. It was shown that a loading magnitude threshold exists above which softening occurs in cartilage. However, in samples that did show softening, we were unable to detect collagen damage. Thus, our results demonstrate that cartilage softening most likely precedes collagen damage.

This chapter is based on the following publication:

Hosseini SM, Veldink MB, Ito K, van Donkelaar CC (2013) Is collagen fiber damage the cause of early softening in articular cartilage? Osteoarthritis and Cartilage 21(1) 136-143

3.1 Introduction

Articular cartilage in diarthrodial joints exhibits unique mechanical properties enabling it to transmit and distribute loads. These biomechanical functions are assured by the extracellular matrix (ECM) consisting primarily of collagen fibrils embedded in a gel of proteoglycans (PG) with low permeability for water flow (Thibault et al. 2002). PGs resist compression while the collagen network withstands tension (Williamson et al. 2003; Ottani et al. 2001; Broom and Poole 1983). These functions are compromised during osteoarthritis (OA), a degenerative joint disease in which deterioration of the ECM occurs (Boschetti and Peretti 2008).

Impact loading and single acute overloads may initiate biological degenerative responses of cartilage (Buckwalter 1995; Guilak 2011). Several studies addressed failure of cartilage following mechanical impact, during which hydrostatic pressure builds as a result of entrapped water within the matrix (Milentijevic et al. 2003; Ateshian et al. 1994; Ateshian and Wang 1994; Solts and Ateshian 1998). Torzilli et al. (1999) used indentation impact loads to the center of bovine cartilage explants with stress magnitudes of 0.5 to 65 MPa at a constant stress rate of 35 MPa/s. Cell death was observed first in the superficial tangential zone (STZ) at stress magnitudes of 10–15 MPa. Matrix damage was initiated at approximately 25 MPa, while impacts > 45 MPa produced strains of > 80% and massive tissue damage. Repo and Finlay (1977) impacted explants of human articular cartilage-on-bone in unconfined compression at strain rates of 500 and 1000 sec^{-1}. Cell death and structural damage initiated at the articular surface and around fissures at strains of 20–30% corresponding to a stress of 25 MPa. Ewers et al. (2001) impacted bovine cartilage explants in unconfined compression using stress rates of 40 MPa/s and 930 MPa/s. Both stress rates deformed the explants to about 50% at 40 MPa peak stress. Cell death was observed around surface fissures and was more extensive in the samples subjected to the lower stress rate.

The above studies involved direct cartilage damage as a consequence of single impact loads. However, primary OA develops over time and the onset is not clear. Already in early or pre-OA stages of OA, the static and dynamic Young's and aggregate moduli of articular cartilage are reduced between 20% and 80% (Mankin et al. 2000; Bonassar et al. 1997; Nieminen et al. 2000; Toyras et al. 1999; Wayne et al. 2003;

Laasanen et al. 2003; Toyras et al. 2003). This involves both tensile and compressive stiffness of the tissue.

The cause of this early change in mechanical properties remains unclear, but it has been speculated that damage in the collagen network, which is another early event in OA (Natoli and Athanasiou 2009; Brown et al. 2012), may be responsible. McCormack and Mansour (1998) noticed that a reduction in tensile strength of cartilage preceded surface damage under repeated compressive loading of 65 N in vitro. To reveal sites of collagen damage, a set of monoclonal mouse antibodies to localize denatured collagen (Col2-3/4M) or enzymatically cleaved collagen (Col2-3/4C_{short}) has been employed (Thibault et al. 2002; Dodge and Poole 1989; Chen et al. 1999; Wilson et al. 2006b). Thibault et al. (2002) showed collagen damage in explants loaded by average peak stresses ranging from 2 to 8 MPa. Chen et al. (1999) showed that collagen damage induced by 5 MPa pressures extended from the superficial layers into the deep zone, when this pressure was sustained from 20 to 120 minutes. In addition, it was shown that collagen damage occurs earlier in thin than in thick cartilage, and this effect was associated with both shear and tensile strains in the fibrillar network (Wilson et al. 2006b). Except for damage to the collagen network, no signs of tissue damage were histologically apparent at the loading magnitudes that were used.

From the above studies it can be concluded that both softening and collagen damage occur in early OA. We may hypothesize that cartilage softening occurs as a result of initial collagen damage. However, because collagen damage and cartilage softening have not yet been determined simultaneously in one study for the very early onset of OA, it remains questionable whether they are associated. The aim of the present study is therefore to evaluate whether indeed, initial collagen damage can be found when tissue softening occurs as a result of excessive mechanical loading.

We approached this question by first identify a threshold load above which significant softening is induced in articular cartilage. The premise is that when we start to identify tissue softening, collagen damage should have reached detectable levels. Therefore, we subsequently evaluated whether collagen damage could be detected using the abovementioned immunohistochemical probe for denatured collagen.

3.2 Materials and methods

3.2.1 Sample preparation and setup description

Osteochondral plugs (*n* = 29, ø7.5 mm, average full-depth cartilage thickness 0.95 mm, average bone thickness 5 mm) were obtained from young bovine carpometacarpal joints and stored at 20°C until testing. Samples were thawed and left to equilibrate in PBS at room temperature for about 30 minutes. Cartilage thickness was determined as the average of the thickness observed at four sides of the biopsy by stereomicroscopy. Samples were fixed by dental cement to the bottom of a 20 mm high bath filled with PBS in such a way that the articular surface of the sample was horizontal.

Samples were indented with a stainless steel spherical indenter (tip radius = 1 mm), using either a Zwick tensile tester (Z010, Zwick Roell, Ulm, Germany) with a 2.5 kN load cell (type Xforce P, Zwick Roell, Ulm, Germany) and TestExpert II software (Version 3.1), or Bose tensile tester (ElectroForce LM1 TestBench, Bose Corporation, Minnesota, USA) with a 20 N load cell. The response of the control groups (below) showed no difference between the two loading systems.

3.2.2 Loading protocols and force relaxation parameters (FRPs)

The experiment contained one control group in which no damage was induced and four experimental groups in which different levels of peak loads were applied. All groups received a baseline loading of 5% indentation, which was initially applied for 90 minutes to ensure equilibrium. Subsequently, each 1500 s, a 600 s period of 10% indentation was applied at a strain rate of 0.001 mm/s, during which relaxation was monitored, followed by 900 s period of 5% baseline indentation. After 600 s during this phase, the indenter was lifted from the sample to obtain a reference 0 N force measurement. These cycles were applied 11 times (Figure 1a, blue line). Superimposed on this control-loading regime (*n* = 6), the other four experimental groups received 10 peak loads during each baseline period. This was either a peak load of 3 N (*n* = 5), 6 N (*n* = 5) or 15 N (*n* = 6), or an increasing peak load (*n* = 7) from 2 to 13 N (Figure 1a, red line). Loads were applied at a strain rate of 0.017 mm/s, and the indenter was lifted at the same rate immediately after reaching the maximum load.

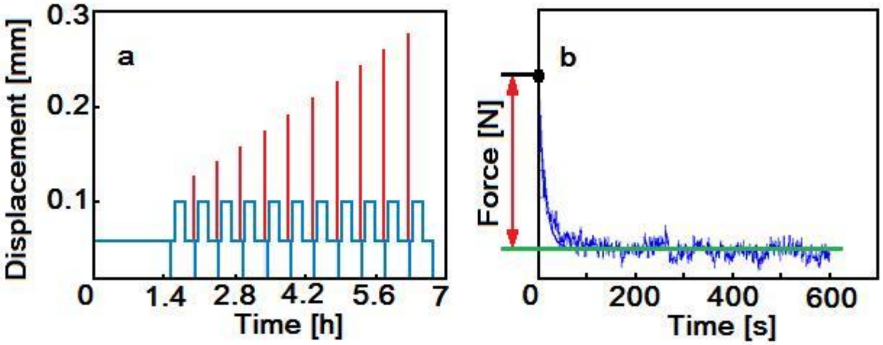

Figure 1 a *Indenter displacement against time to monitor softening (control group, blue line) and to apply peak loads (increasing load group, red line) (Cartilage thickness 1 mm).* ***b*** *Typical relaxation curve during 10% indentation: peak value (black dot), equilibrium value (green line), and force reduction value (red arrow).*

The force relaxation curves at 10% indentation were used to analyze changes in tissue properties as a consequence of the peak loads. Four features were extracted from these curves: peak force, equilibrium force, force reduction value (Figure 1b) and the relaxation time constant which was defined as the time for force to decrease to 37% of its initial peak value. Together, these four extracted features represented the relaxation curve and through the rest of this paper they will be referred to as “Force Relaxation Parameters” (FRP). For comparison between samples and experiments, FRP’s of the control group are subtracted from the experimental groups, after which the data are normalized to their first cycle values.

The four FRPs are the critical features of the time dependent reaction force response of the cartilage samples. During the relaxation phase, water is displaced and loads are gradually transferred to the solid matrix. Given enough time in the relaxation phase, the tissue will reach equilibrium so any change in the FRP indicates alterations in the tissue composition and structure. To evaluate the initiation and progression of softening due to different types of loading, the differences between FRP values of the second and the first relaxation test, and between the last and the first relaxation test were examined.

3.2.3 Histology and biochemical analyses

After loading, cartilage was separated from the subchondral bone using a scalpel. About one third of each sample was dissected and used to determine water-, GAG- and collagen fractions. Per experimental group, explants were lyophilized, weighed dry (A quarter of each sample was weighted (wet weight), cut in small pieces and lyophilized for 24 hours to obtain dry pellets. Samples were reweighted to determine their dry weight), and digested in papain solution (100 mM phosphate buffer, 5 mM L-cystein, 5 mM ethylenediaminetetraacetic acid (EDTA) and125-140 µg/ml papain) at 60°C for 16 h. The sulfated-glycosaminoglycan (sGAG) content was determined using a modification of the assay described by Farndale et al. (1986), with a shark cartilage chondroitin sulfate reference (Sigma). Subsequently, digested tissue samples were hydrolyzed in 6 M hydrochloric acid (Merck, Whitehouse Station, NJ, USA) and hydroxyproline (HYP) quantity was assessed using an assay modified from Huszar et al. (1980) with a trans-4-hydroxyproline (Sigma) reference. Collagen content was obtained by multiplying the hydroxyproline content with 7.6 (Sivan et al. 2006; Kock et al. 2010). GAG- and collagen fractions were normalized to the dry weight.

The remaining two thirds, which included the center of the sample where the indentation was applied, was used for histological analyses. In the most central slices, picrosirius red and safranin O/fast green stainings were evaluated for general histological appearance and for monitoring local changes in PG and collagen content at the site of indentation through the depth of the tissue. Col 2-3/4M and Col 2-3/4C_{short} immunostainings were performed to analyze mechanically induced collagen damage and enzymatically cleaved collagen, respectively (Thibault et al. 2002; Dodge and Poole 1989; Chen et al. 1999; Wilson et al. 2006b). The 7 µm slices were incubated in 1% testicular hyaluronidase (30 min, 37°C), followed by 10% normal horse serum (Col2-3/4M) or 10% normal goat serum (Col2-3/4C_{short}) (30 min, RT), and Col2-3/4M or Col2-3/4C_{short} antibody (1/800, overnight, 4°C). Subsequently, sections were incubated in biotin-labeled horse anti-mouse antibody (Col2-3/4M) or goat anti-rabbit antibody (Col2-3/4C_{short}) (1/400, 1 hour, RT) followed by a biotin streptovidin detection system (30 min). Finally, they were incubated in 10 mg 3',3'diaminobenzidine dissolved in 15 ml PBS with 12 µl 30% H_2O_2 (7 min) and counterstained with Mayer's haematoxylin. Negative controls were incubated in PBS instead of in Col2-3/4M and Col2-3/4C_{short} antibodies. As positive control, a sample was stained that was excessively loaded by compressing it manually using a thin metal plate.

3.2.4 Statistical analyses

Data are represented as mean +/- 95% confidence intervals. Statistical analyses were done using SPSS (Version 19, IBM SPSS Statistics, Chicago, IL). The one sample *t*-test was employed to verify that parameters of the control experiments were not significantly changed during the experiments. Comparisons between experimental groups were performed by one-way ANOVA using Bonferroni post hoc testing to identify specific significant differences. Levene's test and Shapiro-Wilk test were used to test the homogeneity of variance and the normality. Both were used to justify the one-way ANOVA test. Correlations between force relaxation and compositional parameters were tested using the Pearson correlation analysis test. In all cases $p < 0.05$ was considered significant.

3.3 Results

3.3.1 FRP variations

None of the FRP's of the control group was significantly different from zero (all relaxation similar to the first relaxation), and there was no difference between samples evaluated with the two tensile testing systems (data not shown).

The normalized peak (Figure 2) and equilibrium reaction forces (Figure 3) decreased in the groups that received increasing and 15 N peak loading. Negative values for the peak and equilibrium parameters indicate softening. Time constant did not change significantly with peak loading cycles in any group.

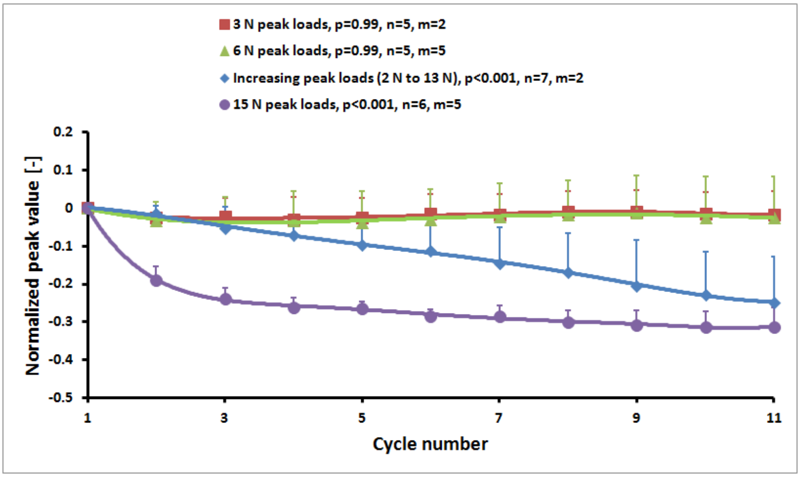

Figure 2 *Normalized peak values (mean + 95% confidence intervals). Reported p-values are those comparing the values of the 11 cycles within each loading protocol. n is the number of independent samples, and m is the number of femurs used to collect samples.*

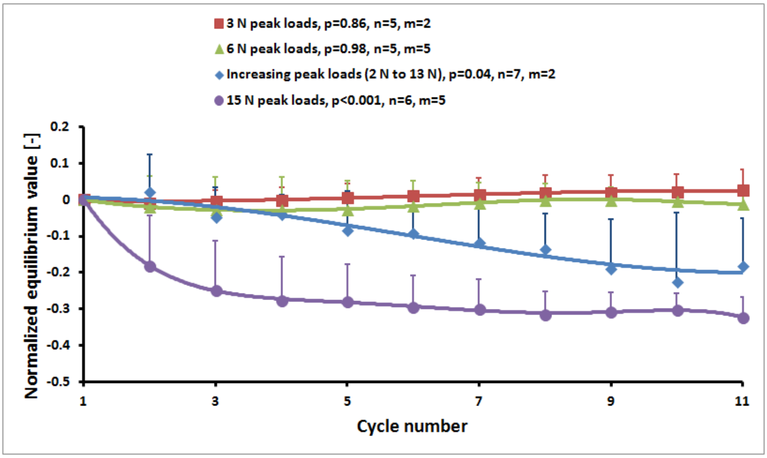

Figure 3 *Normalized equilibrium values (mean + 95% confidence intervals). Reported p-values are those comparing the values of the 11 cycles within each loading protocol. n is the number of independent samples, and m is the number of femurs used to collect samples.*

In the 15 N group, most softening occurred during the first loading cycles as apparent from the difference in FRP values between the second and the first loading cycle (Figure 4a). In the increased loading group, softening steadily increased with increased loading, and was only significant after multiple cycles (Figure 4b). The eventual softening that occurred at the end of the increasing load group and the 15 N group was not significantly different from each other. Groups that received 3 N or 6 N did not differ from control even after ten peak loads (Figure 4b).

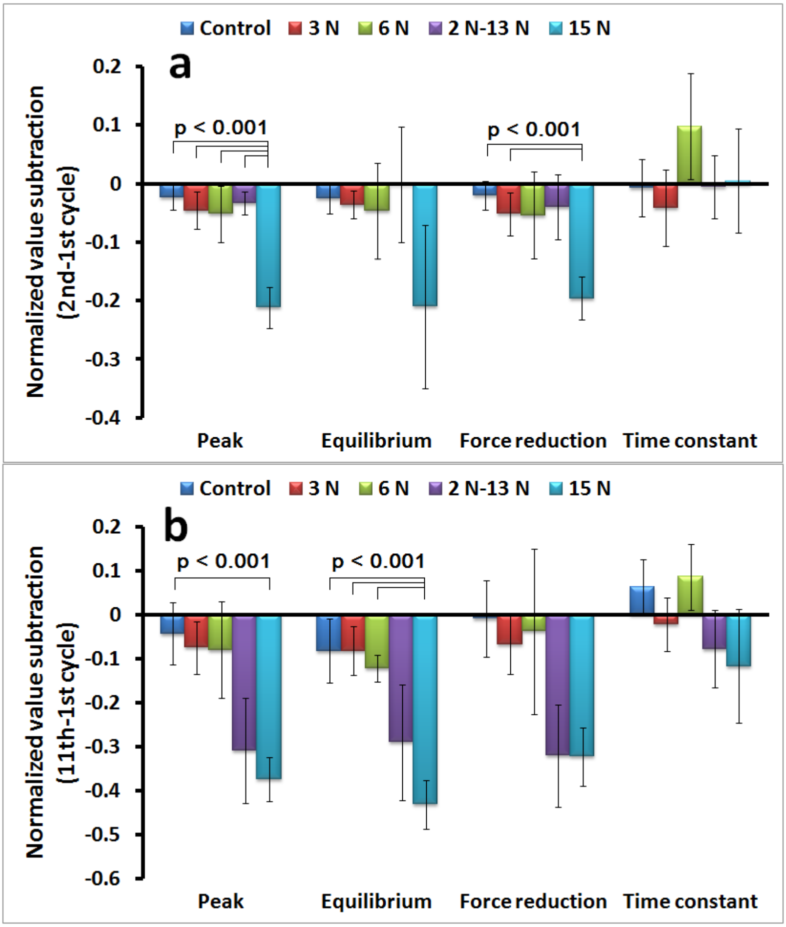

***Figure 4** Bar graph with all FRP per experiment type displayed as subtraction of **a** the second from the first cycle value, **b** the last from the first cycle value. (mean ± 95% confidence intervals).*

3.3.2 Biochemical analyses

Average height of all samples was 0.95 ± 0.12 mm, with no difference between the groups (Figure 5). Also, the biochemical compositions of the samples per group was similar, with only a statistical difference for the average water fraction (after loading) in the increasing peak load group (0.78 ± 0.04) compared to the constant 6 N (0.83 ± 0.02) and 15 N (0.84 ± 0.01) peak load experiments (Figure 5).

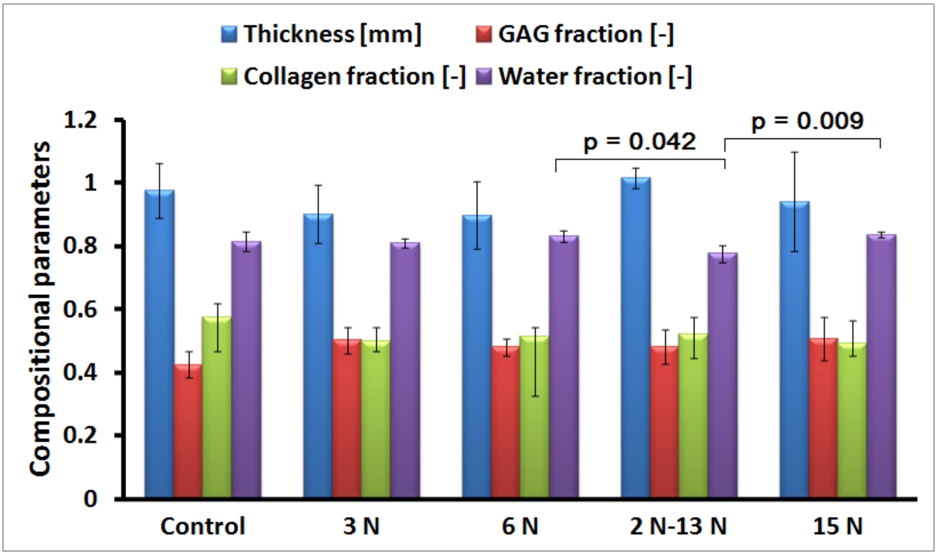

Figure 5 *Average compositional parameters per experiment type. GAG and collagen fractions are normalized to the dried weight of the sample. (mean ± 95% confidence intervals).*

3.3.3 Histology

Picrosirius red and safranin O/fast green staining (Figure 6a-d) revealed that we had both fully mature and immature cartilage samples in our experiments (Toyras et al. 2003; McCormack and Mansour 1998). They are equally distributed among the experimental samples and no correlation with experimental results was found. Moreover, in agreement with our former findings (Wilson et al. 2006b), we could not detect any signs of indentation-induced effects in the tissue by these stainings. Col2-3/4M staining was negative in all samples, while enzymatic damage (Col2-3/4C$_{short}$)

appeared similar in experiments and in unloaded control groups (Figure 6e-h). A severely compressed cartilage sample was used as positive control (Figure 6i).

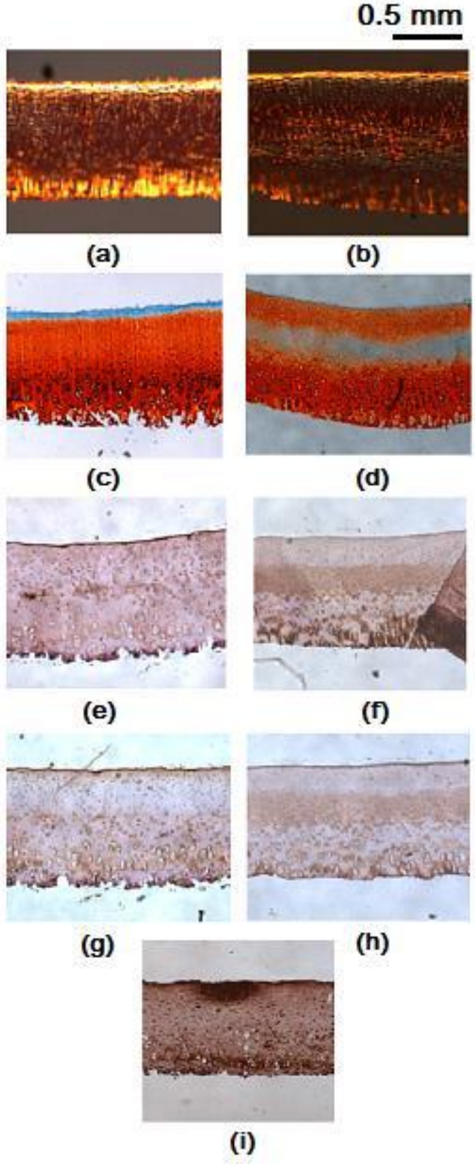

Figure 6 *Typical histological sections from two samples per staining:* ***a,b*** *picrosirius red,* ***c,d*** *safranin O/fast green,* ***e,f*** *Col2-3/4M,* ***g,h*** *Col2-3/4C$_{short}$,* ***i*** *Col2-3/4M positive control.* ***Left*** *from 6 N experiments,* ***right*** *from 15 N experiments.*

3.4 Discussion

For the axial loading with a spherical indenter that we applied in this study, we identified that a threshold loading exists below which cartilage softening does not occur. Samples loaded by 6 N peak loads did not show softening, while a loading of 15 N induced immediate softening in all samples, which on average increased during the two subsequent loading cycles after which it remained constant (Figure 2, Figure 3). Interestingly, histological and immunohistochemical analyses using the Col2-3/4m probe did not show collagen damage in the samples that were softened as a consequence of the 10 repeated 15 N peak loads. Yet, it was shown before that this probe is very sensitive and can pick up very early damage in the collagen network, both as a consequence of high tensile strains and high shear strains (Wilson et al. 2006b). Therefore, we conclude that tissue softening is likely the earliest change in mechanically challenged cartilage, and that most likely, this softening is not the consequence of collagen damage.

In the present study we aimed to identify threshold loading levels at which softening starts. When 6 N or 3 N indentation loads were applied, no softening was apparent in the tissue. This indicates that these loads do not damage the material, and also confirms that the loading protocol used to assess the material properties did not influence the results of the test. At 15 N indentation loading, softening was apparent in most samples, without any other sign of damage. To compare this to other findings in the literature we estimate the applied stresses with our round indenter as follows. With 15 N loading, the maximum indentation depth is around 0.3 mm. This translates into a sample contact area of 1.6 mm^2, and 9.4 MPa average applied stress on the tissue. Because of the round indenter shape, applied stress exceeds 9.4 MPa at the center of the indenter, and declines towards its periphery. In comparison, for normal human activities such as walking and stairs up/down climbing, Morrison (1970a,b) measured patella-femoral and tibial-femoral contact stresses in the range of 3.2-5.3 MPa and 1.3-7.4 MPa, respectively. Physiological cartilage stress levels in the patello-femoral joint were also reported to vary between 1.28 and 12.6 MPa (Matthews et al. 1977), while Smidt measured patello-femoral contact stresses in the range of 1.9-4.8 MPa (Smidt 1973). In vitro mechanical testing of the tibio-femoral joint in neutral position resulted in contact stresses in the range of 0-14 MPa (Riegger-Krugh et al. 1998; Ihn et al. 1993; Fukubayashi and Kurosawa 1980; Brown and shaw 1984; McKellop et al. 1991;

Thambyah et al. 2005), at which levels no damage was apparent in the tissue. In contrary, visible cartilage damage was induced in vitro by applying impact loads of 11 to 36 MPa (Torzilli et al. 1999; Repo and Finlay 1977; Burgin and Aspden 2007; Flachsmann et al. 2005; Jeffrey and Aspden 2006; Kim et al. 2012). These data concur with our result that early softening without visible damage occurred when we applied around 9.4 MPa stress to the cartilage, as this stress level exceeds physiological stress levels, and is below the stress level at which visible damage was found to occur.

The present loading protocol best resembles a former study, where collagen damage was observed to occur after 5 indents using 25 N loads (Wilson et al. 2006b). The present study applied maximum loads of 15 N, as a result of which no collagen damage was observed, but tissue softening was apparent. Because of differences in setups it is difficult to make a direct comparison with indentation studies in which softening was not allowed to occur. From the data published in literature (DiSilvestro and Suh 2001; Wilson et al. 2004; Wilson et al. 2005b), and accounting for the effect of the flat bottom of their indenter compared to our round surface, we derive that the non-damaging indentations that they used should be compared to loads in the order of 5-10 N in our setup. This matches our finding that samples remained unchanged when they received 6 N loading, but did soften when 15 N indents were applied. Interestingly, tissue softening of early osteoarthritic articular cartilage was found to be in the order of 20% to 80% (Mankin et al. 2000; Bonassar et al. 1997; Nieminen et al. 2000; Toyras et al. 1999; Wayne et al. 2003; Laasanen et al. 2003; Toyras et al. 2003). This concurs with the softening that was induced using 15 N loading with our indenter, which was around 40% (Figure 4b).

Some aspects of the study design and results require further analysis. First, we used a round indenter with a radius of 1 mm to induce cartilage softening. With the same indenter at slightly higher forces, collagen damage was found to occur. Obviously, the in vivo shape of opposing cartilage surfaces is different from that of the indenter used in this study. We used an indenter as a model system to induce high strains, locally in the tissue, and to explore whether this would lead to softening, collagen damage or both. Although the strain distribution will be different for different shapes and properties of the indenter, similar phenomena will occur. It is likely that our finding that tissue softening occurs before collagen damage becomes apparent also holds in vivo. Second, the cartilage samples that we included in our study are obtained from young bovines. Histology showed that some samples did not even reach full maturation (Figure

6). We evaluated a possible relationship between tissue maturation and tissue softening, but we did not observe any trends and therefore pooled mature and immature samples. The reason that tissue maturation does not affect our results may be explained by the fact that cartilage maturation starts close to the surface, and ends halfway the depth of the cartilage (van Turnhout et al. 2011). Using a relatively small indenter, the highest strains are induced close to the surface, and also collagen damage was found to occur close to the surface (Wilson et al. 2006b). At this location, all tissues, including the immature samples, showed normal proteoglycan-rich tissue covered with a collagen-rich superficial zone (Figure 6).

The difference between the groups that received 6 N and 15 N indicated that the threshold value to initiate softening in our setup is somewhere in between, with some more variability within these groups than in the 3 N group, likely indicating variability in durability between samples. For some samples, the threshold for softening may be close to 6 N than to 15 N, and vice versa. The same effect is apparent in the group that received increasing levels of loading, which showed the most variable response. Some samples already softened after the first cycles, while other samples only start to become damaged at higher loads. We may speculate that this variability between samples is the results of loading history of the tissue in vivo, possibly reflected by individual tissue composition or sample thickness. Although such sample-specific variation may exist, we did not observe differences in proteoglycan or collagen contents between groups (Figure 5). A statistically significant difference in water fraction exists, the absolute difference is only small and could be considered biologically not meaningful. Also, the group that differs from the other groups is the one that received increasing load levels with time. This group is the least important for the conclusions drawn in this study. Therefore, we consider the observed difference in water fraction unimportant for the interpretation of the results.

Based on our results and previous studies, we postulate that the development of mechanically induced cartilage damage occurs in three steps, which all have a certain threshold level. Above the lowest threshold level, cartilage softening is induced but without visible structural damage. Above a second threshold level, collagen damage is visible at the site of loading. Above the third threshold, macroscopically visible damage occurs. These thresholds are sample specific; with our indenter and loading regime, the first threshold was between 6 and 15 N for most samples, and above 15 N for some. The second threshold is between 15 and 25 N for thin samples and above 25 N for thicker samples (Wilson et al. 2006b). However, the exact forces at which damage occurs may depend on other parameters such as strain rate, as was shown for macroscopic damage (Turley et al. 2011; Nishimuta and Levenston 2012).

It remains speculative which effect caused the softening that we observed. The damage did not affect any parameter directly related to fluid flow, because peak loading did not change the time-constant, and the damage not only affected the peak stress, but also the equilibrium stress level during which fluid flow is absent. Therefore, we propose that the observed decrease in reaction force originates from changes in either the fibrillar or the non-fibrillar components of the tissue, or both. We cannot exclude that the observed softening phenomenon may be due to the intrinsic viscoelastcity of the collagen-proteoglycan matrix. However, long-term viscoelastic effects did not appear in controls and in 3 N and 6 N experiments and the time constants in higher loading experiments were not affected. Therefore, we consider it more likely that the cause of the observed changes is due to the actual changes (damage) in the tissue. Damage to the non-fibrillar PG network is less likely, because PG’s are expected to be more resilient than collagen fibers. Therefore, we anticipate that they would not be damaged before collagen fibers are. Also, we do not expect that our peak loadings induce a loss of PG’s from the tissue. The peak loads were applied for a short period of time, during which significant flow of fluid or transport of (macro)molecules is not expected. Smaller breakdown products of PG’s may have been transported out of the tissue as a consequence of the sustained, 10% loading step, during which equilibrium fluid flow is reached, but in that case also the baseline control experiment would have been affected, which is not the case. Furthermore, no PG staining changes were visible in the histology sections. The remaining explanation is that the collagen network was damaged, yet that we were unable to capture this damage with the Col2-3/4M staining. However, this method has proven very sensitive in the past, and also to stain collagen that was damaged by both excessive tensile and shear loading (Wilson et al. 2006b). Yet, we cannot exclude that a loss of crosslinking or entanglement could have occurred, which may have led to a rearrangement of the collagen network. To explore such effects is part of our future work.

Based on the presence of significant tissue softening and the absence of a positive staining for collagen fiber damage, we conclude that softening of cartilage tissue becomes apparent even before collagen damage can be observed. This invalidates our hypothesis that collagen damage is necessary to cause the earliest tissue softening that occurs in mechanically challenged cartilage. Based on these results and on prior work, we consider cartilage softening the earliest sign of changes in the cartilage after excessive loading, which is followed by collagen damage and visible macroscopic damage when higher loads are applied. Because it is possible to monitor softening in a fast, economical and non-invasive manner, this opens possibilities to very sensitive studies towards understanding the earliest onset of OA.

Chapter 4

How Preconditioning Affects the Measurement of Poro-viscoelastic Mechanical Properties in Biological Tissues

Abstract

It is known that initial loading curves of soft biological tissues are substantially different from subsequent loadings. The later loading curves are generally used for assessing the mechanical properties of a tissue, and the first loading cycles, referred to as preconditioning, are omitted. However, slow viscoelastic phenomena related to fluid flow or collagen viscoelasticity are initiated during these first preconditioning loading cycles and may persist during the actual data collection. When these data are subsequently used for fitting of material properties, the viscoelastic phenomena that occurred during the initial cycles are not accounted for. The aim of the present chapter is to explore whether the above phenomena are significant for articular cartilage, by evaluating the effect of such time-dependent phenomena by means of computational modeling. Results show that under indentation, collagen viscoelasticity dominates the time-dependent behavior. Under UC, fluid-dependent effects are more important. Interestingly, viscoelastic and poroelastic effects may act in opposite directions and may cancel each other out in a stress-strain curve. Therefore, equilibrium may be apparent in a stress-strain relationship, even though internally the tissue is not in equilibrium. Also, the time-dependent effects of viscoelasticity and poroelasticity may reinforce each other, resulting in a sustained effect that lasts longer than suggested by their individual effects. Finally, the results illustrate that data collected from a mechanical test may depend on the preconditioning protocol. In conclusion, preconditioning influences the mechanical response of articular cartilage significantly and therefore cannot be neglected when determining the mechanical properties. To determine the full viscoelastic and poroelastic properties of articular cartilage requires fitting to both preconditioning and post-preconditioned loading cycles.

This chapter is based on the following publication:

Hosseini SM, Wilson W, Ito K, van Donkelaar CC (2013) How preconditioning affects the measurement of poro-viscoelastic mechanical properties in biological tissues. Biomechanics and Modeling in Mechanobiology DOI: 10.1007/s10237-013-0511-2

4.1 Introduction

Analyzing the mechanics of soft biological materials such as articular cartilage has proven to be challenging (Woo et al. 1981; Huyghe et al. 1991; Johson et al. 1996; Carew et al. 2000; Liu and Yeung 2008). These tissues being inhomogeneous and anisotropic with spatially varying microstructures behave non-linearly and time-dependently (Li et al. 2000; Li et al. 2002; Thambyah et al. 2009; Bevill et al. 2010). In cartilage, two distinct mechanisms are responsible for its time-dependent behavior (Mak 1986a; Mak 1986b; Suh and Bai 1998): (a) the frictional drag force when interstitial fluid flows through the porous extracellular matrix (ECM) (i.e. a flow-dependent, poroelastic mechanism), and (b) the time-dependent behavior of both the collagen (Viidik et al. 1968; Haut and Little 1972; Betsch and Baer 1980; Sanjeevi et al. 1982; Haut 1983; Wang et al. 1997; Silver et al. 2002; Li and Herzog 2004; Li et al. 2005) and the proteoglycans (PG) (Mow et al. 1984a; Mow et al. 1984b; Zhu et al. 1993) that constitute the ECM (i.e., a flow-independent, viscoelastic mechanism). The former mechanism is most apparent in proteoglycan-rich tissues such as cartilage, because the osmotic swelling pressure in these tissues interacts with the water content.

A simultaneous prediction of stress-relaxation and dynamic loading under both compression and tension of articular cartilage can be achieved when taking into account flow-dependent, poroelastic and flow-independent, viscoelastic effects, as well as tension–compression nonlinearity (Huang et al. 2001; Huang et al. 2003; Li et al. 2008). Also, the time-dependent responses during unconfined and confined compression, confined swelling and indentation can be captured simultaneously with fibril-reinforced poroviscoelastic swelling models (Wilson et al. 2005b). Thus, simulations corroborate well to experimental data, after constitutive parameters are fitted to distinct experimental datasets (Korhonen and Jurvelin 2010; Saarakkalay et al. 2010; Miller and Morgan 2010). These datasets have in common that they are determined after few initial loading cycles to precondition the tissue and/or the experimental setup. It has long been observed that initial loading curves generated by soft biological tissues are substantially different from subsequent loadings. The later loading curves are generally reported and used for assessing the mechanical properties of a tissue. The first loading cycles, during which the tissue's response slowly changes, are attributed to experimental artifact, considered as preconditioning and thus are omitted in further analyses. The number of reported preconditioning cycles ranges from one (Haut and Little 1972) to a few (3–5)

(Pinto and Patitucci 1980; Carew et al. 1999; Kwan et al. 1993) or more than ten (Woo et al. 1981; Sauren et al. 1983; Myers et al. 1991; Lee et al. 1994; Duncan et al. 1997), depending on the material being tested (Carew et al. 2004) as well as the strain and strain rate applied (Cheng et al. 2009). After these loading cycles the preconditioned tissue may reach a reproducible time-dependent stress-strain response, without progressive changes in the response to additional loading cycles. This is commonly explained by the fact that residual strains that may have been present inside the tissue have been equilibrated by the few initial loading cycles. The result is a tissue that is mechanically conditioned for consistent and reliable measurements (Haut and Little 1972; Kwan et al. 1993; Miller and Morgan 2010), which can be used to determine its mechanical properties (Fung 1993; Carew et al. 2004; Conza 2005; Li and Yeung 2008; Quinn and Winkelstein 2011). For these reasons, preconditioning has become a standard protocol when testing biological tissues (Cheng et al. 2009; Eshel and Lanir 2001).

Few studies reported changes in the mechanical response of tissues during preconditioning. Eshel and Lanir (2001) showed that preconditioning significantly reduced both the slope of the stress–strain relationship, and the stress levels during consecutive stretch cycles for rat dorsal skin. These effects were significant at all strain levels, and increased with strain. After a short unloading period there was significant partial recovery. Sverdlik and Lanir (2002) showed that preconditioning manifested in sheep digital tendons as stress decay in the cyclic phase and as elongation of the tendon’s reference length. These effects intensified with increased strain level and subdued as the strain decreased. They explained their observations by the combination of the irreversible preconditioning and reversible viscoelasticity. Based on these results, it has recently been hypothesized (Lanir and Einat 2012) that preconditioning can be represented as a visco-plastic process, while the time-dependent response in a fully preconditioned tissue is purely viscoelastic, provided the preconditioning strain is higher than the strain during the actual measurements.

Even though preconditioning a tissue before collecting mechanical test data is generally accepted, it may have an effect on the measured mechanical properties. Based on the observation that soft tissues may respond differently depending on the loading sequence applied, Conza (2005) concluded in a review that ‘tissue adaptation to mechanical loading is not unique, making the establishment of a standard preconditioning protocol a difficult task. Part of this conclusion may be related to the fact that slow viscoelastic phenomena, for instance related to fluid flow or collagen viscoelasticity, are initiated during these first preconditioning loading cycles and may persist during the actual collection of the data. When these experimental data are subsequently used for fitting of material properties, the viscoelastic phenomena that occurred during the initial cycles are not accounted for. Consequently, the preconditioning protocol may influence the time-dependent mechanical properties that would be determined by fitting using a computational model.

The present study addresses this potential problem by evaluating the effect of particular preconditioning protocols on the stress-strain relationships of articular cartilage under various loading regimes. Therefore, a composition-based fibril-reinforced, poroviscoelastic swelling model for articular cartilage mechanics was adopted (Wilson et al. 2006a), as a typical example of a model for which previously time-dependent material parameters were fitted to experimental data. Using this model, the stress-relaxation responses of cylindrical articular cartilage plugs that are subjected to cyclic loading in indentation or unconfined compression are evaluated. Typical aspects of these responses are then compared with effects seen during preconditioning. The computational approach allows separating the effects of viscoelastic and poroelastic origin, and their interaction. These are evaluated to provide more insight into the effects of preconditioning.

4.2 Materials and methods

4.2.1 Finite element model

In the validated fibril-reinforced poroviscoelastic swelling model (Wilson et al. 2006a), articular cartilage is assumed as biphasic, consisting of a solid and a fluid phase. The solid phase consisted of a swelling non-fibrillar part, which contains mainly proteoglycans, and a fibrillar part representing the collagen network. For the nonfibrillar part a compressible neo-Hookean model is used. The swelling behavior is implemented as osmotic swelling. The total stress in this model is calculated as (Eq. 1):

$$\boldsymbol{\sigma}_{tot} = -p\mathbf{I} + n_{s,0}\left(\left(1-\sum_{i=1}^{totf}\rho_c^i\right)\boldsymbol{\sigma}_{nf} + \sum_{i=1}^{totf}\rho_c^i\boldsymbol{\sigma}_f^i\right) - \Delta\pi\mathbf{I} \qquad (1)$$

where $n_{s,0}$ is the initial solid volume fraction, $\boldsymbol{\sigma}_{nf}$ is the Cauchy stress in the non-fibrillar matrix, $\boldsymbol{\sigma}^i_f$ is the fibril Cauchy stress in the i^{th} fibril with respect to the global coordinate system, ρ^i_c is the volume fraction of the collagen fibrils in the i^{th} direction with respect to the total volume of the solid matrix and $\Delta\pi$ is the osmotic pressure gradient (Wilson et al. 2006a). In this model, fibrils are assumed to behave viscoelastic. Therefore, they are further introduced below. For details on the implementation of the elastic non-fibrillar stress and osmotic pressure gradient, the reader is referred to earlier work (Wilson et al. 2006a).

The fibrillar part consisted of large primary fibril directions and smaller secondary fibril directions. Bundles of primary fibril directions extended perpendicular from the subchondral bone, splitting close to the articular surface into fibrils curving to a horizontal orientation, flush with the articular surface (Figure 1). The network of secondary fibril directions represents a quasi-isotropic network.

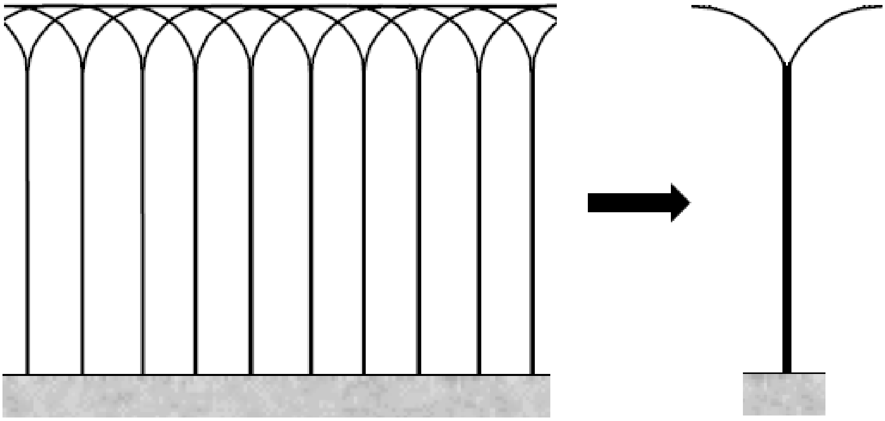

Figure 1 *Orientation of the primary fibril directions as a function of depth.* ***Left:*** *Schematic of the arcade model.* ***Right*** *Orientation of primary collagen fibril directions as implemented in the finite element model.*

In (Wilson et al. 2006a), both types of collagen fibrils were assumed to be viscoelastic, and the fibril Cauchy stress tensor is given by:

$$\boldsymbol{\sigma}_f = \frac{\lambda}{J} P_f \vec{e}_f \vec{e}_f \tag{2}$$

where λ is the elongation of the fibril, P_f is the first Piola-Kirchhoff stress, and e_f is the current fibril direction. Note that this total Cauchy stress of the fibrils is expressed as a function of the deformed surface that a fibril works on. In (Wilson et al. 2006a) the viscoelastic behavior of the collagen fibrils was represented by the two-parameter exponential stress-strain relationship springs S_1, parallel to spring S_2 in series with a linear dashpot with dashpot constant η (Figure 2). Stresses in springs S_1 and S_2 are calculated with Eq. 3 and 4 respectively. Note that the stresses in the dashpot and spring S_2 in Figure 2 are identical. Also, fibers only withstand tension loads (positive strains).

$$P_1 = E_1(e^{k_1\varepsilon_f} - 1) \qquad for \quad \varepsilon_f > 0 \tag{3}$$

$$P_2 = E_2(e^{k_2\varepsilon_e} - 1) = \eta\,\dot{\varepsilon}_v \qquad for \quad \varepsilon_e > 0 \tag{4}$$

where E_1, E_2, k_1 and k_2 are positive material constants, ε_f is the total fibril strain, ε_e is the strain in spring S_2 and ε_v is the dashpot strain. Since the strains in the upper and lower part of the spring system in Figure 2 are the same, the total fibril stress P_f is the summation of P_1 and P_2 (Wilson et al. 2006a).

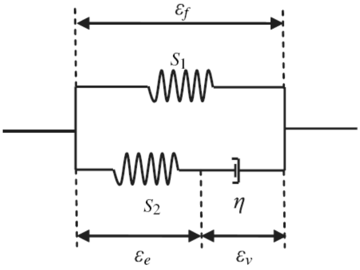

***Figure 2** Schematic model for a viscoelastic collagen fibril (ε_f is the total fibril strain, ε_v the dashpot strain and ε_e the strain in spring S_2) (adopted from Wilson et al. (2006a)).*

By assuming the depth- and strain- dependent permeability, and also accounting for the fact that only the extra-fibrillar fluid can flow out of the tissue, permeability has been calculated by Eq. 5 (Wilson et al. 2006a).

$$k = \alpha(1 - n_{exf})^{-M} \tag{5}$$

where k is the permeability, α and M are positive material constants and n_{exf} current extra-fibrillar fluid fraction.

The values of the model parameters, obtained by fitting to the data of up to 20% compression of cartilage samples (15 different fresh frozen bovine patellae taken from 1-2 year old animals (DiSilvestro and Suh 2001) are as follows (Wilson et al. 2006a): E_1 = 4.316 MPa, E_2 = 19.97 MPa, k_1 = 16.85, k_2 = 41.49, $\eta = 1.424 \times 10^5$ MPa s, $\alpha = 1.767 \times 10^{-16}$ m^4/N s and M = 1.339. The model was implemented in ABAQUS 6.10 (Abaqus Inc., Providence, RI). For more details about this model and the parameters used see (Wilson et al. 2006a).

The cartilage plugs were modeled as axisymmetric with a radius and thickness of 1 mm. In order to apply load, two different rigid nonporous indenters have been used, one round indenter (IND) with a 0.4 mm radius and the other one, a plate (unconfined compression-UC) placed on the cartilage surface (Figure 3). Each model consisted of 850 axisymmetric pore pressure elements (CAX4P) (In order to make sure that the results are independent of the mesh size, mesh dependency up to 4 times finer has been checked.). The nodes at the bottom plane were confined in all directions, and the displacements of the nodes at the symmetry-axis were confined in radial direction. At the top of the model, where the cartilage is not in contact with the indenter, and at the radial edge of the model, zero pore pressure was prescribed, i.e. fluid could flow in and out freely.

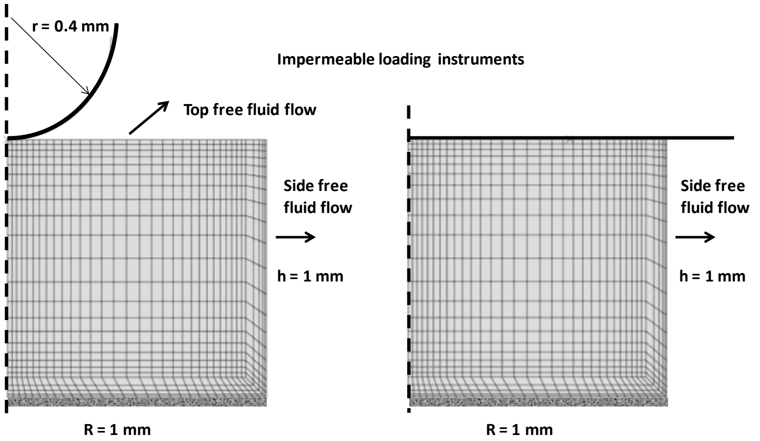

Figure 3 *Meshed used for indentation loading:* ***Left*** *unconfined compression (UC),* ***Right*** *Indentation (IND).*

4.2.2 Loading protocol

In the first step, the tissue was allowed to swell for 30000 s (more than 8 hours) in 0.15 M saline solution. This was to allow the swelling pressure within the tissue to equilibrate against residual tension of the tissue fibers. Since the indenter is free, it moves upwards following the swelling of the tissue. Afterwards the tissue undergoes 5% compression, which is sustained for another 30000 s to ensure complete equilibrium. From this point, a series of strain-relaxation-unstrain between 5% and 10% has been applied to the tissue having 5 relaxation steps of 10% compression level (5 cycles). The time period during which both the 5% and 10% compression are held constant is referred to as recovery time, which is variable between simulations. All the loading-unloading steps happen with 0.001 s^{-1} strain rate. Figure 4 shows the trajectory of the indenter applying load on the tissue.

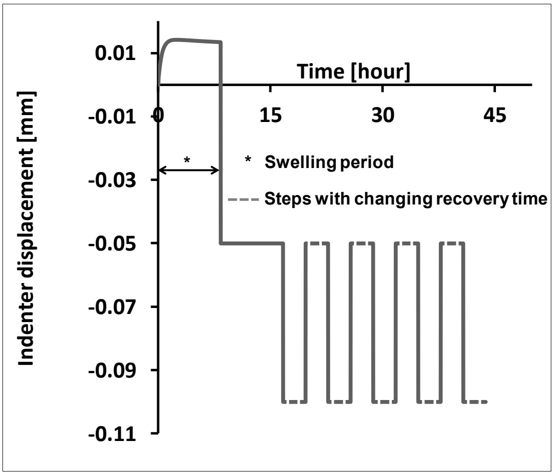

Figure 4: *Indenter displacement when applying load over the tissue for a recovery time of 10800 s.*

4.2.3 Simulations

For ten different recovery times (Table 1), three simulation series of two loading devices (indentation (IND) and unconfined compression (UC), (Figure 3)) were performed (i.e. 60 simulations in total). In the first series of simulations, only the effect of flow-independent viscoelasticity of the matrix was studied. For that purpose, fluid flow was excluded by enforcing zero pore pressure for the whole tissue, i.e. by allowing fluid to flow infinitely fast without resistance. In the second series of simulations, only the effect of flow-dependent poroelasticity was studied. To that purpose, the collagen fibrils were assumed purely elastic by setting η equal to zero (Figure 2). In the third series of simulations, both flow-dependent and fluid-independent viscoelasticity were kept active in the simulations.

Table 1 *Recovery times (s).*

60	80	120	240	360	600	1800	3600	7200	10800

A final set of 10 simulations was performed to illustrate the effect of preconditioning on the result of a single relaxation experiment. Therefore, a sustained relaxation experiment with 10% compression was simulated, after the tissue was preconditioned with 9 loading cycles with different recovery times (Table 1).

4.2.4 Data analysis

To represent the typical measurements during an experiment, the reaction force of the tissue was monitored during the indentation or unconfined compression loading over time. From these data, the five peak force values were determined immediately at the beginning of each of the five 10% loading steps. Finally, the effect of preconditioning was quantified as the normalized difference in values of the peak force between subsequent compressive loading steps *i* (Eq. 6).

$$\text{Normalized peak force difference} = \frac{\text{Peak}_{i+1} - \text{Peak}_{i}}{\text{Peak}_{i}}, (i = 1\text{-}5) \quad (6)$$

4.3 Results

Because a larger area of the tissue is compressed during UC than during IND, the total reaction force was higher in UC (Figure 5).

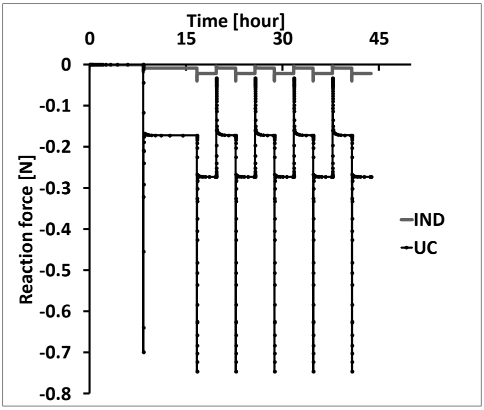

Figure 5 *Resulting reaction force during two complete simulations of one IND and one UC loading protocol with 10800 s recovery time between each change in applied load. Both poroelasticity and collagen viscoelasticity are included.*

Regardless of whether flow-independent viscoelastic, flow-dependent poroelastic, or the combination of both conditions was included in the simulations, the equilibrium value reached the same reaction force during sustained compression (Figure 6). However, as expected the magnitude of the peak and the relaxation curve after the peak depended on the viscoelastic behavior of the tissue (Figure 6).

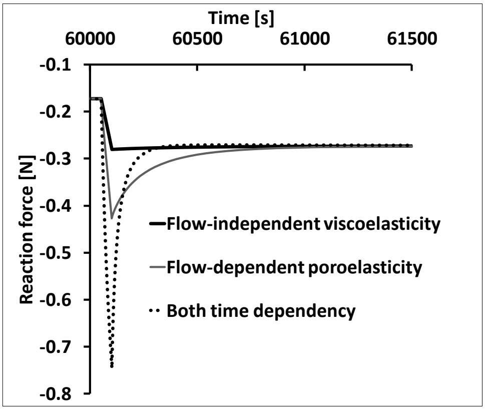

Figure 6 *The relaxation curves of 10800 s recovery time of UC simulations of the first 10% compression step. Solid line: flow-independent viscoelastic matrix, Solid line with dots: flow-dependent poroelastic tissue, Dashed line: both are included. This figure shows only 1500 s of the 10800 s relaxation curves, until curves reach equilibrium.*

Depending on the experimental conditions, the curves in Figure 6 were different for subsequent loading cycles. These differences were most apparent for the peak reaction force in experiments with short recovery times. The absolute value of these peaks might increase or decrease with subsequent loading cycles, depending on the type of loading (IND vs. UC) and the properties of the matrix (flow-dependent poroelastic tissue vs. flow-independent viscoelastic matrix) (Figure 7).

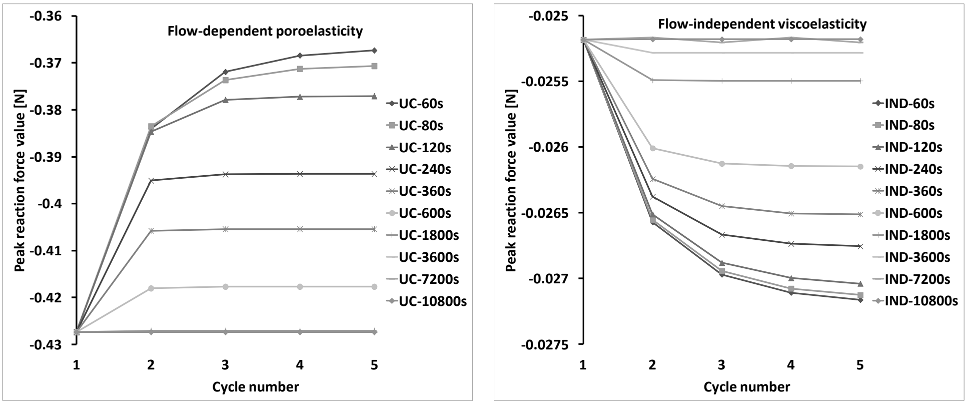

Figure 7 *Illustration of the differences in response, depending on the applied loading condition and on the type of time-dependency that is included. The curves show the peak reaction forces in subsequent 10% compression cycles.* ***Left*** *UC with flow-dependent poroelastic tissue,* ***Right*** *IND with flow-independent viscoelastic matrix. (Data points are connected by lines only for more clarity.)*

The normalized difference between the peak values of the first and second loading cycle (Eq. 6, with i = 1) are plotted against the recovery time used in the simulations (Table 1) (Figure 8). This evaluation showed several phenomena. First, in simulations in which only matrix viscoelasticity was taken into account, the first peak was always smaller in absolute value than the second one, while this was opposite in the case where the matrix was elastic, but the tissue was poroelastic. Second, flow-dependent poroelastic effects were more dominant under UC loading compared to IND, while the opposite was true for matrix viscoelasticity, which was more effective under IND. Third, with the current parameter values, effects induced by fluid-independent matrix viscoelasticity seem to be effective over a wider range of recovery times than fluid-dependent effects. Finally, in simulations where both fluid-dependent and fluid-independent effects were included, which is the physiological condition, it might take even longer for the peaks to reach equilibrium compared to when either one of them was present alone. Also, depending on recovery time allowed, subsequent peak values might either increase or decrease (positive or negative values in Figure 8).

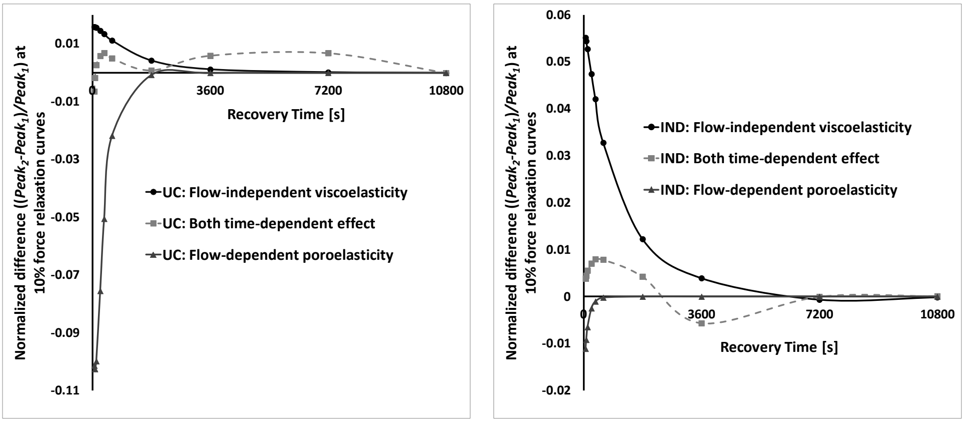

Figure 8 *Plot of the normalized difference between the first and second peak values ((Peak$_2$-Peak$_1$)/Peak$_1$) as a function of the recovery time allowed between loading cycles,* ***Left*** *UC,* ***Right*** *IND.* ***NB:*** *the dots are the results of actual simulations. These are interconnected for clarity of the figure, but care should be taken during interpretation of this extrapolation.*

Subsequently, we evaluated whether this difference between the first and second peak-values (Figure 8) would reduce between subsequent cycles, as this is what is normally observed during tissue preconditioning. Indeed, the normalized difference between subsequent peaks reduced (Figure 9). Very small variations between peak values at longer recovery times were apparent for the simulations with matrix viscoelasticity.

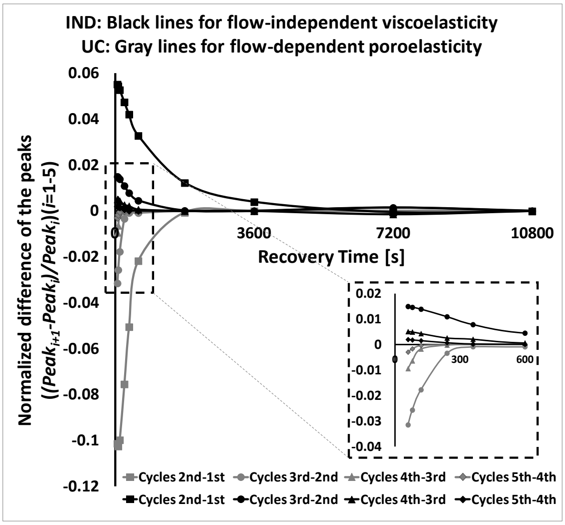

Figure 9 *Normalized difference between subsequent peak values for cycles (i = 1-5) as a function of the recovery time allowed between loading cycles ((Peak$_{i+1}$-Peak$_i$)/Peak$_i$). The zoomed region shows the first 600 s of the graph.*

A sustained relaxation test gave different peak forces and relaxation times, depending on the duration of the 9 preconditioning cycles that were applied. Regardless of the preconditioning protocol, the equilibrium values were identical in all simulations (Figure 10-Left). During these 10 preconditioning cycles, the absolute value of the peak force either decreased (recovery times ≤ 120 s) or increased (recovery times ≥ 240 s) with cycle number, until they all equilibrated after 2 to 9 cycles (Figure 10-Right).

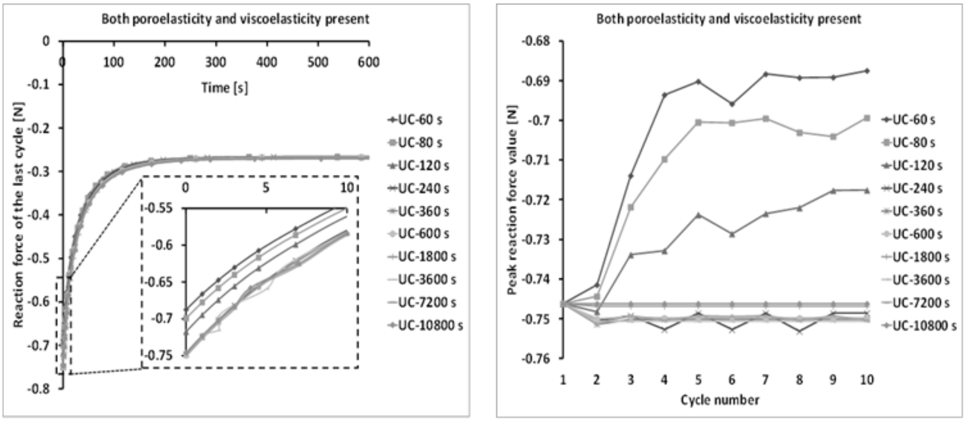

Figure 10 Left *The first 600 seconds of sustained UC relaxation tests after 10 preconditioning cycles with various relaxation times per cycle.* ***Right*** *The peak reaction force values change during preconditioning. With short recovery times in the preconditioning cycles, the absolute value of the reaction force decreases, while it increases with longer relaxation times and becomes consistent with recovery times in the order of hours. (****Right*** *Data points are connected by lines only for more clarity.)*

Moreover, to illustrate that internal processes may not be equilibrated even though the reaction force on the indenter is in equilibrium, the reaction force, the maximal principal strain in the non-fibrillar matrix, the strain in one of the primary fibers, and the strain in one of the secondary fibers with an oblique direction are evaluated for an integration point in the top surface of the cartilage, close to the edge of the indenter (Figure 11). The reaction force equilibrates after approximately 1500 s, while the other parameters continue to change over the entire 10800 s of indentation.

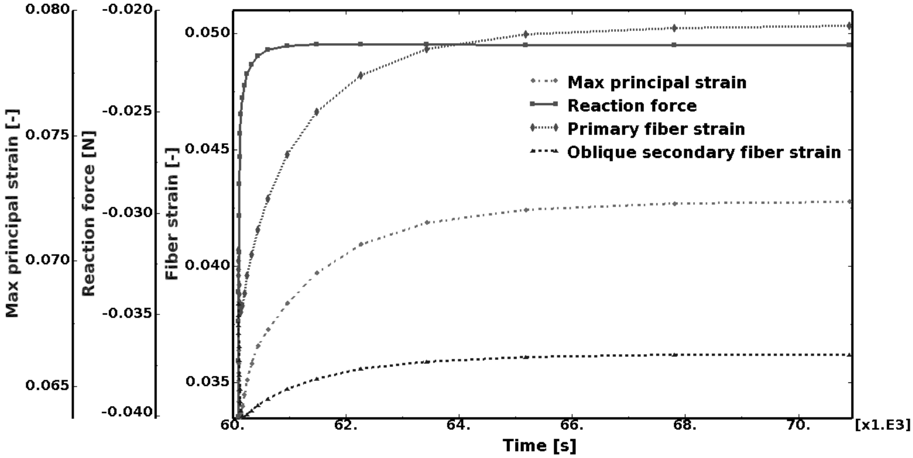

Figure 11 *The reaction force on the indenter, and the maximal principal strain, primary and secondary fiber strain in an integration point of an element under the edge of the indenter. The curves are derived during the fifth indentation of a simulation with 10800 s recovery time in between indentation periods, when both poroelasticity and collagen fiber viscoelasticity are present.*

4.4 Discussion

The objective of this study was to explore the importance of time-dependent effects of fluid flow and of solid matrix viscoelasticity on the stress-relaxation response of cartilage, when the tissue was preconditioned prior to performing the actual measurements. The hypothesis was that these two time-dependent phenomena together change the mechanical response of the tissue during the first cycles, and that this effect occurs during the first preconditioning cycles in a mechanical test. Thus, by omitting the preconditioning cycles, the significance of the viscoelastic response of the tissue would be lost as a result of the preconditioning. This would be particularly important when such experimental data were used for fitting viscoelastic material parameters using computational models.

Indeed, simulations with a fibril-reinforced poroviscoelastic swelling model showed results that corresponded to typical preconditioning effects. First, peak-reaction forces between successive loading steps were not identical, and differences between subsequent peaks decreased with the number of loading cycles applied (Figure 7). Second, these differences decreased when more recovery time was allowed between subsequent loading steps (Figure 7, Figure 8). The number of preconditioning cycles to reach equilibrium depended on the loading protocol, used. This is in agreement with experiments, in which the number of required preconditioning cycles varies from one to several (Haut and Little 1972; Carew et al. 1999; Kwan et al 1993; Pinto and Patitucci 1980; Duncan et al. 1997; Lee et al. 1994; Myers et al. 1991; Sauren et al. 1983; Woo et al. 1981) depending on the material and the strain and strain rate (Carew et al. 2004; Cheng et al. 2009). Third, the effects of the first loading cycle remained present for a long time (more than two hours), as apparent from internal conditions in the tissue (stress-strain (Figure 11) and pore pressure distribution in the tissue (data not shown)), even though after few loading cycles the reaction force appeared to stabilize. When only fluid-dependent poroelasticity or only collagen viscoelasticity was accounted for, steady state was reached faster than when both effects interacted (Figure 8). Finally, the exact effect of interaction between collagen viscoelasticity and poroelastic matrix, the total time dependent behavior, is very complex and therefore not well predictable (Figure 8). This had two main reasons. First, collagen viscoelasticity and fluid-dependent effects had opposite effects on the change in reaction force during subsequent loading cycles. Second, it was shown that the relative importance of flow-dependent and flow-independent phenomena depends on the loading protocol, i.e. under indentation the collagen viscoelastic effects are more important than under unconfined compression. The opposite is true for flow-dependent poroelastic effects (Figure 8, Figure 9). In conclusion, the above effects make the total tissue response during an experiment difficult to interpret and may mask that a tissue is not in equilibrium, even though the reaction force appears constant.

The time-dependent response of a tissue to mechanical loading is very complex, because of the interaction between two separate non-linear and time-dependent effects: one related to collagen matrix viscoelasticity and one to flow-dependent poroelasticity. Fundamentally, if one of them is not in equilibrium, then by definition the other one is not in equilibrium as well. In addition, the viscoelastic collagen network is strongly anisotropic in nature. Hence, the viscoelastic behavior also has directionality. This combination of two viscoelastic effects, one of which has an orientation, makes the total tissue response over time complex and difficult to predict without the use of computational models such as the one used in the present study. Yet, regardless of the time interval during the preconditioning protocol, similar to an ordinary time-dependent material, a repeatable stress-strain response can be obtained after some repeated loading cycles (Figure 10b). At that time, the tissue has changed from one stress state to another. Consequently, the stress relaxation response for the same tissue is different, depending on the preconditioning protocol (Figure 10a).

The above effects were evaluated in articular cartilage, because in this tissue both viscoelastic and poroelastic phenomena are known to play an important role (Haung et al. 2001; Haung et al. 2003; Li et al. 2008). This allowed using a fibril-reinforced poroviscoelastic swelling model that was developed and validated for articular cartilage in the past (Wilson et al. 2004; Wilson et al. 2005b; Wilson et al. 2006a; Wilson et al. 2007). For this particular model, all relevant time-dependent material parameters, including those for collagen viscoelasticity and flow-dependent effects have already been determined (Wilson et al. 2006a). Finally, both unconfined compression and indentation experiments have been evaluated, because based on our expertise, these two loading cases have been anticipated to induce distinct fluid flows and collagen strain patterns.

All flow-independent viscoelastic behavior was accounted for by the collagen network, while proteoglycans were assumed elastic (neo-Hookean) (Wilson et al. 2006a) even though they were known to behave viscoelastic (Mow et al. 1984a; Mow et al. 1984b; Zhu et al. 1993). This choice has not led to an underestimation of the effect of matrix viscoelasticity, as the material parameters for collagen and proteoglycans were fitted together to experimental data. Consequently, the contribution of proteoglycan viscoelasticity was accounted for by the collagen. If both solid matrix components would have been considered viscoelastic, this would have added another time-dependent characteristic to the model, which would have resulted in even more complex material behavior. In principle, proteoglycan viscoelasticity would have had the same effect as collagen viscoelasticity, yet with different characteristic time constant.

Flow-dependent poroelastic effects and flow-independent collagen viscoelastic effects had an opposite effect on the peaks in successive loading steps (negative vs. positive points in Figure 8 and Figure 9). The reason was that when the viscoelastic fibrils were not given enough recovery time after straining, they remained stressed and therefore the tissue acted stiffer in the next loading cycle (Haung et al. 2001; Haung et al. 2003; Li et al. 2008). When water was expressed during deformation and the recovery time was insufficient for the water to flow back in, then the hydrostatic pressure was lower in the next loading cycle and therefore the tissue appeared softer. Both effects were consistent under both indentation and unconfined compression. However, because during indentation fibers were strained more, the effect of flow-independent viscoelasticity was more pronounced. Unconfined compression induced more fluid flow, resulting in a response dominated by tissue poroelasticity. Hence, which of the flow-dependent or flow-independent phenomenon dominated, depended on the exact loading applied. Therefore it was impossible to identify a consistent required recovery time for mechanical testing of cartilage tissue in general. Typical recovery times for equilibrating flow-independent and flow-dependent effects were in the order of 5400 s and 1800 s for 10% unconfined compression and 6300 s and 600 s for 10% indentation. The time to reach equilibrium in the unconfined compression experiment concurs with the observations by Huang et al. (2003), who observed that 3000-5000 s relaxation periods were required to reach equilibrium in 5% unconfined compression testing. Similar to the present study, they concluded that the long duration originated from the viscoelastic response of the solid matrix under tension. Obviously, recovery times were obtained for 10% compression applied in this study, and changing the load magnitude and conditions may change the recovery times.

If what is considered preconditioning is the result of this interaction between two time-dependent phenomena, then this has important implications to experimental, numerical and combined studies addressing the mechanical properties of biological tissues. First, it implies that the mechanical properties that are determined experimentally after preconditioning are not true mechanical properties, but should be considered apparent mechanical properties after a pre-stress is introduced in the tissue. Second, if preconditioning effects are in fact time-dependent mechanical effects of the tissue, then preconditioning effects can and should be captured by numerical models that simulate transient effects of mechanical loading. Third, if output by such models is to be compared to experimental data after preconditioning, then these models should go through similar preconditioning cycles. For the latter reason, parameter fits to experimental data should include the experimental preconditioning loading cycles, in other words preconditioning cycles should be run with the numerical model before fits are being performed to the preconditioned experimental data.

After preconditioning in vitro, biological tissue may remain in the preconditioned state for a long time and they may not return to the initial state after even considerable equilibration. In theoretical models however, the combination of viscoelasticity, poroelasticity and poroviscoelasticity would eventually restore the initial state of the tissue, albeit this may be a very slow process. Possibly, because of the very long time to full equilibration, experimental observations were not sufficiently long to reach full equilibrium prior to the experiments. Alternatively, it is possible that other phenomena may be apparent in tissues, which are not part of the presented theoretical model, such as residual stresses in the tissue as a consequence of sample harvesting or handling. Such effects may be accounted for by sufficient preconditioning of the tissue.

4.5 Conclusion

The tissue response to mechanical loading is the result of a complex interaction between two time-dependent effects: those that originate from the reinforcing viscoelastic collagen network, and those that relate to the poroelastic tissue. During repeated loading, collagen viscoelasticity and fluid flow have opposite effects on the tissue reaction force and may partly mask each other’s effects. Their relative importance depends on the nature of the applied load, and on the exact loading protocol used. Importantly, the present study suggests that rather than eliminating residual stresses from the tissue during preconditioning, initial loading cycles may introduce residual stresses in the viscoelastic collagen network. These additional residual stresses change the mechanical state of the tissue, resulting in a repeatable stress-strain response of the tissue that is dependent on the employed preconditioning protocol.

CHAPTER 4

Chapter 5

A Numerical Model to Study Mechanically Induced Initiation and Progression of Damage in Articular Cartilage

Abstract

Proteoglycan loss and surface roughening, early signs of osteoarthritis, are likely preceded by softening of the ground substance and the collagen network. Insight in their relative importance to progression of osteoarthritis may assist the development of treatment strategies for early osteoarthritis. To support interpretation of experimental data, a numerical model is proposed that can predict damage progression in cartilage over time, as a consequence of excessive mechanical loading. The objective is to assess the interaction between ground substance softening and collagen fiber damage using this model. An established cartilage mechanics model is extended with the assumption that excessive strains may damage the ground substance or the collagen network, resulting in softening of the overstrained constituent. During subsequent loading cycles the strain may or may not cross a threshold, resulting in damage to stabilize or to progress. To evaluate how softening of the ground substance and collagen may interact, damage progression is computed when either one of them, or both together are allowed to occur during stepwise increased loading. Softening in the ground substance was predicted to localize in the superficial and transitional zone and resulted in cartilage softening. Collagen damage was most prominent in the superficial zone, with more diffuse damage penetrating deeper into the tissue, resulting in adverse strain gradients. Effects were more pronounced if both constituents developed damage in parallel. Ground substance softening and collagen damage have distinct effects on cartilage mechanopathology, and damage in either one of them may promote each other.

This chapter is based on the following publication:

Hosseini SM, Wilson W, Ito K, van Donkelaar CC (2013) A numerical model to study mechanically induced initiation and progression of damage in articular cartilage. Osteoarthritis and Cartilage DOI: 10.1016/j.joca.2013.10.010

5.1 Introduction

Articular cartilage derives this biomechanical function from the constitution of its extracellular matrix (ECM), which consists of a strongly hydrated ground substance, mainly consisting of proteoglycans (PGs), reinforced by a tension-resistant fibrillar collagen network. The PGs attract water through osmotic pressure, therewith resisting compression and straining the collagen. Unfortunately, this load-bearing construction may become damaged when cartilage is subjected to excessive mechanical conditions, and such damage is likely to progress into osteoarthritis (OA) (Thibault et al. 2002; Jeffrey et al. 1997; Jeffrey et al. 1995; Anderson et al. 2011). Early signs of OA include PG loss and cartilage surface roughening, which proceeds into fibrillation with cracks penetrating deeper into the tissue at later stages (Chen and Broom 1998; Radin et al. 1978; Pelletier et al. 1983; Guilak et al. 1994; Clark and Simonian 1997). It is apparent that these changes reduce tissue stiffness under tension (Akizuki et al. 1986; McCormack and Mansour 1998; Kleemann et al. 2005; Guilak et al. 1994), compression and shear, and increase permeability (LeRoux and Setton 2002). It has become apparent that initial damage may start before PGs are lost and the surface roughens. As a consequence of loading with an indenter, collagen damage was detected below the cartilage surface, but it did not necessarily become apparent at the surface (Wilson et al. 2006b). Similar loading conditions were later associated with cartilage softening (Hosseini et al. 2013a). These effects may corroborate with observations of damage to the collagen fiber structure at the microscopic scale in early OA tissue (Chen and Broom 1998; Chen and Broom 1999; Broom et al. 2001). However, softening also occurred without detectible collagen damage or loss of PGs from the tissue. Therefore, it was proposed that softening may result from damage to the PG-rich ground substance (Hosseini et al. 2013a), or from the interaction between proteoglycans and collagen at the microscopic scale (Elliot et al. 2000; Thambyah and Broom 2007).

Because together they determine the mechanical properties of articular cartilage, softening or either the ground substance or the collagen network may affect the strains experienced by the other. However, the importance of such interaction to the progression of cartilage damage is unknown. Various mechanisms can be postulated. Softening of the ground substance may reduce the compressive properties of the cartilage and this may subsequently put the collagen network at risk of overstraining. Alternatively, softening of the collagen network may allow the ground substance to attract more water, resulting in local tissue swelling. This may further weaken the tissue, which could result in excessive straining during mechanical loading. Indeed, OA was found to develop in animals that were treated with either collagenases or stromelysins (Tesch et al. 2004; Eyre 2004), indicating that both PGs and collagen are essential to joint homeostasis. Yet, these studies did not reveal the mechanism by which softening of the PGs and collagen network may interact, and effects not related to tissue mechanics such as inflammation, may have played a role.

Therefore, the importance of softening in the ground substance, damage to the collagen network, and the possible interaction between these two for the progression of cartilage damage remains speculative. Yet, such insight may be useful for future development of therapies to treat early OA. To explore these effects experimentally is challenging. Therefore, a numerical approach is adopted, using a composition-based model that includes collagen fiber-reinforcement, ground substance stiffness and tissue swelling due to PGs, and constitutes a physiological organization of the collagen structure and a depth-dependent collagen and PG density (Wilson et al. 2007; Julkunen et al. 2008a). To study progression of cartilage damage with this model requires extension, such that softening of the collagen network and of the ground substance may progress independently over time as a result of mechanical conditions in the tissue.

The objective of the present study is to present such damage progression model, and to employ it to explore whether and how damage in the PG-rich ground substance may advance damage in the collagen network and vice versa. For this purpose, simulations are compared in which cartilage is excessively loaded under four hypothetical conditions. The first condition is when no damage is allowed to develop in the cartilage as a reference. Second, damage is only allowed to develop in the fibrillar network. Third, damage only develops in the ground substance. Fourth, damage may develop in both the fiber network and the ground substance.

5.2 Materials and methods

5.2.1 Cartilage mechanics model

A composition-based, fiber-reinforced, poroviscoelastic biphasic swelling model is adopted (Wilson et al. 2006a; Wilson et al. 2007; Hosseini et al. 2013b), in which cartilage is assumed to consist of a porous solid matrix saturated with water. The solid consists of a PG-rich ground substance and a fibrillar part representing the collagen network. The ground substance has a particular stiffness and contains fixed negative charges associated with the PGs, which induce osmotic swelling. The viscoelastic fibrillar network is implemented in 2D as a collection of 2 primary and 4 secondary fiber directions per integration point, where the dominating primary fiber directions are oriented such that they represent the arcade-like organization. The total stress ($\boldsymbol{\sigma}_{tot}$) in the cartilage is then determined by the combination of hydrostatic, non-fibrillar and fibrillar matrix stresses and osmotic pressure ($\Delta\pi$) (Eq. 1).

$$\boldsymbol{\sigma}_{tot} = -p\mathbf{I} + n_{s,0}\left(\left(1-\sum_{i=1}^{totf}\rho_c^i\right)\boldsymbol{\sigma}_{nf} + \sum_{i=1}^{totf}\rho_c^i\boldsymbol{\sigma}_f^i\right) - \Delta\pi\mathbf{I} \tag{1}$$

where p is the hydrostatic pressure, $\mathbf{I}$ is the unit tensor, $n_{s,0}$ is the initial solid volume fraction, $\boldsymbol{\sigma}_{nf}$ is the Cauchy stress in the non-fibrillar matrix, $\boldsymbol{\sigma}_{if}$ is the fiber Cauchy stress in the i^{th} fiber with respect to the global coordinate system, ρ_c^i is the volume fraction of the collagen fibers in the i^{th} direction with respect to the total volume of the solid matrix and $\Delta\pi$ is the osmotic pressure gradient. The non-fibrillar and fibrillar stress terms are defined per unit area of the non-fibrillar and fibrillar areas respectively.

The non-fibrillar matrix stress can be calculated by the following formula, which depends on the amount of deformation, the amount of solid and shear modulus G_m (Wilson et al. 2006a; Wilson et al. 2007):

$$\boldsymbol{\sigma}_{nf} = -\frac{1}{6}\frac{\ln(J)}{J}G_m\mathbf{I}\left[-1+\frac{3(J+n_{s,0})}{(-J+n_{s,0})}+\frac{3\ln(J)Jn_{s,0}}{(-J+n_{s,0})^2}\right]+\frac{G_m}{J}(\mathbf{F}\cdot\mathbf{F}^T-J^{2/3}\mathbf{I}) \tag{2}$$

where J is the determinant of the deformation tensor $\boldsymbol{F}$.

The fiber Cauchy stress tensor is as follows:

$$\boldsymbol{\sigma}_f = \frac{\lambda}{J}P_f\vec{e}_f\vec{e}_f \tag{3}$$

where λ is the elongation of the fiber, P_f is the first Piola-Kirchhoff stress, and e_f is the current fiber direction. The total Cauchy stress of the fibers is expressed as a function of the deformed surface that a fiber works on. The viscoelastic behavior of the collagen fiber was represented by the two-parameter exponential stress-strain relationship springs S_1, parallel to a spring S_2 in series with a linear dashpot with dashpot constant η. Stresses P_1 and P_2 in springs S_1 and S_2 are calculated as

$$P_1 = E_1(e^{k_1 \varepsilon_f} - 1) \qquad for \quad \varepsilon_f > 0$$

$$P_2 = E_2(e^{k_2 \varepsilon_e} - 1) = \eta \dot{\varepsilon}_v \qquad for \quad \varepsilon_e > 0 \tag{4}$$

with E_1, E_2, k_1 and k_2 positive material constants, ε_f the total fiber strain, ε_e the strain in spring S_2 and ε_v the dashpot strain. Fibers are assumed to withstand tension (positive strains), but not compression. The total fiber stress P_f is the summation of P_1 and P_2 (Wilson et al. 2006a). The values of the model parameters used are (Wilson et al. 2006a): E_1 = 4.316 MPa, E_2 = 19.97 MPa, k_1 = 16.85, k_2 = 41.49, η = 1.424 × 10^5 MPa s, G_m = 0.903 MPa. For formulations of the osmotic pressure and strain dependent permeability the reader is referred to Wilson et al. (2006a, 2007).

5.2.2 Damage model

The mechanics model is extended with a description of damage. Basically, it is assumed that when the deviatoric strain value in the ground substance exceeds a particular threshold, this would soften the matrix. For the fiber network, it is assumed that when the strain in the direction of the fibers exceeds a threshold, these fibers soften. As there may be a distribution of strains in the ground substance or in the collagen fibers, softening accumulates over time when during subsequent cycles a larger portion of the ground substance or fibers become damaged.

This theory is implemented using a damage parameter D, which represents the relative amount of damaged material and has a value between 0 and 1. The effective stress for either the nonfibrillar or the fibrillar matrix then becomes

$$\tilde{\boldsymbol{\sigma}} = \frac{\boldsymbol{\sigma}}{1 - D} \tag{5}$$

The damage parameter D can be expressed as a function of a history variable κ_z, which equals the maximal value of the equivalent strain over time. The damage evolution law for D in the present study is defined similar for the fibrillar and the nonfibrillar matrix as:

$$D = \begin{cases} 0 & if\ \kappa_z \leq \kappa_{0,z} \\ \frac{\kappa_{c,z}}{\kappa_z}\frac{\kappa_z - \kappa_{0,z}}{\kappa_{c,z} - \kappa_{0,z}} & if\ \ \kappa_{0,z} < \kappa_z < \kappa_{c,z} \\ 1 & if\ \kappa_z \geq \kappa_{c,z} \end{cases} \tag{6}$$

where $\kappa_{0,z}$ is the value of κ_z at which damage starts, and $\kappa_{c,z}$ is the value of κ_z at which the total tissue is damaged ($z = \{f, nf\}$ for the fibrillar (f) and nonfibrillar part (nf)).

For the equivalent strain (ε_{eq}) in the collagen fibres the strain in the direction of the collagen fibers was used:

$$\varepsilon_{eq,f}(\vec{x}) = \varepsilon_f(\vec{x}) \tag{7}$$

and for the nonfibrillar matrix the deviatoric strain equals:

$$\varepsilon_{eq,nf}(\vec{x}) = \frac{1}{3}\sqrt{(\varepsilon_{p1}(\vec{x}) - \varepsilon_{p2}(\vec{x}))^2 + (\varepsilon_{p1}(\vec{x}) - \varepsilon_{p3}(\vec{x}))^2 + (\varepsilon_{p2}(\vec{x}) - \varepsilon_{p3}(\vec{x}))^2}$$

(8)

where ε_{pi} are the principal strains.

In a uniaxial stress situation, and assuming that the equivalent strain equals the axial strain, Eq. 6 results in linear softening, followed by complete loss of stiffness at $\kappa_{c,z}$ (Figure 1).

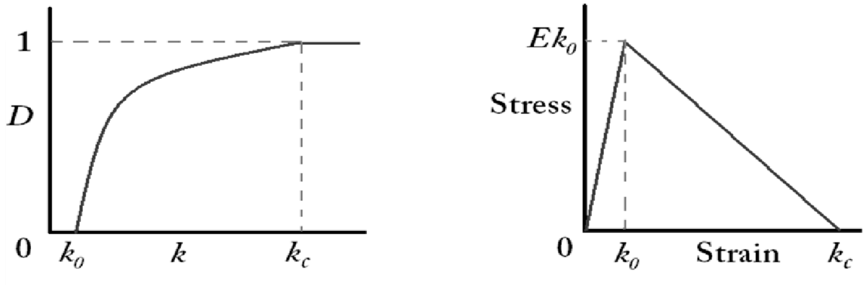

Figure 1 *Damage model, showing the damage variable (D) as a function of the strain history variable (κ, ranging from κ_0 to κ_c)* ***left*** *and the corresponding softening of the constituent, visualized by the stress-strain behavior of the tissue* ***right****.*

Damage thresholds ($\kappa_{0,z}$, $\kappa_{c,z}$) for the fibrillar and nonfibrillar matrix are based on data from the literature (Williamson et al. 2003; Haut 1986; Wang 2006; Stammen et al. 2001). For the fibrillar part, it is assumed that damage start at 8% strain, and that damage is complete at 18% strain in the fibre direction ($\kappa_{0,f}$ = 0.08; $\kappa_{c,f}$ = 0.18). The more compliant ground substance is assumed to be damaged at strains above 30%, with complete failure at 60% strain magnitude ($\kappa_{0,nf}$ = 0.30; $\kappa_{c,nf}$ = 0.60).

It should also be mentioned that though the continuum damage modeling as developed above seems mathematically true and physically meaningful, computational solutions may fail to converge to a meaningful result as a consequence of refinement of the spatial discretization (mesh-dependent results). This is because of the fact that when damage occurs in one finite element, due to increase in load, damage in that specific element with specific thickness starts to grow and that specific element experiences inelastic unloading (softening or post-peak regime) while the neighboring elements yet do not reach the criterion for damage initiation so they are unloaded elastically to keep the force balance in the whole system. By decreasing the element size, damage accumulation only happens in the same region but in the new smaller elements. This mesh dependency is not so much due to the numerical implementation, but rather due to a shortcoming of the underlying continuum theory, which results in a localized damage accumulation (Peerlings et al. 1998; Peerlings 2007). In case simulations remain in the stable material regime, then the use of a local model such as developed here will be acceptable, otherwise in order to trust the results and making sure that they are physically meaningful mesh independency of the results must be checked and satisfied.

5.2.3 Simulations

A 2D model of articular cartilage (5.5 mm wide, 1 mm high; 1950 pore pressure plane strain elements with 4-node bilinear displacement CPE4P) was loaded with a round-end impermeable indenter (1 mm diameter) (Figure 2) in ABAQUS 6.10 (Abaqus Inc., Providence, RI). The bottom is fixed in all directions to represent cartilage attachment to bone. Water is free to leave the tissue from the sides and top of the sample in which there is no contact with the indenter. The spatial distribution of PG and collagen, and the orientation of collagen are taken from the literature (Wilson et al. 2006a; Wilson et al. 2007).

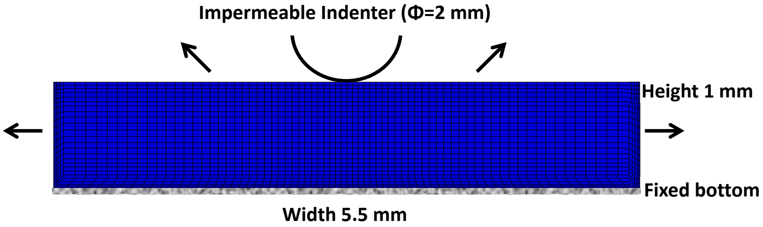

Figure 2 *2D Finite element mesh of the cartilage sample and the indenter. The bottom is fixed to simulate attachment to the bone. Arrows indicate free surfaces with unrestricted water flow.*

First, the tissue was allowed to equilibrate for 8 hours in 0.15 M solution, during which the tissue swelled approximately 1%. Subsequently, the indenter compressed the tissue in four steps of 10% compression to 10, 20, 30 and 40% of the original tissue height at a strain rate of 0.1% s^{-1}. Each loading step was followed by 2 hours of stress-relaxation. This protocol is simulated for four different conditions. First, a control case in which no damage was allowed to develop in the cartilage (No damage). Second, damage was only permitted to develop in the fibers (Fiber damage only). Third, damage was only permitted to develop in the ground substance (Ground substance damage only). Fourth, damage was permitted develop in both the fibers and the ground substance (Both fiber and ground substance damage). Fiber damage is computed at each location for each fiber in the six directions. For visualization purpose, the total fiber network damage per location is represented as the average damage in all fibers and weighted for their respective densities (Eq. 9):

$$D_{FibrillarNetwork} = \frac{C(D_{P1} + D_{P2}) + D_{S1} + D_{S2} + D_{S3} + D_{S4}}{2C + 4} \quad (9)$$

where D_P and D_S are the damage parameter in each primary and secondary fiber direction respectively and C = 3.009, which is the relative density of the primary fiber direction with respect to the secondary fiber directions (Wilson et al. 2006a).

In addition to the simulations described above, the possible effect of localization of damage has been studied by comparing simulations with different mesh sizes. More specific, the results of the simulation of ‘Both fiber and ground substance damage’ is compared with a separate simulation with a double finer mesh size to check the effect of mesh dependency.

5.3 Results

As the loading increased, damage developed in both the fibrillar network and ground substance. The area where damage occurred was different for the two components (Figure 3a-d). These locations remained largely the same, regardless of whether damage occurred in only one of the components (Figure 3a,b) or in both (Figure 3c,d), but if both were allowed to occur, the ground substance damage penetrated deeper and fiber network damage was enhanced (Figure 3e).

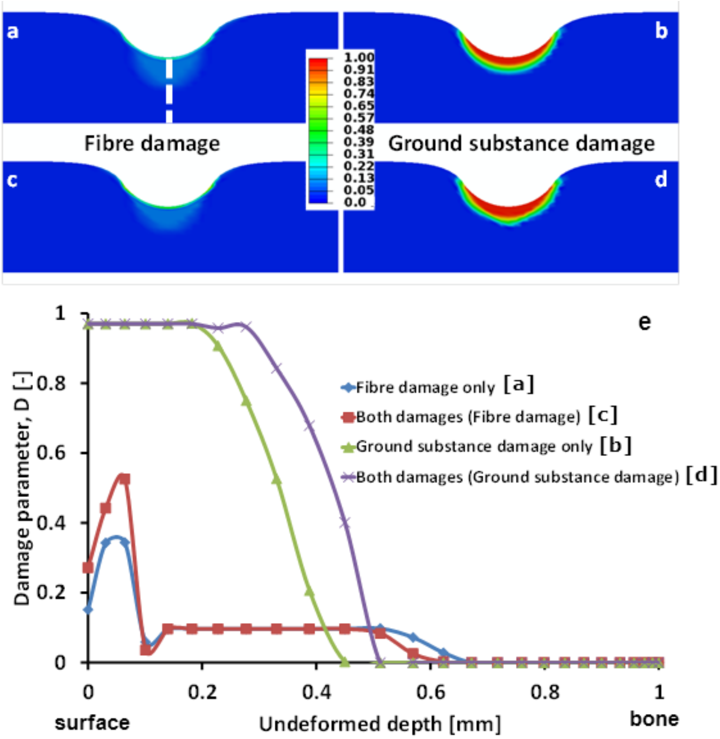

Figure 3 *Damage distribution in the fibers* ***(a,c)*** *and the ground substance* ***(b,d)*** *at the end of the loading protocol when only fiber damage* ***(a)****, only ground substance damage* ***(b)****, or both are allowed to occur in parallel* ***(c,d)****. Colors represent the magnitude of damage parameter D, which is quantitatively shown in* ***(e)*** *as a function of depth from the surface (0 mm) to the bone (1 mm) over an imaginary line centrally under the indenter (indicated as a dash line in* ***(a)****).*

To obtain a better insight in the damage development, ground substance and fiber matrix damage were evaluated separately and as a function of the depth of indentation. Ground substance softening started at the surface and gradually developed deeper into the tissue (Figure 4a). Maximal damage remained located at the surface, and there was a steep transition from highly damaged areas to deeper undamaged regions. Initial superficial damage started already at 10% indentation loading, because even at this low external indentation, due to the round shape of the indenter the local strains inside the tissue exceeded 30%.

Damage in the fiber network started in the transition zone, i.e. in the area underneath the surface, while the superficial zone remained intact (Figure 4b). When the indentation depth reached higher strain levels, damage penetrated into the deeper areas of the cartilage, while more intense damage occurred in the superficial zone (Figure 4b).

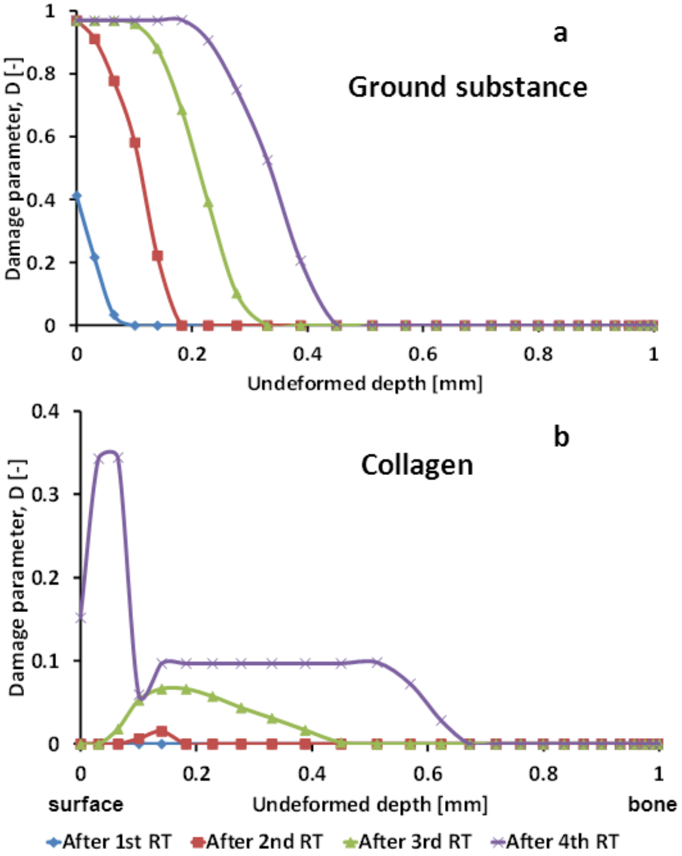

Figure 4 *The profile of damage at the end of the stress-relaxation period following each of the four subsequent loading cycles shows progression of the damage over time. The horizontal axis represents an imaginary line centrally under the indenter from the surface (0 mm) to the bone (1 mm), similar to Figure 3e.* ***a*** *damage in the ground substance,* ***b*** *damage in the collagen fiber network.*

The magnitude and location of fiber damage varied with the fiber direction. For fibers parallel to the surface, which are part of the pool of secondary fibers, the damage was more severe than for perpendicular or oblique fibers (Figure 5). Secondary fibers show more intense damage underneath the surface, while primary fibers are damaged in the superficial zone after more severe loading (Figure 4). Due to the lower volume fraction of the secondary fibers their effect on the total stress might be less than the effect of the damage in the primary fibers. The fibers in vertical direction did not damage because they did not undergo tension during the applied loading protocol, while oblique fibers did not damage because the strain in their direction did not exceed the threshold ($\kappa_{0,f}$ = 0.08) (data not shown).

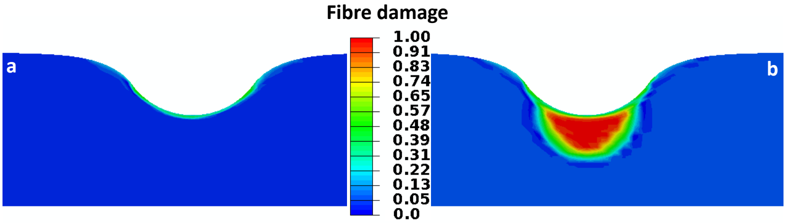

Figure 5 *Damage in the fibrillar network was dependent on the fiber orientation, as shown here for the simulation in which fiber damage was only allowed to occur.* ***a*** *damage in one of the primary fibers with an arcade-like orientation.* ***b*** *damage in the secondary fiber compartment that has a horizontal orientation.*

Compared with undamaged cartilage, the peak force and the equilibrium relaxation force decreased when damage developed in the tissue (Figure 6). The magnitude of these changes depended on the nature of damage, with ground substance softening reducing the stiffness more than fiber damage.

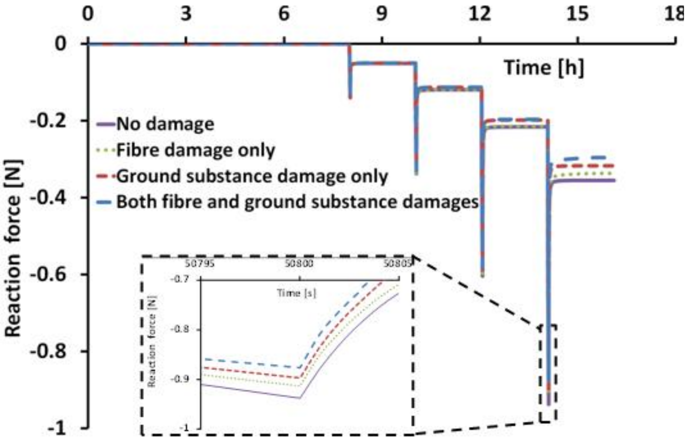

Figure 6 *Reaction force during the four simulations over time, where strain was increased to 10, 20, 30 and 40% after 8, 10, 12 and 14 hours, respectively. A magnification is included of the peak values after 40% strain was applied.*

Moreover, the local damage in the tissue not only changed the local effective stress, but also the distribution of strains inside the tissue, as illustrated by maximum principal strain at the end of the 40% indentation (Figure 7). Compared with the strain distribution in undamaged tissue (Figure 7a), the distribution of strains was less affected by softening of the ground substance (Figure 7c) than by damage in the fibers (Figure 7b,d). When both damages are present, the effect on strain was most distinctive, with sharp transition areas centrally under the surface (Figure 7d).

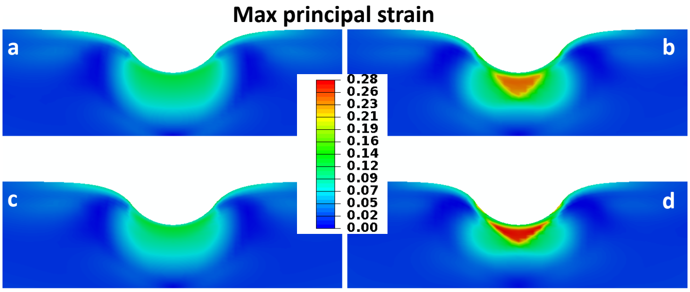

***Figure 7** Maximum principal strain distributions, 2 hours after 40% indentation was applied, in case no damage was allowed to develop **(a)**, or damage developed in the fibers **(b)**, the ground substance **(c)** or both **(d)**.*

The effect of localization of damage is checked by comparing simulations with two mesh densities. The damage distribution for both ground substance damage and collagen fiber damage are slightly different between these meshes (Figure 8), although the damage pattern remains qualitatively comparable. Similarly, there is a minor effect on the reaction force (Figure 9) and peak stress (data not shown) in the relaxation experiment.

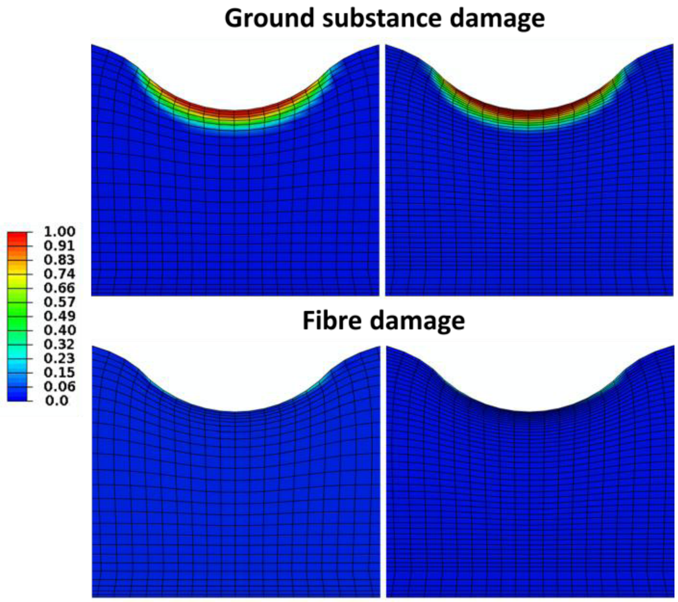
Ground substance damage
1.00
0.91
0.83
0.74
0.66
0.57
0.49
0.40
0.32
0.23
0.15
0.06
0.0
Fibre damage

Figure 8 *Ground substance damage **(Top)**, the fiber damage **(Bottom)** at the end of 30% compression for original mesh (the mesh used in all other simulations) **(Left)** and double finer mesh **(Right)**.*

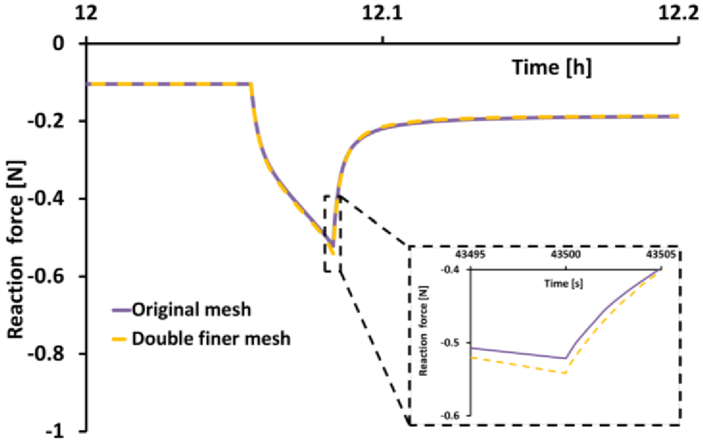

Figure 9 *Reaction force during the 30 % compression for the simulation 'Both fiber and ground substance damage' for the two different mesh densities. A magnification of the peak values is included.*

5.4 Discussion

A damage progression model for articular cartilage is presented, based on an established composition-based model for cartilage mechanics. It can independently predict the development of softening in the ground substance and damage in the fibrillar network over time and as a function of mechanical loading. The model is employed to evaluate theoretical effects of ground substance softening and collagen damage on tissue softening, and to explore whether damage in the ground substance may advance damage in the collagen network and vice versa. Ground substance softening is predicted to develop over a larger area than collagen damage under the applied indentation loading (Figure 3). Cartilage softening, an important measure for cartilage function, is affected earlier and to a greater extent by damage in the ground substance than by collagen damage. Softening due to ground substance damage is promoted by additional collagen damage (Figure 6). Collagen damage has a more pronounced effect on the magnitude and distribution of strains inside the tissue, and this effect is more prominent when the ground substance is allowed to soften simultaneously (Figure 7). The concentration of high strains and the strain gradients that develop underneath the surface in the transitional zone (Figure 7 b,d) seem unfavorable and may be speculated to be detrimental to the cartilage in the long term, possibly also via effects on chondrocyte viability. Summarized, the simulations suggest that ground substance softening is more essential to cartilage softening, while damage to the collagen induces an unfavorable strain field in the tissue. Additionally, due to mechanical interaction between the ground substance and the collagen fibers, damage to either one of them can promote damage in the other. Alternatively formulated, the results suggest that if the components are intact, they protect each other from developing damage.

The above conclusions, however, need to be considered with care. They depend on the validity of the model, and the presented model has not yet been validated thoroughly against experimental data. It is an extension of a validated composition based model for cartilage, which includes reinforcement with a visco-elastic fiber network, and biphasic swelling. The biphasic swelling approach was analytically validated for swelling values in the physiological range of cartilage (Wilson et al. 2007), and material parameters for swelling, nonfibrillar matrix and the fiber network have been fitted simultaneously to unconfined and confined compression, indentation and free swelling data from the literature (Wilson et al. 2005b; Wilson et al. 2006a).

Subsequently, the model has proven to be valuable to understand several aspects of cartilage mechanics, enforcing the validity of this approach. However, the damage model that is now added has not yet been validated for cartilage. The description using a damage parameter and a strain history variable is common in polymer science (Geers et al. 1999), and the relationship between these parameters that was employed here (Eq. 6) is the simplest version of this approach. Although a more difficult damage law may turn out to apply for cartilage in the future, variations are not anticipated to change the general conclusions. The most important and critical unknown factors are the four values that were chosen as damage thresholds ($\kappa_{0,f}$, $\kappa_{c,f}$, $\kappa_{0,nf}$, and $\kappa_{c,nf}$ (Eq. 6 and Figure 1)). The exact values for these thresholds, which represent damage in a continuum including a range of fibers that may experience different strain magnitudes, are unknown. The values that are used have been estimated from experiments on articular cartilage in which damage was induced by indentation, confined and unconfined loading in tension and compression, and under various loading rates (Williamson et al. 2003; Haut 1986; Wang 2006; Park et al. 2004; Stammen et al. 2001; Haung et al. 2005; Butler et al. 1978; Pins et al. 1997). However, these studies reveal significant variability. Earlier studies showed failure strain of collagen-rich superficial zone cartilage in the order of 25-40% (Kempson et al. 1973; Roth and Mow 1980) which is in agreement with Haung et al. (2005) who neither observed failure in a tensile test of articular cartilage till 16% strain, nor in confined compression till 50% strain, and with computationally predicted failure strains of collagen in the order of 25-30% (Wilson et al. 2006b). These data, however, are measured in intact cartilage and not on collagen fibers. Tearing of collagen in tendons occurred over 4% stretch and macroscopic failure occurred beyond 8–10% strain (Wang 2006; Butler et al. 1978). Failure of self-assembled collagen fibers that were cross-linked at either zero or 50% stretch failed at 15.59% or 11.65% strain, respectively (Pins et al. 1997).

Taking into account their variability in these experimental studies, we implemented collagen damage to start failing at strains of 8%, and assumed complete failure would have occurred when strain was 10% more. The ground substance is assumed to be more compliant than the reinforcing collagen network, because otherwise the collagen would not be effective. Hence, ground substance softening was assumed to start at 1.5 times the strain at which collagen was assumed to rupture (30%), and to completely fail at double that strain. To evaluate the effect of the chosen parameter values for $\kappa_{0,z}$ and $\kappa_{c,z}$, a simple parameter variation study was performed.

Although the size of the affected area and the magnitude of damage depend on these values, the locations of damage, the patterns of damage progression over time, and the nature of the interaction between damage in the ground substance and the collagen fibers are insensitive to these parameters. This insensitivity is also illustrated by noting that damage initiates earlier and progresses more rapidly in the ground substance than in the fibers (Figure 6), even though $\kappa_{0,nf}$ for the ground substance is three times larger than $\kappa_{0,f}$ for the fibrillar network.

Although full validation of the damage model has not yet been performed, the output may be compared with literature data to evaluate the predictions. Reduction in mechanical properties over time with progression of tissue damage (Figure 6) is known to occur experimentally and clinically (McCormack and Mansour 1998; Kleemann et al. 2005; Hosseini et al. 2013a; Temple et al. 2007; Buckwalter et al. 1994; Langelier and Buschmann 2003; Kempson et al. 1973; Akizuki et al. 1987). In agreement with the present findings (combine Figure 4 and Figure 6), it has been shown that cartilage softening after indentation already occurs before collagen damage can be observed (Hosseini et al. 2013a). Also, the prediction that compromised ground substance may affect the failure mechanics of collagen and vice versa, was previously observed, although this involved tensile testing and not compression (Kempson et al. 1973). The regions in which damage is predicted to occur are probably the best data for validation. The location of predicted ground substance damage matches with experimental and clinical observations of PG loss (Wilson et al. 2006b; Lin et al. 2004; Wu et al. 2002; Hollander et al. 1995; Lorenz and Richter 2006). Loss of saffranin-O staining starts at the articular surface (Lin et al. 2004) and this area increases with increased loading, while a sharp transition remains between the PG-rich and the PG-poor tissue (Lin et al. 2004). This concurs with the predictions (Figure 3b,d,e and Figure 4). It should be noted that PG loss was not incorporated as such in the model, because ground substance weakening was assumed to occur, but the fixed charge density remained constant. However, it makes sense that damaging of the ground substance precedes the loss of PGs. The rationale is that excessive straining may fracture the PGs into smaller fragments, which would subsequently be able to diffuse out of the tissue into the synovial fluid. However, this takes time, which may explain why no loss of PGs was seen immediately after damage was induced by indentation (Hosseini et al. 2013b).

Collagen damage also increases with tissue loading. Intense staining for collagen damage is found selectively in the superficial zone of human OA cartilage, while more diffuse collagen damage penetrates deeper into the tissue over a larger area (Lin et al. 2004). It has been shown that the deeper and diffuse collagen damage may precede the more intense damage in the superficial zone when excessive indentation is applied (Wilson et al. 2006b). Also, collagen already exhibits impaired load bearing properties already in very early OA tissue (Thambyah et al. 2012). All these data suggest that the collagen network may be mechanically compromised in the transitional or deeper zone before visible damage such as fissures become apparent at the surface. This is in agreement with the present predictions. Finally, the peculiar triangular pattern of strains and the sharp transition between high and low strained areas in the tissue corresponds with recent publications on internal collagen structure in severely loaded articular cartilage as observed with DIC (Bevill et al. 2010). Even though the loading protocol that was used in the latter study was different (single vs. double indenter) it may be speculated that the strains penetrated similarly into the tissue. In a previous numerical study using the same composition based model employed here (Hosseini et al. 2013b), yet without damage, the global strain patterns of the experiments by Bevill et al. (2010) were corroborated. However, the sharp transitions were not seen in the model, which may now be speculated to be caused by initial tissue damage in the experiments (Bevill et al. 2010), which was not included in former simulations (Hosseini et al. 2013b).

To the best of our knowledge, it is for the first time that a damage model has been used for a fibril reinforced poroviscoelastic model of articular cartilage. It was employed to study the damage initiation and progression in each component of cartilage as well as the interaction between them for promoting damage. The relatively simple linear softening damage evolution law has the advantage that only two parameters govern the damage evolution for each component of the cartilage ($\kappa_{0,z}$, $\kappa_{c,z}$). Though these parameters are unknown for articular cartilage, since they have a clear physical meaning it is possible to find acceptable values for them in literature. More advanced exponential (Mazars and Pijaudier-Cabot 1989; Peerlings et al. 1998) and modified power-law softening (Geers et al. 1998) exist, but these laws have the drawback that the number of unknown parameters increases, which would have to be fitted to relevant experimental data. Unfortunately, such data is sparse for cartilage. The goal of this study was to gain more understanding in the role of collagen and proteoglycans damage during damaging of cartilage. Hence, it was not the goal to obtain the perfect set of unique material parameters, or to provide an in-depth quantitative interpretation of the results. Therefore, the choice for the damage model is less demanding.

However, the results should be interpreted with care because a local damage model has been used. This means that damage predicted by the present model may localize in particular elements, in this case the damage model becomes ill-posed. Alternative non-local damage models use a characteristic length scale that smoothen the effect of deformation and damage and therefore precluding localization. In gradient-enhanced models, similar to the nonlocal models, discontinuities are smoothened so that strains remain finite (de Vree et al. 1995; Peerlings et al. 1998; Peerlings 2007). However, the use of present local damage model is acceptable, provided that the simulations stay within the stable part of material mechanical behavior. Otherwise, if mechanical stability is lost, the model becomes ill-posed and numerical solutions become physically meaningless due to localization. The results contain several indications that the effect of localization was minor. First, Figure 3 a-d and Figure 5 show that damage in neither the fibrillar network nor in the ground substance has accumulated in one specific element or a number of specific neighboring elements, but is rather smooth. The smooth curves in Figure 3e and the strain distribution in Figure 7 support this idea.

Yet, the best way to check for localization in the present simulations is by evaluating whether there is a mesh-dependency in the solution. Indeed, the distribution of damage in the collagen network shows slight mesh dependency (Figure 8). Similarly, mesh-dependency had a minor effect on the peak-load and the relaxation curve, indicating a small effect of localization. However, in agreement with the above arguments, it is shown that these effects were small and the overall locations of the damage pattern and the stress-relaxation curves remained similar and physiologically realistic.

There are several reasons why the material may remain mechanically stable, and localization and mesh dependency in our simulations may be limited. First, even when the ground substance loses stiffness, the collagen fiber network consisting of fibers in different directions still reinforces the cartilage material. Second, the viscoelasticity of the collagen fibers partially may contribute to keep the mechanical behavior of the whole system in a stable region. Third, the hydrostatic swelling pressure remains present, and this has a significant contribution to the stability of the model when the stiffness of the ground substance or collagen fibers drops. Fourth, the nature of experiment, which involves step-wise stress-relaxation, allows the tissue to equilibrate under constant strains. Therefore, possible localization effects are not continually affecting the results, and their effects are not as significantly as they would be under a regular tensile test in which the tissue is continually elongated.

Also, 3D rather than 2D modeling may be required for particular future studies. However, this is not essential for the first assessment of the interaction between ground substance softening and collagen damage, which is the objective of the present study.

5.5 Conclusion

A cartilage damage progression model is proposed and employed to explore effects of ground substance softening and collagen fiber damage on cartilage mechanopathology. Even though thorough validation is still required, predictions of the locations and magnitudes of damage in both constituents, and the effects thereof on cartilage softening and tissue strain corroborate well with the literature.

Based on the results, it is concluded that damage to the ground substance has more pronounced effects on cartilage softening, while damage to the collagen network results in adverse strain localizations inside the tissue. Importantly, it is shown that damage to either one of them can promote damage in the other, while an intact collagen network may protect the ground substance from softening and vice versa.

Chapter 6

General Discussion

CHAPTER 6

6.1 Discussion

Osteoarthritis (OA) is a degenerative disease of synovial joints characterized by pain and disability, and involves damage of articular cartilage and changes to the underlying bone. By the age of 55 to 65 years, up to 85% of all people have some degree of OA in one or more joints. Earlier changes in the joints associated with the development of OA may already occur in young people. Since articular cartilage is an avascular tissue that has very low capability of repair, such damage is progressive, for younger patients, joint-preserving treatments are aimed for, which include modern techniques such as Autologous Chondrocyte Transplantation (ACT) or Matrix-associated Chondrocyte Transplants (MACT), established techniques such as debridement or mosaic plasty (OATS), and joint-loading modification through joint-distraction or osteotomy. However, the clinical outcome of these interventions is suboptimal, partly because treatment is performed at relatively late stages of the disease. It is hypothesized that earlier intervention would be preferred for the more aggressive cases. However, to identify those cases is difficult. Thus, it is of interest to predict the time course of damage progression in cartilage. It is believed that mechanical overloading plays a crucial role in OA initiation and progression. Therefore, to understand OA development, insight into the mechanical conditions inside the cartilage is required.

Computational models, in particular using the finite element method, enable to study the mechanical conditions in cartilage tissue under physiological or pathological loading regimes. Many computational models have been developed and used to simulate and analyze articular cartilage. Mostly these models investigate stress or strain distribution inside the cartilage, trying to correspond the regions of high stress or strain concentration to damaged regions in actual cartilage tissue. However, to the best of our knowledge, there has not been any fiber reinforced computational model, which actually uses damage mechanics, to investigate damage initiation and progression in different components of cartilage tissue.

In this thesis, we have addressed this important research area on the mechanically induced damage of cartilage components. This was approached using both experimental and computational approaches. In our experiments, we aimed to determine the loading threshold, which triggers very early cartilage softening, and we aimed to evaluate whether collagen damage would be causing this softening. The results of the experiments provided us with the observation that softening occurred, which was apparent from a reduction in the reaction force, even though there was no collagen damage visible in immunohistological staining. This observation invalidated our hypothesis that cartilage early softening starts from collagen damage.

However, full interpretation of the experimentally observed cartilage softening remained difficult, because part of the softening may have been caused by a slow time-dependent tissue response.

Mechanical overloading not only affects the structural organization of the tissue that might lead to softening and damage but also at the same time depending on the loading condition it affects the viscoelastic and poroelastic response of the tissue. Reaction force, the parameter that we measured in our experiments is the resultant of all the changes that happen in the tissue. That is why it is very difficult to correlate the reaction force changes to a specific phenomenon, namely damage or change in time dependent characteristics. From our experiments, it remained speculative which effect caused the softening that we observed. The damage did not affect any parameter directly related to fluid flow, because peak loading did not change the time-constant, and the damage not only affected the peak stress, but also the equilibrium stress level during which fluid flow is absent. Therefore, we proposed that the observed decrease in reaction force might have originated from damage in either the fibrillar or the non-fibrillar components of the tissue, or both. However, we could not exclude another possible explanation for the observed softening phenomenon, which is that long-term intrinsic viscoelastic effects in the collagen PG matrix are responsible. Therefore, in Chapter 4 and 5, we investigated each of these two possibilities separately, using our cartilage model.

We concluded that the time-dependent response of a tissue to mechanical loading is very complex, because of the interaction between two separate non-linear and time-dependent effects: one related to collagen matrix viscoelasticity and one to flow-dependent poroelasticity. Fundamentally, if one of them is not in equilibrium, then by definition the other one is not in equilibrium as well. Previous studies have suggested that the choice of preconditioning strain may influence the equilibrium condition as well as the measured properties (Carew et al. 2000; Carew et al. 2004; Pinto and Patitucci 1980; Woo 1982; Sverdlik and Lanir 2002; Gefen et al. 2003). The load level at equilibrium greatly depends on the loading applied to the tissue. June et al. (2009) also reported that cartilage stress relaxation proceeds slower at higher compressive strains.

Cheng et al. (2009) suggested that “the preconditioning strain should be reported and the highest strain being used in the study should be used for preconditioning. This is important to allow meaningful comparison of test data within the study and also with other studies.” Our investigation on the effect of preconditioning and the fact that the reaction force of the cartilage is influenced by recovery time in a repetitive loading regime strengthens the idea that part of the softening behavior observed in our experiments may not occur because of structural damage in the cartilage samples, but may be due to the time dependent behavior of the tissue. To explore the other possible explanation of our experimental results, which is that structural damage occurred in the cartilage samples, a damage progression model for articular cartilage has been presented, based on an established composition-based model for cartilage mechanics. It can independently predict the development of softening in the ground substance and damage in the fibrillar network over time and as a function of mechanical loading. The simulations suggest that ground substance softening is more essential to cartilage softening, while damage to the collagen induces an unfavorable strain field in the tissue that might lead to further progression of damage. Additionally, due to mechanical interaction between the ground substance and the collagen fibers, damage to either one of them can promote damage in the other.

In addition to the softening at the very early stages of cartilage damage and osteoarthritis, fibrillation, clefts and fissures occurring at the surface of the tissue and penetrating into the deep zones of cartilage are among the signs of cartilage damage and osteoarthritis. These phenomena will reduce the functionality of the cartilage tissue, because it compromises the distribution and transfer of the load in the joint. In this thesis we employed our cartilage code to investigate the role of the superficial tangential zone of the cartilage. Our findings show that the mechanical importance of the superficial zone comes from both the architecture of the collagen fibers as well as the variation in ECM composition through the depth of the tissue. The horizontal orientation of the collagen fibers on the surface of the tissue is significant to avoid concentration of mechanical deformation on the directly loaded regions. Using the horizontal direction of the collagen fibers, cartilage distributes the applied loads from the directly loaded to the neighboring unloaded regions. Glaser and Putz (2002) also observed that superficial zone of cartilage distributes the loads to larger portions of the contact area rather than only the directly loaded regions. They also concluded that this capability of the superficial zone that prevents localization of loading contributes to avoid peaks of surface tensile strain. Several authors considered that any kind of damage to the superficial zones facilitates the development of damage to other regions on the surface as well as in the deeper zones and consequently the chances for OA to occur increases remarkably (Saxena et al. 1991; Cotta and Puhl 1970; Roth and Mow 1980; Thambyah and Broom 2006; Thambyah et al. 2009; Bevill et al. 2010).

The above discussion of the logic and approach taken in this thesis to understand aspects of cartilage damage is schematically represented in Figure 1.

At the start of this project, the cartilage mechanics model existed and was already published (e.g. Wilson et al. 2006a). In Chapters 2 and 4, this model was applied to study effects of early cartilage damage, i.e. STZ damage and tissue softening. Chapter 5 presented for the first time an extended model that includes the actual development of cartilage damage over time. This model allowed us to study the mechanical behavior of articular cartilage when structural changes due to overloading occur. It revealed how damage in the fibers and in the ground substance may individually develop, and how these components may interact with each other while damage is progressing. Even though the model may require further enhancement and quantitative validation is pending, this work has provided significant insights in the etiology of early cartilage damage development. Also it has provided input for the development of new hypotheses, which are presently being explored experimentally in our group.

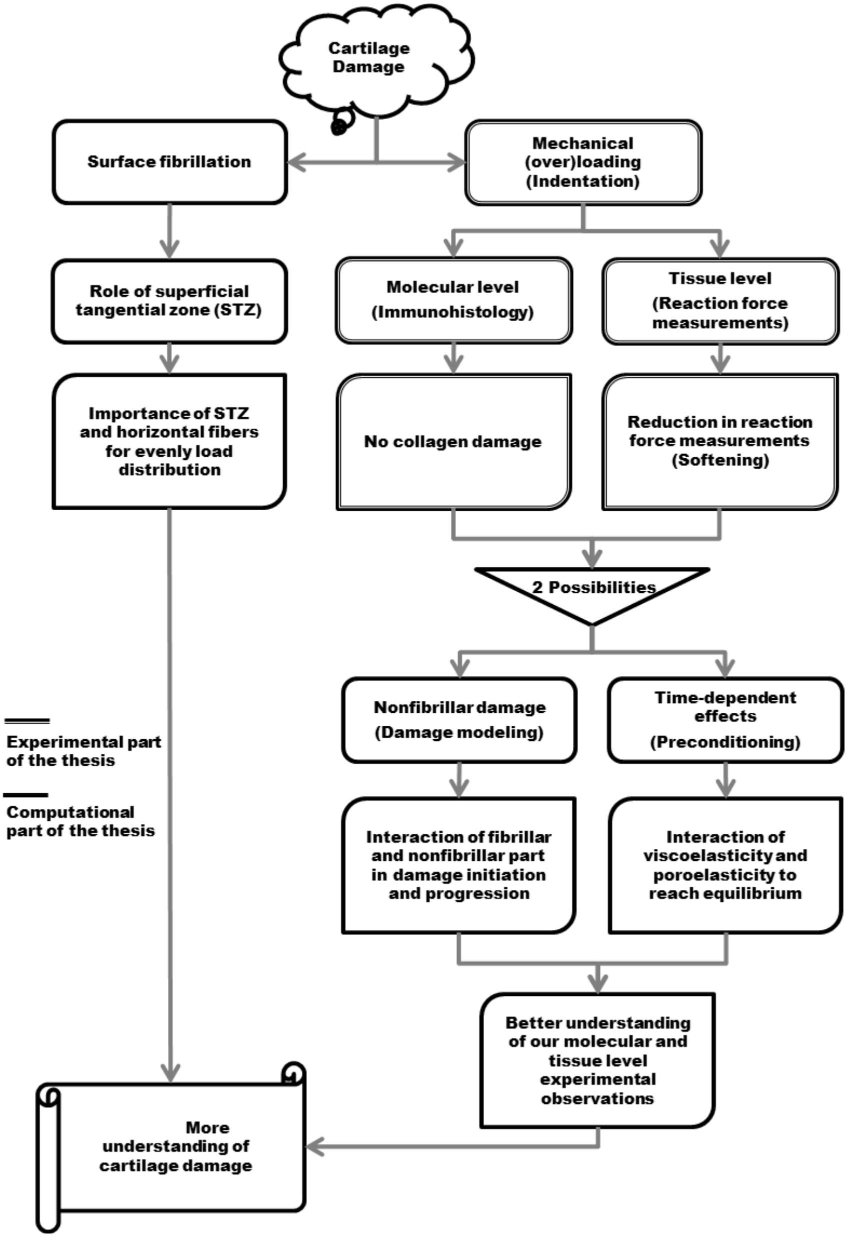
Cartilage Damage
Surface fibrillation
Mechanical (over)loading (Indentation)
Role of superficial tangential zone (STZ)
Molecular level (Immunohistology)
Tissue level (Reaction force measurements)
Importance of STZ and horizontal fibers for evenly load distribution
No collagen damage
Reduction in reaction force measurements (Softening)
2 Possibilities
Nonfibrillar damage (Damage modeling)
Time-dependent effects (Preconditioning)
Experimental part of the thesis
Computational part of the thesis
Interaction of fibrillar and nonfibrillar part in damage initiation and progression
Interaction of viscoelasticity and poroelasticity to reach equilibrium
Better understanding of our molecular and tissue level experimental observations
More understanding of cartilage damage

Figure 1 *The schematic representation showing the logic and approach taken in this thesis to understand some aspects of cartilage damage as well as an indication of an overview of how the individual studies of this thesis fit together.*

6.2 Recommendations for future studies in the field cartilage damage

6.2.1 Follow up of the present work

In our experiments, after applying load to the samples that resulted in softening, we find neither collagen damage nor PG loss in the histology sections. We proposed that the collagen network was damaged; however, we were unable to capture this damage with the Col2-3/4M staining. Actually, this method has proven to be very sensitive in the past to stain collagen that was damaged by both excessive tensile and shear loading (Wilson et al. 2006b). Yet, we cannot exclude that a loss of crosslinking or entanglement could have occurred, which may have led to a rearrangement of the collagen network. To observe such effects would require investigation of loaded articular cartilage at an ultrastructural level, for instance using electron microscopy.

In our computational modeling of cartilage damage, so far we investigated damage initiation and progression of early damage, before macroscopic damage can be observed. There are several options, which can be added to this computational model. Speculating on the damage mechanisms that may occur, collagen fibers may rupture upon excessive straining. Similarly, PG aggregates may breakdown into smaller fragments, and the connectivity between aggregates may be lost. This would likely result in matrix softening. As a consequence, the smaller PG fractions may diffuse out of the cartilage, thus causing the loss in Safranin O staining in the damaged region. We did not observe such a loss of PG staining in our samples, which were frozen immediately after damaging. It is possible that PG fragments should be given a longer time to diffuse out of the tissue, which could be the topic of a future study.

If PG loss would occur over time, it would not only affect the stiffness of the ground substance, but it would also lower the fixed charge density in the tissue. This effect of PG loss has not been considered in the present model, but it is well possible to add this to the damage progression model in the future. Also, PG diffusion and leakage over time could be implemented.

The other extensions relate to the damage model and the way it can be implemented. In this work, we have employed the linear softening damage evolution law. There are also other softening models such as an exponential and a modified power-law. Since the mechanical behavior of both collagen fibers and the ground substance are not linear, these two models may be more accurate. However, it should be noted that these models have more parameters, which make them more difficult to measure and validate. Moreover, the damage model in this work has been implemented in a local way. However, to improve this work and in order to prevent localization (mesh-dependency), theoretically it is better to use a nonlocal or enhanced gradient method for the damage evolution (de Vree JHP et al. 1995; Peerlings et al. 1998, Peerlings 2007). Future developments and experimental data sets will be required to further develop the damage evolution law for collagen and PG in cartilage.

6.2.2 Towards a clinically viable tool

The ultimate aim of the present model development is to use it as a tool that can be used to predict progression of OA, given current conditions of the joint and the patient. A key question that such model may for instance help to answer, is whether for a particular patient, OA progression will be aggressive or mild, and under which circumstances adaptive or degenerative responses would prevail. To develop a tool that can assist in making such difficult prognostic evaluations will be very challenging, and we will have to overcome significant hurdles before the present cartilage damage model will become a clinically viable tool. These include factors related to obtaining patient-specific model input, the model itself, validation of the predictions, and the ultimate practical implementation in the clinic.

The model is based on the finite element method, by which realistic geometries can be created, and an advanced cartilage material model that includes realistic contents and structure of the constituents. In principal, these are all measurable in explants. However, it is most challenging to include patient-specific tissue geometry, patient-specific tissue structure and composition and patient-specific tissue loading conditions. For the geometry, it may be speculated that the development of high-resolution imaging techniques based on X-ray and MR, in combination with the developments in automated image analysis and segmentation may make it possible in the future to use patient-specific geometries.

However, within this geometry, quantitative patient-specific spatial distributions of tissue structure and composition are also required, and this poses a more significant challenge. This is especially important when aiming for the identification of early OA, when the tissue softens and the contents change, yet the geometry is still relatively normal. Advances in the field of MR imaging are promising and may eventually be able to deliver the requested data. For instance, it is possible to derive biomechanical properties of cartilage (Niemminen et al. 2004; Julkunen et al. 2008b; Julkunen et al. 2013) the arrangement of the collagenous network (Nieminen et al. 2001; Xia 1998), spatial variations in PG content (Nissi et al. 2004) and fixed charge density distribution (Silvast et al. 2009) from MRI measurements. It may be expected that such data can also be derived from patients in the future. Finally, patient-specific loading conditions may already be derived from human movement analyses in an inverse approach.

With patient-specific input, the prediction of damage progression by the model will also become patient-specific. However, even when appropriate patient-specific input data would be available, it is a major computational challenge to perform realistic simulations using all these data. The model would have to include the presently used material model for cartilage, and at the same time capture the realistic joint geometry in 3D. This requires a very large number of elements, and consequently long computation times. In addition, joint kinematics is important for the development of OA throughout a joint. This poses additional requirements to the model. For instance, kinematic constraints such as ligaments, menisci and muscle forces will have to be incorporated. Although such simulations are presently impossible, the developments of faster computers and computational approaches may make such simulations possible in the future. In addition to more advanced numerical implementation of damage development, as discussed before, a cartilage degeneration model would also have to include the biological response to (adverse) mechanical loading, as well as a repair response to the damage. Modeling such responses in physiologically realistic ways is another major challenge that we have only started to dive into. Of particular interest are computational models that are being developed to understand the development of cartilage under well-controlled conditions during tissue engineering.

When these developments are complete, the next challenge is to validate that this model can indeed be used to objectively predict the time course of OA progression in a patient-specific manner. Simulations of OA progression should be performed, starting with patient-specific input data. For tuning and subsequent validation, computed predictions of structural and compositional changes in cartilage and bone should be corroborated against data from prospective clinical studies that include imaging data of OA progression at various stages of the disease. Such data are presently being collected in various studies in the world, for example in the Genetics, Arthrosis and Progression (GARP) study at the Leiden University Medical Center in The Netherlands.

After model validation, the final challenge is to implement a numerical tool into clinic practice. Collaboration with clinicians during the validation phase or even earlier, will be essential, but is in itself insufficient to achieve this. Likely, it requires participation of people with engineering backgrounds, such as medical engineers who are currently being trained in our own department as well as elsewhere around the world.

In conclusion, major challenges will need to be overcome before the model in its present form may become a clinically viable tool. Some of these hurdles cannot be taken with the present technical possibilities. However, there are significant developments in each of these areas, which may enable their use when time comes. Therefore, the development of a clinically useable cartilage damage progression will remain at the forefront of what is technologically feasible.

6.3 General conclusion

In conclusion, the first steps in the development of a damage model have been taken in this thesis. Starting from a fibril reinforced poroviscoelastic swelling model, which is a composition-based approach to model cartilage mechanics, damage was introduced such that it could be attributed to particular aspects of the tissue, i.e. to collagen or ground substance. Although further validation of the model is required for early as well as more progressive tissue damage, the potential benefits of this model are apparent. It opens possibilities for understanding fundamental aspects of OA initiation and progression. For instance, it allows unraveling the specific effects of collagen damage or ground substance weakening, which in turn provide significant complementary insights to experimental studies using tissue explants or animals.

References

Akizuki S, Mow VC, Müller F, Pita JC, Howell DS, Manicourt DH (1986) Tensile properties of human knee joint cartilage: I. Influence of ionic conditions, weight bearing and fibrillation on the tensile modelus. Journal of Orthopaedic Research 4, 379–392.

Akizuki S, Mow VC, Muller F, Pita JC, Howell DS (1987) Tensile properties of human knee joint cartilage. II. Correlations between weight bearing and tissue pathology and the kinetics of swelling. Journal of Orthopaedic Research 5, 173–186.

Anderson DD, Chubinskaya S, Guilak F, Martin JA, Oegema TR, Olson SA, Buckwalter JA (2011) Post-traumatic osteoarthritis: Improved understanding and opportunities for early intervention. Journal of Orthopaedic Research 29(6), 802-809.

Armstrong CG, Lai WM, Mow VC (1984) An analysis of the unconfined compression of articular cartilage. Journal of Biomechanical Engineering 106(2), 165–173.

Ateshian GA, Lai WM, Zhu WB, Mow VC (1994) An asymptotic solution for the contact of two biphasic cartilage layers. Journal of Biomechanics 27(11), 1347-1360.

Ateshian GA, Wang H (1994) A theoretical solution for the frictionless rolling contact of cylindrical biphasic articular cartilage layers. Journal of Biomechanics 28(11), 1341-1355.

Bank RA, Soudry M, Maroudas A, Mizrahi J, Tekoppele JM (2000) The increased swelling and instantaneous deformation of osteoarthritic cartilage is highly correlated with collagen degradation. Arthritis & Rheumatism 43(10), 2202-2210.

Benninghoff A (1925) Form und Bau der Gelenkknorpel in ihren Beziehungen zur Funktion. Z Zellforsch 2, 783–862.

Betsch DF, Baer E (1980) Structure and mechanical properties of rat tail tendon. Biorheology 17, 83-94.

Bevill SL, Thambyah A, Broom ND (2010) New insights into the role of the superficial tangential zone in influencing the microstructural response of articular cartilage to compression. Osteoarthritis and Cartilage 18, 1310-1318.

Bonassar LJ, Sandy JD, Lark MW, Plaas AH, Frank EH, Grodzinsky AJ (1997) Inhibition of cartilage degradation and changes in physical properties induced by IL-1beta and retinoic acid using matrix metalloproteinase inhibitors. Arch Biochem Biophys 344, 404–412.

Boschetti F, Peretti GM (2008) Tensile and compressive properties of healthy and osteoarthritic human articular cartilage. Biorheology 45, 337-344.

Broom ND, Chen MH, Hardy A (2001) A degeneration-based hypothesis for interpreting fibrillar changes in the osteoarthritic cartilage matrix. Journal of Anatomy 199(Pt 6), 683–698.

Broom ND, Poole CA (1983) Articular cartilage collagen and proteoglycans their functional interdependency. Arthritis & Rheumatism 26(9), 1111–1119.

Brown CP, Houle MA, Chen M, Price AJ, Légaré F, Gill HS (2012) Damage initiation and progression in the cartilage surface probed by nonlinear optical microscopy. Journal of the Mechanical Behavior of Biomedical Materials 5(1), 62-70.

Brown TD, Shaw DT (1984) In vitro contact stress distribution on the femoral condyles. Journal of Orthopaedic Research 2(2), 190–199.

Brown TD, Singerman RJ (1986) Experimental determination of the linear biphasic constitutive coefficients of human fetal proximal femoral chondroepiphysis. Journal of Biomechanics 19(8), 597–605.

Buckwalter JA (1995) Osteoarthritis and articular cartilage use, disuse and abuse: experimental studies. J Rheumatol 43(Suppl), 13-15.

Buckwalter JA, Hunziker EB, Rosenberg LC, Coutts R, AdamsM, Eyre D (1991) Articular cartilage: Composition and structure. In: Wo Sl, Buckwalter JA(eds) Injury and repair of musculoskeletal soft tissues, 2nd edn. American Acedemy of Orthopaedic Surgeons, Park Ridge 405–425.

Buckwalter JA, Lane LE (1997) Athletics and osteoarthritis. The American Journal of Sports Medicine 25, 873-881.

Buckwalter JA, Mankin HJ (1998) Articular cartilage: degeneration and osteoarthritis, repair, regeneration, and transplantation. Instr Course Lect (American Academy of Orthopedic Surgery) 47, 487-504.

Buckwalter JA, Mow VC, Ratcliffe A (1994) Restoration of Injured or Degenerated Articular Cartilage. Journal of the American Academy of Orthopaedic Surgeons 2(4), 192-201.

Burgin LV, Aspden RM (2007) A drop tower for controlled impact testing of biological tissues. Medical Engineering & Physics 29, 525-530.

Bursac PM, Obitz TW, Eisenberg SR, Stamenovic D (1999) Confined and unconfined stress relaxation of cartilage: appropriateness of a transversely isotropic analysis. J Biomech 32, 1125-1130.

Butler DL, Grood ES, Noyes FR, Zernicke RF (1978) Biomechanics of ligaments and tendons. Exercise and Sport Sciences Reviews 6, 125–181.

Carew EO, Barber JE, Vesely I (2000) Role of Preconditioning and Recovery Time in Repeated Testing of Aortic Valve Tissues: Validation Through Quasilinear Viscoelastic Theory. Annals of Biomedical Engineering 28, 1093–1100.

Carew EO, Garg A, Barber JE, Vesely I (2004) Stress Relaxation Preconditioning of Porcine Aortic Valves. Annals of Biomedical Engineering 32(4), 563–572.

Carew EO, Talman EA, Boughner DR, Vesely I (1999) Quasilinear viscoelastic theory applied to internal shearing of porcine aortic valve leaflets. J Biomech Eng 121, 386–392.

Chahine NO, Wang CC, Hung CT, Atheshian GA (2004) Anisotropic strain-dependent material properties of bovine articular cartilage in the transitional range from tension to compression. J Biomech 37(8), 1251–1261.

Charlebois M, McKee MD, Buschmann MD (2004) Nonlinear tensile properties of bovine articular cartilage and their variation with age and depth. Journal of Biomechanical Engineering 126(2), 129-137.

Chen CT, Burton-Wurster N, Lust G, Bank RA, Tekoppele JM (1999) Compositional and metabolic changes in damaged cartilage are peak-stress, stress-rate, and loading-duration dependent. Journal of Orthopaedic Research 17(6), 870–879.

Chen MH, Broom ND (1998) On the ultrastructure of softened cartilage: a possible model for structural transformation. Journal of Anatomy 192, 329-341.

Chen MH, Broom ND (1999) Concerning the ultrastructural origin of large-scale swelling in articular cartilage. Journal of Anatomy 194(Pt 3), 445-461.

Chen SS, Falcovitz YH, Schneiderman R, Maroudas A, Sah RL (2001) Depth-dependent compressive properties of normal aged human femoral head articular cartilage: relationship to FCD. Osteoarthritis and Cartilage 9, 561–569.

Cheng S, Clarke EC, Bilston LB (2009) Short Communication-The effects of preconditioning strain on measured tissue properties. Journal of Biomechanics 42, 1360–1362.

Clark JM (1985) The organization of collagen in cryofractured rabbit articular cartilage – a scanning electron-microscopic study. J Orthop Res 3,17-29.

Clark JM (1991) Variation of collagen fiber alignment in a joint surface: a scanning electron microscope study of the tibial plateau in dog, rabbit, and man. J Orthop Res 9, 246-257.

Clark JM, Simonian PT (1997) Scanning electron microscopy of ‘fibrillated’ and ‘malacic’ human articular cartilage: technical considerations. Microsc Res Techn 37, 299-313.

Conza N (2005) PART 3: Tissue preconditioning. Engineering Issues in Experimental Biomedicine Series.

Cotta H, Puhl W (1970) Oberßa¨chenbetrachtungen des Gelenkknorpels. Arch Orthop Unfall-Chir 68, 152-164.

de Vree JHP, Brekelmans WAM, van Gils MAJ (1995) Comparison of nonlocal approaches in continuum damage mechanics. Computers and Structures 55, 581–588.

DiSilvestro MR, Suh JK (2001) A cross-validation of the biphasic poroviscoelastic model of articular cartilage in unconfined compression, indentation, and confined compression. Journal of Biomechanics 34, 519–525.

Dodge GR, Poole AR (1989) Immunohistochemical detection and immunochemical analysis of type II collagen degradation in human normal, rheumatoid, and osteoarthritic articular cartilages and in explants of bovine articular cartilage cultured with interleukin 1. Journal of Clinical Investigation 83, 647–661.

Donzelli PS, Spilker RL, Ateshian GA, Mow VC (1999) Contact analysis of biphasic transversely isotropic cartilage layers and correlations with tissue failure. Journal of Biomechanics 32, 1037-1047.

Duncan AC, Boughner D, Vesely I (1997) Viscoelasticity of dynamically fixed bioprosthetic valves. II. Effect of glutaraldehyde concentration. J Thorac Cardiovasc Surg 113, 302–310.

Elliot DM, Guilak F, Vail TP, Wang JY, Setton LA (2000) Tensile properties of articular cartilage are altered by meniscectomy in a canine model of osteoarthritis, Journal of Orthopaedic Research 18(3), 383–392.

Eshel H, Lanir Y (2001) Effects of Strain Level and Proteoglycan Depletion on Preconditioning and Viscoelastic Responses of Rat Dorsal Skin. Annals of Biomedical Engineering 29(2), 164–172.

Ewers BJ, Dvoracek-Driksna D, Orth MW, Haut RC (2001) The extent of matrix damage and chondrocyte death in mechanically traumatized articular cartilage explants depends on rate of loading. Journal of Orthopaedic Research 19(5), 779–784.

Eyre DR (2004) Collagens and Cartilage Matrix Homeostasis. Clinical Orthopaedics & Related Research 427,118-122.

Farndale RW, Buttle DJ, Barrett AJ (1986) Improved quantitation and discrimination of sulphated glycosaminoglycans by use of dimethylmethylene blue. Biochemica et Biophysica Acta 883, 173-177.

Flachsmann R, Kim W, Broom N (2005) Vulnerability to Rupture of the Intact Articular Surface with Respect to Age and Proximity to Site of Fibrillation: A Dynamic and Static-Investigation. Connective Tissue Resarch 46, 159-169.

Fukubayashi T, Kurosawa H (1980) The contact area and pressure distribution pattern of the knee. A study of normal and osteoarthrotic knee joints. Acta Orthop Scand 51(6), 871–879.

Fung YC (1993) Biomechanics: Mechanical Properties of Living Tissues, 2nd ed. New York: Springer 277–292.

Garcia JJ, Aliero NJ, Haut RC (1998) An Approach for Stress Analysis of Transversely Isotropic Biphasic Cartilage Under Impact Load. J Biomech Eng 120, 608-613.

Geers MGD, de Borst R, Brekelmans WAM, Peerlings RHJ (1998) Strain-based transient-gradient damage model for failure analyses. Computer Methods in Applied Mechanics and Engineering, 160, 133-153.

Geers MGD, de Borst R, Brekelmans WAM, Peerlings RHJ (1999) Validation and internal length scale determination for a gradient damage model: application to short glass-fibre-reinforced polypropylene. International Journal of Solids and Structures. 36(17), 2557–2583.

Gefen A, Gefen N, Zhu Q, Raghupathi R, Margulies SS (2003) Age-dependent changes in material properties of the brain and brain case of the rat. J Neurotrauma 20(11), 1163-1177.

Glaser C, Putz R (2002) Functional anatomy of articular cartilage under compressive loading Quantitative aspects of global, local and zonal reactions of the collagenous network with respect to the surface integrity. Osteoarthritis and Cartilage 10, 83-99.

Guilak F (2011) Biomevhanical factors in osteoarthritis. Best practice & Research clinical rheumatology 25, 815-823.

Guilak F, Ratcliffe A, Lane N, Rosenwasser MP, Mow VC (1994) Mechanical and biochemical changes in the superficial zone of articular cartilage in canine experimental osteoarthritis. Journal of Orthopaedic Research 12, 474–484.

Halloran JP, Sibole S, van Donkelaar CC, van Turnhout MC, Oomens CWJ, Weiss JA, Guilak F, Erdemir A (2012) Multiscale mechanics of articular cartilage: potentials and challenges of coupling musculoskeletal, joint, and microscale computational models. Annals of Biomedical Engineering 40(11), 2456-2474.

Haut RC (1983) Age-dependent influence of strain rate on the tensile failure of rat-tail tendon. ASME J Biomechanical Eng 105, 296-299.

Haut RC (1986) The influence of specimen length on the tensile failure properties of tendon collagen. Journal of Biomechanics 19(11), 951-955.

Haut RC, Little RW (1972) A constitutive equation for collagen fibers. J Biomech 5, 423-430.

Hollander AP, Pidoux I, Reiner A, Rorabeck C, Bourne R, Poole AR (1995) Damage to type II collagen in aging and osteoarthritis starts at the articular surface, originates around chondrocytes, and extends into the cartilage with progressive degeneration. J Clin Invest 96, 2859–2869.

Hosseini SM, Veldink MB, Ito K, van Donkelaar CC (2013a) Is collagen fibre damage the cause of early softening in articular cartilage? Osteoartjritis and Cartilage 21(1), 136-143.

Hosseini SM, Wu Y, Ito K, van Donkelaar CC (2013b) The importance of superficial collagen fibrils for the function of articular cartilage. Biomechanics and Modeling in Mechanobiology. DOI 10.1007/s10237-013-0485-0

Huang C-Y, Mow VC, Ateshian GA (2001) The role of flow-independent viscoelasticity in the biphasic tensile and compressive responses of articular cartilage. J Biomech Eng 123, 410-417.

Huang C-Y, Soltz MA, Kopacz M, Mow VC, Ateshian GA (2003) Experimental verification of the roles of intrinsic matrix viscoelasticity and tensioncompression non-linearity in the biphasic response of cartilage. J Biomech Eng 125, 84-93.

Huang C-Y, Stankiewicz A, Ateshian GA, Mow VC (2005) Anisotropy, inhomogeneity, andtension–compression nonlinearity of human glenohumeral cartilage in finite deformation. Journal of Biomechanics 38, 799–809.

Hunziker E (1992) Articular artilage structure in humans and experimental animals. In:Kuettner KE, Peyron JG, Schleyer R, Hascall VC, (eds) Articular Cartilage and Osteoarhritis. Raven Press, New York, 183–199.

Huszar G, Maiocco J, Naftolin F (1980) Monitoring of collagen and collagen fragments in chromatography of protein mixtures. Analytical Biochemistry 105(1), 424-429.

Huyghe JM, Houben GB, Drost MR, van Donkelaar CC (2003) An ionised/non-ionised dual porosity model of intervertebral disc tissue. Biomechanics and Modeling in Mechanobiology 2, 3–19.

Huyghe JM, Janssen JD (1997) Quadriphasic mechanics of swelling incompressible porous media, Int. J. Engng Sci. 35, 793-802.

Huyghe JM, van Campen DH, Arts T, Heethaars RM (1991) The constitutive behaviour of passive heart muscle tissue: a quasi-linear viscoelastic formulation. J Biomech 24, 841-849.

Huyghe JM, Wilson W, Malakpoor K (2009) On the thermodynamical admissibility of the triphasic theory of charged hydrated tissues. ASME J. Biomech. Eng. 131 p. 044504.

Ihn JC, Kim SJ, Park IH (1993) In vitro study of contact area and pressure distribution in the human knee after partial and total meniscectomy. Int Orthop 17(4), 214–218.

Jeffrey JE, Aspden RM (2006) The Biophysical Effects of a Single Impact Load on Human and Bovine Articular Cartilage. Journal of Engineering in Medicine 220, 677-686.

Jeffrey JE, Anne Thomson L, Aspden RM (1997) Matrix loss and synthesis following a single impact load on articular cartilage in vitro. Biochimica et Biophysica Acta 1334(2-3), 223-232.

Jeffrey JE, Gregory DW, Aspden RM (1995) Matrix damage and chondrocyte viability following a single impact load on articular cartilage. Archieves of biochemistry and biophysics 322(1), 87-96.

Johson GA, Liversay GA, Woo S L-Y, Rajagopal KR (1996) A single integral finite strain viscoelastic model of ligaments and tendons. J Biomech Eng 118, 221-226.

Julkunen P, Korhonen RK, Nissi MJ, Jurvelin JS (2008b) Mechanical characterization of articular cartilage by combining magnetic resonance imaging and finite-element analyses-a potential functioning imaging technique. Physics in Medicine and Biology, 53(9), 2425-2438.

Julkunen P, Wilson W, Isaksson H, Jurvelin JS, Herzog W, Korhonen RK (2013) A review of the combination of experimental measurements and fibril-reinforced modeling for investigation of articular cartilage and chondrocyte response to loading. Computational and Mathematical Methods in Medicine Volume 2013, Article ID 326150, 23 pages.

Julkunen P, Wilson W, Jurvelin JS, Rieppo J, Qu CJ, Lammi MJ, Korhonnen RK (2008a) Stress–relaxation of human patellar articular cartilage in unconfined compression: Prediction of mechanical response by tissue composition and structure. Journal of Biomechanics 41(9), 1978-1986.

June RK, Ly S, Fyhrie DP (2009) Cartilage stress-relaxation proceeds slower at higher compressive strains. Archives of Biochemistry and Biophysics 483, 75–80.

Kempson GE, Muir H, Pollard C, Tuke M (1973) The tensile properties of the cartilage of human femoral condyles related to the content of collagen and glycosaminoglycans. Biochem Biophys Acta 297, 465–472.

Khoshgoftar M, Wilson W, Ito K, van Donkelaar CC (2013) The effect of tissue-engineered cartilage biomechanical and biochemical properties on its post-implantation mechanical behavior. Biomechanics and Modeling in Mechanobiology 12, 43-54.

Kim W, Thambyah A, Broom N (2012) Does prior sustained compression make cartilage-on-bone more vulnerable to trauma? Clinical Biomechanics 27(7), 637-645.

Kleemann RU, Krocker D, Cedraro A, Tuischer J, Duda GN (2005) Altered cartilage mechanics and histology in knee osteoarthritis: relation to clinical assessment (ICRS Grade). Osteoarthritis and Cartilage 13, 958-963.

Kock LM, Ravetto A, van Donkelaar CC, Foolen J, Emans P, Ito K (2010) Tuning the differentiation of periosteum-derived cartilage using biochemical and mechanical stimulation. Osteoarthritis and Cartilage 18(11), 1528-1535.

Korhonen RK, Jurvelin JS (2010) Compressive and tensile properties of articular cartilage in axial loading are modulated differently by osmotic environment. Medical Engineering & Physics 32, 155–160.

Kurz B, Jin M, Patwari P, Cheng DM, Lark MW, Grodzinsky AJ (2001) Biosynthetic response and mechanical properties of articular cartilage after injurious compression. Journal of Orthopaedic Research 19, 1140-1146.

Kwan MK, Lin T H-C, Woo S L-Y (1993) On the viscoelastic properties of the anteromedial bundle of the anterior cruciate ligament. J Biomech 26, 447–452.

Laasanen MS, Toyras J, Korhonen RK, Rieppo J, Saarakkala S, Nieminen MT, Hirvonen J, Jurvelin JS (2003) Biomechanical properties of knee articular cartilage. Biorheology 40, 133–140.

Lai WM, Hou JS, Mow VC (1991) A triphasic theory for the swelling and deformation behaviors of articular cartilage. ASME J Biomech Eng 113, 245–258.

Lai WM, Mow VC, Sun DD, Ateshian GA (2000) On the electric potentials inside a charged soft hydrated biological tissue: streaming potential versus diffusion potential. J Biomech Eng 122(4), 336-346.

Langelier E, Buschmann MD (2003) Increasing strain and strain rate strengthen transient stiffness but weaken the response to subsequent compression for articular cartilage in unconfined compression. Journal of Biomechanics 36, 853–859.

Lanir Y, Einat R (2012) Viscoelasticity and preconditioning in soft tissues: old dilemmas, new paradigm, ESB2012: 18th Congress of the European Society of Biomechanics.

Lee JM, Haberer SA, Pereira CA, Naimark WA, Courtman DW, Wilson GJ (1994) High strain rate testing and structural analysis of pericardial bioprosthetic materials. In: Biomaterials' Mechanical Properties ASTM STP 1173, edited by H. E. Kambic, and A. T. Yakabori. Philadelphia: ASTM 19–42.

LeRoux MA, Setton LA (2002) Experimental and biphasic FEM determinations of the material properties and hydraulic permeability of the meniscus in tension. ASME J. Biomech. Eng. 124, 315–321.

Lipshitz H, Etheridge R, Glimcher MJ (1975) In vitro wear of articular cartilage. J Bone Joint Surg 57, 527–537.

Li LP, Buschmaan MD, Shirazi-Adl A (2000) A Fibril reinforced nonhomogeneous poroelastic model for articular cartilage: inhomogeneous response in unconfined compression. Journal of Biomechanics 33, 1533-1541.

Li LP, Herzog W (2004) The role of viscoelasticity of collagen fibers in articular cartilage: Theory and numerical formulation. Biorheology 41, 181–194.

Li LP, Herzog W, Korhonen RK, Jurvelin JS (2005) Communication The role of viscoelasticity of collagen fibers in articular cartilage: axial tension versus compression. Medical Engineering & Physics 27, 51-57.

Li LP, Korhonen RK, Jurvelin JS, Herzog W (2008) Fluid pressure driven fibril reinforcement in creep and relaxation tests of articular cartilage. Medical Engineering & Physics 30, 182–189.

Li LP, Shirazi-Adl A, Buschmaan MD (2002) Alterations in mechanical behaviour of AC due to changes in depth varying material properties a nonhomogenous poroelastic model study. Computer methods in biomechanics and biomedical engineering 5(1), 45-52.

Lin PM, Chen C-T C, Torzilli PA (2004) Increased stromelysin-1 (MMP-3), proteoglycan degradation (3B3- and 7D4) and collagen damage in cyclically load-injured articular cartilage. Osteoarthritis and Cartilage 12, 485–496.

Liu Z, Yeung K (2008) The Preconditioning and Stress Relaxation of Skin Tissue. Journal of Biomedical & Pharmaceutical Engineering 2(1), 22-28.

Lorenz H, Richter W (2006) Osteoarthritis: Cellular and molecular changes in degenerating cartilage. Progress in Histochemistry and Cytochemistry 40, 135–163.

Macirowski T, Tepic S, Mann RW (1994) Cartilage stresses in the human hip joint. Journal of Biomechanical Engineering 116(1), 10–18.

Matthews LS, Sonstegard DA, Henke JA (1977) Load bearing characteristics of the patello-femoral joint. Acta Orthopaedica Scand 48, 511-516.

Mak AF (1986a) The apparent viscoelastic behavior of articular cartilage – the contributions from the intrinsic matrix viscoelasticity and interstitial fluid flows. J Biomech Eng 108, 123–130.

Mak AF (1986b) Unconfined compression of hydrated viscoelastic tissues: a biphasic poroviscoelastic analysis. Biorheology 23, 371–383.

Mankin HJ, Mow VC, Buckwalter JA (2000) Articular cartilage repair and osteoarthritis. Buckwalter JA, Einhorn TA, Simon SR, Editors, Orthopaedic basic science: biology and biomechanics of the musculoskeletal system, (2nd ed), American Academy of Orthopaedic Surgeons, Rosemont, IL. 471–488.

Mansour JM, Mow VC (1976) The permeability of articular cartilage under compressive strain and at high pressures. Journal of Bone and Joint Surgery 58(4), 509–516.

Maroudas A (1968) Physicochemical properties of cartilage in the light of ion exchange theory. Biophys J 8, 575–595.

Maroudas A, Bannon C (1981) Measurement of swelling pressure in cartilage and comparison with the osmotic pressure of constituent proteoglycans. Biorheology 18, 619–632.

Maroudas A, Wachtel E, Grushko G, Katz EP, Weinberg P (1991) The effect of osmotic and mechanical pressures on water partitioning in articular cartilage. Biochimica et Biophysica Acta 1073, 285–294.

Mazars J, Pijaudier-Cobat G (1989) Continuum damage theory – application to concrete. Journal of Engineering Mechanics 115, 345-365.

McCormack T, Mansour JM (1998) Reduction in tensile strength of cartilage precedes surface damage under repeated compressive loading in vitro. Journal of Biomechanics 31, 55–61.

McCutchen CW (1982) Cartilage is poroelastic, not viscoelastic (including an exact theorem about strain energy and viscous loss, and an order of magnitude relation for equilibration time. Journal of Biomechanics 15(4), 325–327.

McKellop HA, Sigholm G, Redfern FC, Doyle B, Sarmiento A, Luck Sr JV (1991) The effect of simulated fracture-angulations of the tibia on cartilage pressures in the knee joint J Bone Joint Surg Am 73(9), 1382–1391.

Milentijevic D, Helfet DL, Torzilli PA (2003) Influence of Stress Magnitude on Water Loss and Chondrocyte Viability in Impacted Articular Cartilage. Journal of Biomechanical Engineering 125(5), 594 (8 pages).

Miller GJ, Morgan EF (2010) Use of microindentation to characterize the mechanical properties of articular cartilage: comparison of biphasic material properties across length scales. Osteoarthritis and Cartilage 18, 1051-1057.

Morrison JB (1970a) The mechanism of the knee joint in relation to normal walking. Journal of Biomechanics 3, 51-61.

Morrison JB (1970b) The mechanics of muscle function in locomotion. Journal of Biomechanics 3, 431-451.

Mow VC, Fithian DC, Kelly MA (1989) Fundamentals of articular cartilage and meniscus biomechanics in articular cartilage and knee joint function: Basic Science and Arthroscopy, J. W. Ewing, Ed., pp. 1–18, Raven Press, New York, NY, USA.

Mow VC, Holmes MH, Lai WM (1984a) Fluid transport and mechanical properties of articular cartilage: a review. J Biomech 17, 377-394.

Mow VC, Mak AF, Lai WM, Rosenberg LC, Tang LH (1984b) Viscoelastic properties of proteoglycan subunits and aggregates in varying solution concentrations. J Biomech 17, 325-238.

Mow VC, Guo XE (2002) Mechano-electrochemical properties of articular cartilage: their inhomogeneities and anisotropies. Annual Review of Biomedical Engineering 4, 175–209.

Mow VC, Kuei SC, Lai WM, Armstrong CG (1980) Biphasic creep and stress relaxation of articular cartilage in compression: theory and experiments. Journal of Biomechanical Engineering 102, 73–84.

Myers BS, McElhaney JH, Doherty BJ (1991) The viscoelastic responses of the human cervical spine in torsion: experimental limitations of quasi-linear theory, and a method for reducing these effects. J Biomech 24, 811–817.

Natoli RM, Athanasiou KA (2009) Traumatic loading of articular cartilage: Mechanical and biological responses and post-injury treatment. Biorheology 46, 451-485.

Nieminen MT, Toyras J, Laasanen MS, Silvennoinen J, Helminen HJ, Jurvelin JS (2004) Prediction of biomechanical properties of articular cartilage with quantitative magnetic resonance imaging. Journal of Biomechanics 37(3), 321-328.

Nieminen MT, Toyras J, Rieppo J, Hakumaki JM, Silvennoinen J, Helminen HJ, Jurvelin JS (2000) Quantitative MR microscopy of enzymatically degraded articular cartilage. Magn Reson Med 43, 676–681.

Nieminen MT, Rieppo J, Töyräs J, Hakumäki JM, Silvennoinen J, Hyttinen MM, Helminen HJ, Jurvelin JS (2001) T2 relaxation reveals spatial collagen architecture in articular cartilage: a comparative quantitative MRI and polarized light microscopic study. Magnetic Resonance in Medicine 46(3), 487–493.

Nishimuta JF, Levenston ME (2012) Response of cartilage and meniscus tissue explants to in vitro compressive overload. Osteoarthritis and Cartilage 20(5), 422–429.

Nissi MJ, Töyräs J, Laasanen MS, Rieppo J, Saarakkala S, Lappalainen R, Jurvelin JS, Nieminen MT (2004) Proteoglycan and collagen sensitive MRI evaluation of normal and degenerated articular cartilage. Journal of Orthopaedic Research 22(3), 557–564.

Ottani V, Raspanti M, Ruggeri A (2001) Collagen structure and functional implications. Micron 32(3), 251–260.

Park S, Hung CT, Ateshian GA (2004) Mechanical response of bovine articular cartilage under dynamic unconfined compression loading at physiological stress levels. Osteoarthritis and Cartilage 12, 65-73.

Pearle AD, Warren RF, Rodeo SA (2005) Basic Science of Articular Cartilage and Osteoarthritis Clin Sports Med 24, 1–12.

Peerlings RHJ, de Borst R, BrekelmansWAM, Geers MGD (1998) Gradient-enhanced damage modelling of concrete fracture Mechanics of Cohesive-Frictional Materials 3, 323–342.

Pearlings RHJ (2007) Damage mechanics, Lecture notes for the course ‘damage mechanica’ (4K060), Eindhoven University of Technology.

Pelletier JP, Martel-Palletier J, Altman RD, Ghandur (Mnaymneh) L, Hower DS, Woessner JF (1983) Collagenolytic activity and collagen matric breakdown of the articular cartilage in de Pond-Nuki dog model of osteoarthritis. Arthritis Rheum 26, 866–874.

Pins GD, Huang EK, Christiansen DL, Silver FH (1997) Effects of static axial strain on the tensile properties and failure mechanisms of self-assembled collagen fibres. J Appl Polym Sci 63, 1429-1440.

Pinto JG, Patitucci PJ (1980) Visco-elasticity of passive cardiac muscle. J Biomech Eng 102, 57–61.

Quinn KP, Winkelstein BA (2011) Preconditioning is Correlated With Altered Collagen Fiber Alignment in Ligament. J Biomech Eng 133(6), 064506.

Radin EL, Ehrlich MG, Chernack R, Abernethy P, Paul IL, Rose RM (1978) Effect of repetitive impulsive loading on the knee joints of rabbits. Clin Othop 131, 288–293.

Repo RU, Finlay JB (1977) Survival of articular cartilage after controlled impact. J Bone Jt Surg 59(8), 1068-1076.

Riegger-Krugh C, Gerhart TN, Powers WR, Hayes WC (1998) Tibiofemoral contact pressures in degenerative joint disease. Clin Orthop 348, 233–245.

Rieppo J, Hyttinen MM, Lappalainen R, Jurvelin JS, Helminen HJ (2004) Spatial determination of water, collagen and proteoglycan contents by Fourier transform infrared imaging and digital densitometry. Trans ORS 1021.

Rieppo J, Töyräs J, Nieminen MR, Jurvelin JS, Helminen HJ (2005) Spatial mapping of cartilage collagen and proteoglycans by FT-IRS. Trans ORS 1484.

Rolauffs B, Muehleman C, Li J, Kurz B, Kuettner KE, Frank E, Grodzinsky AJ (2010) Arthritis & Rheumatism 62(10), 3016-3027.

Römgens AM, van Donkelaar CC, Ito K (2013) Contribution of collagen fibers to the compressive stiffness of cartilaginous tissues, Biomechanics and Modeling in Mechanobiology 12(6), 1221-1231.

Roth V, Mow VC (1980) The intrinsic tensile behavior of the matrix of bovine articular cartilage and its variation with age. J Bone Joint Surg 62A(7), 1102-1117.

Saarakkalay S, Julkunenz P, Kivirantay P, Makitalo J, Jurvelin JS, Korhonen RK (2010) Depth-wise progression of osteoarthritis in human articular cartilage: investigation of composition, structure and biomechanics. Osteoarthritis and Cartilage 18, 73-81.

Sanjeevi R, Somanathan N, Ramaswamy D (1982) A viscoelastic model for collagen fibres. J Biomech 15, 181-183.

Sauren AAHJ, van Hout MC, van Steenhoven AA, Veldpaus FE, Janssen JD (1983) The mechanical properties of porcine aortic valve tissues. J Biomech 16, 327–337.

Saxena RK, Sahay KB, Guha SK (1991) Morphological changes in the bovine articular cartilage subjected to moderate and high loadings. Acta Anat 142, 152-157.

Setton LA, Zhu W, Mow VC (1993) The biphasic poroviscoelastic behavior of articular cartilage: role of the surface zone in governing the compressive behavior. Journal of Biomechanics 26(4-5), 581–592.

Shapiro EM, Borthakur A, Kaufman JH, Leigh JS, Reddy R (2001) Water distribution patterns inside bovine articular cartilage as visualized by 1H magnetic resonance imaging. Osteoarthritis and Cartilage 6, 533–538.

Schinagl RM, Ting MK, Price JH, Sah RL (1996) Video microscopy to quantitate the inhomogeneous equilibrium strain within articular cartilage during confined compression. Ann Bionied Eng 24, 500-512.

Schinagl RM, Gurskis D, Chen AC, Sah RL (1997) Depth-dependent confined compression modulus of full-thickness bovine articular cartilage. J Orthop Res 15, 499-506.

Shirazi R, Shirazi-Adl A (2008) Deep vertical collagen fibrils play a significant role in mechanics of articular cartilage. Journal of Orthopaedic 26(5), 608-615.

Shirazi R, Shirazi-Adl A, Hurtig M (2008) Role of cartilage collagen fibrils networks in knee joint biomechanics under compression. Journal of Biomechanics 41, 3340-3348.

Siegmund T, Allen MR, Burr DB (2008) Failure of mineralized collagen fibrils: Modeling the role of collagen cross-linking. Journal of Biomechanics 41, 1427-1435.

Silvast TS, Jurvelin JS, Aula AS, Lammi MJ, Töyräs J (2009) Contrast agent-enhanced computed tomography of articular cartilage: association with tissue composition and properties. Acta Radiologica 50(1), 78–85.

Silver FH, Ebrahimi A, Snowhill PB (2002) Viscoelastic properties of self-assembled type I collagen fibers: Molecular basis of elastic and viscous behaviors. Conn Tiss Res 43, 569-580.

Sivan S, Merkher Y, Wachtel E, Ehrlich S, Maroudas A (2006) Correlation of swelling pressure and intrafibrillar water in young and aged human intervertebral discs. Journal of Orthopaedic Research 24(6), 1292-1298.

Smidt GI (1973) Biomechanical analysis of knee flexion and extension. Journal of Biomechanics 6, 79-92.

Soulhat J, Buschmann MD, Shirazi-Adl A (1999) A fibrilnetwork-reinforced biphasic model of cartilage in unconfined compression. Journal of Biomechanical Engineering 121(3), 340–347.

Solts MA, Ateshian GA (1998) Experimental verification and theoretical prediction of cartilage interstitial fluid pressurization at an impermeable contact interface in confined compression. Journal of Biomechanics 31(10), 927-934.

Soltz MA, Ateshian GA (2000) A Conewise Linear Elasticity mixture model for the analysis of tension-compression non-linearity in articular cartilage. J Biomech Eng 122, 576-586.

Stammen JA, Williams S, Ku DN, Guldberg RE (2001) Mechanical properties of a novel PVA hydrogel in shear and unconfined compression. Biomaterials 22, 799-806.

Suh JK, Bai S (1998) Finite element formulation of biphasic poroviscoelastic model for articular cartilage. J Biomech Eng 120, 195–201.

Sverdlik A, Lanir Y (2002) Time-Dependent Mechanical Behavior of Sheep Digital Tendons, Including the Effects of Preconditioning. Journal of Biomechanical Engineering 124(1), 78–84.

Temple MM, Bae WC, Chen MQ, Lotz M, Amiel D, Coutts RD, Sah RL (2007) Age- and site-associated biomechanical softening of human articular cartilage of the femoral condyle. Osteoartjritis and Cartilage 15(9), 1042-1052.

Temple-Wong MM, Bae WC, Chen MQ, Bugbee WD, Amiel D, Coutts RD, Lotz M, Sah RL (2009) Biomechanical, structural and biochemical indices of degenerative and osteoarthritic deterioration of adult human articular cartilage of the femoral condyl. Osteoarthritis and Cartilage. 17(11), 1469-1476.

Tesch AM, MacDonald MH, Kollias-Baker C, Benton HP (2004) Endogenously produced adenosine regulates articular cartilage matrix homeostasis: enzymatic depletion of adenosine stimulates matrix degradation. Osteoarthritis and Cartilage 12(5), 349-359.

Thambyah A, Broom N (2006) Micro-anatomical response of cartilage-on-bone to compression: mechanisms of deformation within and beyond the directly loaded matrix. J Anat 209(5), 611-622.

Thambyah A, Broom ND (2007) On how degeneration influences load-bearing in the cartilage–bone system: a microstructural and micromechanical study. Osteoarthritis and Cartilage 15(12), 1410-1423.

Thambyah A, Goh JCH, Das De S (2005) Contact stresses in the knee joint in deep flexion. Medical Engineering and Physics 27, 329-335.

Thambyah A, Zhao L, Broom ND (2009) Microstructural response and fluid flow mechanisms in cartilage loading: new insights using a novel indentation method. Journal of Strain Analysis 44(5), 319-326.

Thambyah A, Zhao J-Y, Bevill SL, Broom ND (2012) Macro-, micro- and ultrastructural investigation of how degeneration influences the response of cartilage to loading. Journal of the Mechanical Behavior of Biomedical Materials 5(1), 206–215.

Thibault M, Poole AR, Buschmann MD (2002) Cyclic compression of cartilage/bone explants in vitro leads to physical weakening, mechanical breakdoan of collagen and release of matrix fragments. Journal of Orthopaedic Research 20, 1265-1273.

Torzilli PA, Grigiene R, Borrelli Jr J, Helfet DL (1999) Effect of impact load on articular cartilage: cell metabolism and viability, and matrix water content. Journal of Biomechanical Engineering 121(5): 433-441.

Torzilli PA, Mow VC (1976a) On the fundamental fluid transport mechanisms through normal and pathological articular cartilage during function. I the formulation," Journal of Biomechanics 9(8), 541–552.

Torzilli PA, Mow VC (1976b) On the fundamental fluid transport mechanisms through normal and pathological articular cartilage during function. II. The analysis, solution and conclusions. Journal of Biomechanics 9(9), 587–606.

Toyras J, Rieppo J, Nieminen MT, Helminen HJ, Jurvelin JS (1999) Characterization of enzymatically induced degradation of articular cartilage using high frequency ultrasound. Phys Med Biol 44, 2723–2733.

Toyras J, Laasanen MS, Saarakkala S, Lammi MJ, Rieppo J, Kurkijarvi J, Lappalainen R, Jurvelin JS (2003) Speed of sound in normal and degenerated bovine articular cartilage. Ultrasound Med Biol 29, 447–454.

Turley S, Thambyah A, Firth E, Broom N (2011) Failure mechanisms of cartilage-on-bone tissues and the influence of loading history. Advanced Materials Research 275, 139-142.

Urban JP (1994) The chondrocyte: a cell under pressure. Br J Rheum 33, 910-908.

van Turnhout MC, Kranenbarg S, van Leeuwen JL (2011) Contribution of postnatal collagen reorientation to depth-dependent mechanical properties of articular cartilage. Biomechanics and Modeling in Mechanobiology 10(2), 269-279.

Viidik Q (1968) A rheological Model for Uncalcified Parallel-Fibriled Collagenous Soft Tissue. J Biomech 1, 3-11.

Wang CCB, Chahine NO, Hung CT, Ateshian GA (2003) Optical determination of anisotropic material properties of bovine articular cartilage in compression. Journal of Biomechanics 36(3), 339-353.

Wang CC, Guo XE, Sun D, Mow VC, Ateshian GA, Hung CT (2002) The functional environment of chondrocytes within cartilage subjected to compressive loading: a theoretical and experimental approach. Biorheology 39, 11-25.

Wang J H-C (2006) Review Mechanobiology of tendon. Journal of Biomechanics 39, 1563-1582.

Wang JL, Parnianpour M, Shirazi-Adl A, Engin AE (1997) Failure criterion of collagen fiber: Viscoelastic behavior simulated by using load control data. Theor Appl Fracture Mech 27, 1-12.

Wayne JS, Kraft KA, Shields KJ, Yin C, Owen JR, Disler DG (2003) MR imaging of normal and matrix-depleted cartilage: correlation with biomechanical function and biochemical composition. Radiology 228, 493–499.

Williamson AK, Chen AC, Masuda K, Thonar MA, Sah RL (2003) Tensile mechanical properties of bovine articular cartilage: Variations with growth and relationships to collagen network components. Journal of Orthopaedic Research 21(5), 872–880.

Wilson W, Huyghe JM, van Donkelaar CC (2006a) A composition-based cartilage model for the assessment of compositional changes during cartilage damage and adaptation. Osteoarthritis and Cartilage 14(6), 554–560.

Wilson W, Huyghe JM, van Donkelaar CC (2007) Depth dependent compressive equilibrium properties of articular cartilage explained by its composition. Biomechanics and Modeling in Mechanobiology 6, 43–53.

Wilson W, van Burken C, van Donkelaar CC, Buma P, van Rietbergen B, Huiskes R (2006b) Causes of mechanically induced collagen damage in articular cartilage. Journal of Orthopaedic Research 24, 220–228.

Wilson W, van Donkelaar CC, van Rietbergen C, Ito K, Huiskes R (2004) Stresses in the local collagen network of articular cartilage: a poroviscoelastic fibril-reinforced finite element study. Journal of Biomechanics 37(3), 357–366.

Wilson W, van Donkelaar CC, Huyghe JMRJ (2005a) A comparison between mechano-electrochemical and biphasic swelling theories for soft hydrated tissues. Journal of Biomechanical Engineering: Transactions of the ASME 127(1), 158-165.

Wilson W, van Donkelaar CC, van Rietbergen B, Huiskes R (2005b) A fibril-reinforced poroviscoelastic swelling model for articular cartilage. J Biomech 38(6), 1195-1204.

Wilson W, van Donkelaar CC, van Rietbergen B, Huiskes R (2005c) The role of computational models in the search for the mechanical behaviour and damage mechanisms of articular cartilage. Med. Eng. Phys. 27, 810–826.

Wong M, Wuethrich P, Buschmann MD, Eggli P, Hunziker EB (1997) Chondrocyte biosynthesis correlates with local tissue strain in statically compressed adult articular cartilage. J Orthop Res 15, 189-196.

Wong M, Wuethrich P, Eggli P, Hunziker EB (1996). Zone-specific cell biosynthesis activity in mature bovine articular cartilage: a new method using confocal microscopic stereology and quantitative autoradiography. Journal of Orthopedic Research 14, 424–432.

Woo SL (1982) Mechanical properties of tendons and ligaments. I. Quasi-static and nonlinear viscoelastic properties. Biorheology 19(3), 385–396.

Woo SL-Y, Gomez MA, Akeson WH (1981) The time and history-dependent viscoelastic properties of the canine medial collateral ligament. J Biomech Eng 103, 293-298.

Wu W, Billinghurst RC, Pidoux I, Antoniou J, Zukor D, Tanzer M, Poole AR (2002) Sites of collagenase cleavage and denaturation of type II collagen in aging and osteoarthritic articular cartilage and their relationship to the distribution of matrix metalloproteinase 1 and matrix metalloproteinase 13. Arthritis Rheum 46(8), 2087–2094.

Xia Y (1998) Relaxation anisotropy in cartilage by NMR microscopy (μMRI) at 14-μm resolution. Magnetic Resonance in Medicine 39(6), 941–949.

Zhu W, Mow VC, Koob TJ, Eyre DR (1993) Viscoelastic shear properties of articular cartilage and the effects of glycosidase treatments. J Orthop Res 11, 771-781.

Acknowledgements

Foremost, I would like to express my sincere gratitude to my supervisor Dr. Rene van Donkelaar for the continuous support of my PhD study and research, for his patience, motivation, enthusiasm, and immense knowledge. His guidance helped me in all the time of my research. I could not have imagined having a better and nicer advisor and mentor for my PhD research. Working with him, I never felt ignored or unreasonably stressed. Rene, I am very much appreciative of all the good things I learned from you and all the knowledge you transferred to me.

Moreover, I would like to specially thank my promoter, Prof. Keita Ito, the person from whom I learned more about scientific thinking, scientific discussion and scientific judgment. The way he looked into the "cause and effect" of a phenomenon was so amazing for me. Having so many individual and group meetings with him during my PhD research made me a more critical person in case of describing an observation and finding a solution for a problem. Keita, I also very much appreciate you for building up the capability of conducting independent research in me.

My gratitude is also extended to the members of my PhD defense committee: Prof. Dr. Klaas Nicolay, Prof. Dr. Ir. Nico Verdonschot, Prof. Dr. Dan L Bader, Prof. Dr. Ir. Marc Geers and Dr. Wouter Wilson for their kind acceptance to be in the committee, their interest in my thesis, their inputs and finally their approval of my thesis.

My special thanks also go to our group secretary, Janneke Cuijpers, for her very kind helps in many administrative issues and also to Leo Wouters for his helps in many computer, laptop and networking problems.

I would also like to express my thankfulness to Pooya, Wouter, Jacques, Veronique, Javad, Peter, Juan, Ron, Poh and Lorenza for their being very open to have fruitful discussion with me on my project whenever I asked them. Many of my special thanks also go to two of my hard working students, Mariska Veldink and Yabin Wu for their very well-done job. I am also very grateful to all of my colleagues in Material Technology institute specifically my friends in Orthopaedic Biomechanics group that provided me with very nice working environment.

I am also thankful to my international colleagues and friends together with them I had great time and enjoyable social life during my stay in the Netherlands/Europe:

Gregory & Effi, Juan & Sol, Francesca, Chiara, Giulia, Lieke, Anderes & Lorenza, Patrik, Juan carlos & Gabi, Francesco & Pein, Rene, Patrick & Doina. I also appreciate all the kindness of my Persian friends together with them I never felt lonely and distanced from home: Amin, Pooya & Solmaz, Hamid & Azar, Javad, Amin & Parisa, Mohammad & Flora, Ali & Niloofar, Hamed & Negar, Kamyar & Pegah, Salman & Leila, Hossein & Samaneh, Arash & Farimah, Hamidreza & Marzieh, Saeed & Samaneh, Sara, Arash, Mohammad & Afrooz, Mohammad & Samaneh, Hadi, Ali & Erfaneh, Saeed, Mona, Raheleh, Hamed and Pooyan & Ellaheh.

Another stanch supporter and fan was a special friend of mine, Faisal, who I met at the end of my first year of my PhD in Eindhoven, but he became one of my best friends in my life. I had great times of scientific, philosophical and social discussions with him. He was all supportive and understanding of my PhD life. Faisal, I appreciate you very much for all the invaluable times we had together.

I would also like to gratefully acknowledge all my colleagues in CAE department of DSM Ahead for their being so kind and understanding towards my situation that I was sometimes busy at work with different issues of my thesis writing, revising and publishing.

Last, but certainly not least, I must acknowledge with tremendous and deep thanks from my heart and my soul the support from my parents, Esmaeil and Adibeh, and my brothers, Hamid and Saeed. They never let me feel I was far from them. There are no words that can express my gratitude and appreciation for all you have done and been for me. I love you from the bottom of my heart and I am forever indebted to you for giving me life, your love, and your heart.

Sayyed Mohsen Hosseini (Reza)

Curriculum Vitae

Sayyed Mohsen Hosseini whose nickname is Reza was born on August 19th, 1982, in Gonbadekavoos, a city in northern Iran. After finishing high-school in Mathematics and Physics in Mashhad in 2000, he entered Islamic Azad University of Mashhad, where he obtained his bachelor’s degree in Mechanical Engineering (Solid Mechanics and Design) in 2004. During his bachelor’s, he was elected as the chief of “The Scientific Committee of Mechanical Engineering Department (Student Branch)”. At the same time, he was also in charge of managing the Iranian Society of Mechanical Engineers (ISME), for the student branch of Khorasan.

In 2004, Reza entered the Biomedical Engineering Department at Amirkabir University of Technology (Tehran Polytechnic) where is the Center of Excellence in Biomedical Engineering in Iran. There, he did his master’s thesis entitled “Design of a Tactile Sensing System for Detecting an Embedded Object in Simulated Biological Tissue” under the supervision of Prof. Siamak Najarian, leading to the patent of a medical device called “Tactile Tumor Detector”. During his master’s, Reza significantly contributed to the establishment of two laboratories in the Biomedical Engineering Department: Biorobotics and Virtual Reality Laboratory, and Artificial Tactile Sensing and Robotic Surgery Laboratory.

In 2007, Reza received a grant to do a research on his patent under the supervision of Prof. Seyed Mohsen Towliat Kashani and Prof. Siamak Najarian, in Baqiyatallah Medical Sciences University, Tehran, Iran. The title of his research was "Sensitivity and Specificity Determination of Physical Examination and Tactile Tumor Detector Device in the Detection of Breast Masses in Comparison to Sonography as the Gold Standard". Having participated in the 14th Razi Medical Sciences Research Festival, Reza was titled as the “Young Researcher” and on 22nd of December 2008 he was awarded by the President of Iran, Mahmoud Ahmadinejad. At the same period, Reza had a position as a lecturer in Islamic Azad University of Saveh.

Reza moved to the Netherlands, in April 2009, to do his PhD at Eindhoven University of Technology (TU/e), where he joined the Orthopaedic Biomechanics group chaired by Prof. Keita Ito. The title of his PhD research accomplished under supervision of Dr. Rene van Donkelaar was “Towards a Damage Model for Articular Cartilage”. One reviewer of his PhD publications expressed: “The authors have tackled a long standing and important research question--the mechanical damage of cartilage components--they are to be congratulated for doing so.”

Since May 2013, Reza has started a new career as a Research Scientist / CAE Engineer at DSM Engineering Plastic Business Group in Materials Science Center, DSM Ahead BV, located at Chemelot Campus, Geleen, the Netherlands.